Synthesis and characterization of III-V colloidal semiconductor nanocrystals doped with rare-earth ions

Thuy Dieu Thi Ung

UNIVERSITÉ DE GRENOBLE

INSTITUTE OF MATERIALS SCIENCE

THÈSE

Pour obtenir le grade de

DOCTEUR DE L'UNIVERSITÉ DE GRENOBLE
Spécialité Chimie Physique Moléculaire et Structurale

Préparée dans le cadre d'une cotutelle entre
L'UNIVERSITÉ DE GRENOBLE ET **INSTITUTE OF MATERIALS SCIENCE**

Présentée et soutenue publiquement par

THUY DIEU THI **UNG**

le **17 Décembre 2010**

SYNTHÈSE ET CARACTÉRISATION DE NANOCRISTAUX COLLOÏDAUX DE SEMI-CONDUCTEURS III-V DOPÉS PAR DES TERRES RARES

Thèse dirigée par **Quang Liem NGUYEN** et **Peter REISS**

JURY

Prof. Xavier MARIE	*INSA Tolouse*	Rapporteur
Prof. Christophe DUJARDIN	*Université Claude Bernard Lyon*	Rapporteur
Prof. Daniel LE SI DANG	*Institut Néel Grenoble*	Examinateur
Prof. Thu Nga PHAM	*Institute of Materials Science*	Examinateur
Prof. Adam PRON	*CEA Grenoble*	Examinateur
Prof. Quang Liem NGUYEN	*Institute of Materials Science*	Directeur de thèse
Dr. Peter REISS	*CEA Grenoble*	Codirecteur de thèse

Laboratoire d'Electronique Organique Moléculaire et Hybride
Institut Nanosciences et Cryogénies, CEA Grenoble, France

Laboratoire de Matériaux Optoélectroniques
Institute of Materials Science, VAST, Vietnam

THÈSE

Pour obtenir le grade de

DOCTEUR DE L'UNIVERSITÉ DE GRENOBLE
Spécialité Chimie Physique Moléculaire et Structurale

Préparée dans le cadre d'une cotutelle entre
L'UNIVERSITÉ DE GRENOBLE ET **INSTITUTE OF MATERIALS SCIENCE**

Présentée et soutenue publiquement par

THUY DIEU THI **UNG**

le **17 Décembre 2010**

SYNTHÈSE ET CARACTÉRISATION DE NANOCRISTAUX COLLOÏDAUX DE SEMI-CONDUCTEURS III-V DOPÉS PAR DES TERRES RARES

Thèse dirigée par **Quang Liem NGUYEN** et **Peter REISS**

Laboratoire d'Electronique Organique Moléculaire et Hybride
Institut Nanosciences et Cryogénies, CEA Grenoble, France

Laboratoire de Matériaux Optoélectroniques
Institute of Materials Science, VAST, Vietnam

DECLARATION BY RESEARCH SCHOLAR

I hereby declare that the thesis entitled "**Synthesis and characterization of III-V colloidal semiconductor nanocrystals doped with rare-earth ions**", submitted for the Degree of ***Doctor of Philosophy*** to the University Joseph Fourier, has been performed by me in the sandwich regime between IMS/VAST (Vietnam) and UJF, CEA (France) under the supervision of Prof. Nguyen Quang Liem and Dr. Peter Reiss. The work is original and has not been submitted in part or full by me for any other degree or diploma to this or any other University.

Ung Thi Dieu Thuy

To my Professors

To my beloved Parents

Acknowledgements

I would like to express my appreciation to my supervisors, *Prof. Nguyen Quang Liem and Dr. Peter Reiss*, for their guidance and support. Their tireless enthusiasm and new ideas have always helped me continue working, though things seemed rather hopeless at times during the project. They taught me a lot both in science mind and in social life. Additional thanks for prompt and perfect corrections of our manuscripts. My deepest personal regards are due for them forever.

I sincerely acknowledge *Prof. Adam Pron* and *Prof. Daniel Le Si Dang* for their valuable help in every possible way through fruitful discussions and corrections of my manuscript.

I would like to thank to *Prof. Jean-pierre Travers* for allowing me the great opportunity to carry out my research work in his lab.

I would like to express my deepest gratitude to members of my graduate committee for their guidance and collaboration in the development of this work.

I am thankful to the secretaries *Ms Catherine Pascal*, *Ms Gwenaëlle Stephan* and *Ms Magali Pourtier*. I was lucky to have them for any required help and more...

A special thanks to *postdoc Liang Li for* guiding my first steps in operating the experimental setup and discussion.

My heartfelt thank *Le Quang Phuong* and *Tran Thi Kim Chi*, who initially helped me for the time-resolved photoluminescence measurement and fruitful discussion.

I also thank *Dr. Le Quang Huy* for XRF measurement.

I wish to express my sincere gratitude to Institute of Materials Science (IMS, Vietnam), Commission of Atomic Energy (CEA Grenoble, France) and University of Grenoble (France) for allowing me the opportunity to do Doctor's degree.

The work described in this thesis was carried out in IMS, CEA Grenoble and was supported by the Evariste Galois fellowship of the French Ministry of Foreign Affairs and the funding of CEA-DRI. I want to thank everyone who helped me make this work possible; specially my colleagues from Optoelectronic Materials (Vietnam) and Molecular Organic and Hybrid Electronics (France) Laboratories for useful collaboration, stimulating discussions and hospitality.

During the thesis, I also received a great help from MORICEAU, CROS and CHARBONNEL families. I am especially grateful for their friendship, which encouraged me

to overcome many difficulties in my life. Especially, they cared for me during my illness and made me feeling like my parents. I wish to take this opportunity to thank them.

I also want to thank all my friends, who have encouraged and supported me in everything I do.

Finally, without the support and endless love of my parents, I would not have been the person I am. They were, are, and will be forever the most important source of encouragement to me. Any words are not sufficient to thank my family. This thesis is dedicated to them.

Summary

This thesis focuses on the synthesis of III-V colloidal semiconductor nanocrystals (NCs) doped with rare earth (RE) ions by various synthetic methods. Nearly monodisperse series of InP and In(Zn)P core NCs as well as of strongly luminescent InP/ZnS and In(Zn)P/ZnS core/shell NCs were successfully synthesized by reaction of the In precursor (indium myristate) with different phosphorous precursors such as yellow phosphorous, PH_3 gas or $P(TMS)_3$ in the non-coordinating solvent 1-octadecene. The prepared NCs were characterized by powder XRD, TEM, EDX, XRF, UV-vis absorption and steady-state (SSPL) as well as time-resolved photoluminescence (TRPL) spectroscopy. Alloy In(Zn)P and In(Zn)P/ZnS QDs were synthesized in a heating-up one-pot method by adding zinc stearate during the nucleation and growth process of InP NCs. The alloy In(Zn)P/ZnS QDs showed high PL quantum yield (QY) up to 70% and their emission could easily be tuned in the range from 480 to 590 nm (FWHM: 50 nm) by varying the Zn^{2+}:In^{3+} molar ratio and the reaction temperature. The high PL QY is rationalized by band-edge fluctuation occurring in the In(Zn)P alloy structure, which contributes to the confinement of photoexcited carriers.

Eu-doped In(Zn)P/ZnS NCs were successfully synthesized in a three-step one-pot method, namely (step 1) synthesis of the In(Zn)P host NCs; (step 2) Eu-dopant growth; (step 3) synthesis of the outer ZnS shell. Complementary optical measurements – absorption, PL, PLE, phosphorescence and TRPL spectroscopy – confirmed the successful doping of the In(Zn)P/ZnS NCs with Eu and revealed resonant energy transfer between the In(Zn)P host and the Eu^{3+} guest ions.

Finally, we have studied the influence of the surrounding environment on the optical characteristics of alloy In(Zn)P/ZnS QDs by comparing close-packed NC films and colloidal solutions. The SSPL spectra from the close-packed In(Zn)P/ZnS NCs are peaking at shorter wavelengths in comparison with those taken from the colloidal ones. In addition, TRPL studies show that the close-packed In(Zn)P/ZnS NCs possess a shorter luminescence decay time and a strongly increased spectral shift with the delay time from the excitation moment in comparison with the colloidal ones. Förster resonance energy transfer and/or excited charge-carrier transfer between the In(Zn)P/ZnS NCs are the main reasons for the observed behavior. The evidence of charge-carrier transfer in close-packed layers of In(Zn)P/ZnS QDs is very important for their integration into optoelectronic devices, such as QD LEDs or LEFETs.

Content

List of Figures

List of Tables

List of Abbreviations

Å	Angstrom
d-dots	Doped quantum dots
EDX	Energy Dispersive X-ray spectroscopy
eV	Electron Volt
Eu(MA)	Europium myristate
Eu-oleate	Europium oleate
FWHM	Full Width at Half Maximum
hr	Hour
HRTEM	High Resolution Transmission Electron Microscopy
$In(Ac)_3$	Indium acetate
$In(MA)_3$	Indium myristate
LED	Light Emitting Diode
LQY	Luminescence Quantum Yield
MA	Myristic acid
μL	Microlitre
min	Minute
mL	Mililitre
NCs	Nanocrystals
nm	Nanometer
NPs	Nanoparticles
ODE	1-octadecene
PL	Photoluminescence
PLE	Photoluminescence Excitation
$P(TMS)_3$	Tris-(trimethylsilyl)phosphine
QD	Quantum dot
RE	Rare earth
SSPL	Steady-state Photoluminescence
TEM	Transition Electron Microscopy
$(TMS)_2S$	bis(trimethylsilyl) sulfide
TOP	Trioctylphosphine
TOPO	Trioctylphosphin oxide
TRPL	Time-resolved Photoluminescence
UV-Vis	Ultraviolet-Visible
XRD	X-rays Diffraction

XRF	X-rays Fluorescence spectroscopy
$Zn(EX)_2$	Zinc ethylxanthate
Zn-oleate	Zinc otearate
$ZnSt_2$	Zinc stearate

Introduction

The term “nanoparticles” (NPs) means that materials have the form of individual particles with a size below 100 nm. In this size range, the ratio of atoms on the surface to the atoms in the volume (proportional to 1/ r) is large meaning that one should consider the *contribution of the surface atoms* (including their dangling bonds) in various characteristics of the NPs. For easy evaluation and imagination, it is calculated that a 1-nm NP is composed of ~30 atoms of which 99% are resident on the surface; a 2-nm one is composed of ~250 atoms of which 80% are resident on the surface; a 4-nm one is composed of ~4000 atoms of which 40% are resident on the surface. Even the number of atoms per particle is small these atoms can arrange in the crystalline structure observed in the bulk material. In such a case a NP is called to be a nanocrystal (NC). In addition and more important, on the nanometer scale, there is a very interesting effect on the charge carriers, namely the “*quantum confinement effect*” which occurs if the size of NCs is comparable to twice the Bohr radius of its exciton. In this case, the NC is referred to as a quantum dot (QD).

Because of the specific characteristics arising from the nanometer size mentioned above, NPs/NCs/QDs have become interesting objects for both basic and applied research. For basic/fundamental research, most of interests have been focused on the quantum confinement effect and the energy levels of charge carriers involved in the optical/electrical processes, the interaction between excitation light and QDs, the energy transfer inside and between the QDs etc. For applied research, in the past decade, various QDs of II-VI and III-V semiconductors have been synthesized for their promising applications in biological labeling [1-3], opto-electronic devices including light emitting diodes (LEDs) and solar cells (SC) [4-12], as well as in photocatalysis[13]. For biological labeling, CdSe and CdTe semiconductor QDs exhibit strong luminescence at various colors in the visible and near infrared (NIR) range without the requirement of a specific excitation wavelength because of the semiconductor crystalline nature with a very large cross section for absorption of photons having energy higher than the bandgap. In contrast, biological labeling using organic dyes needs specific excitation wavelength resonant to the

molecule energy levels. Though the first paper on labeling of using CdSe/ZnS QDs [14] has been cited more than 5000 times, this work has to be considered as a proof-of-principle due to the intrinsic toxicity of Cd-based QDs.

To overcome this problem, the synthesis of various other types of semiconductor QDs has been developed. Among them, QDs of InP and $CuInS_2$ have been synthesized and turned-out to be very promising candidates for the above mentioned applications [15–20]. One reason for the choice of InP is that bulk InP possesses a direct bandgap of 1.27 eV and its excitonic Bohr diameter is 22 nm [21] therefore InP QDs emit in the visible and NIR spectrum because of quantum confinement of charge carriers on the nanometer scale. Until 2005, there have not been many publications on QDs of III-V semiconductors in general and on InP in particular because of difficulties in the materials preparation [22–26]. For InP QDs synthesis, one can mention efforts from several groups such as Nozik *et al*. and Peng *et al*. who used all organometallic precursors with stabilizers in high boiling temperature organic solvents [24–27,30]; Alivisatos *et al*. who used $InCl_3$ as the In source and a similarly organometallic precursor for P, with a sophisticated procedure [27]; Weller *et al*. who used the same route determined by Nozik *et al*. with attention to the shelling and etching process to study surface states of InP NPs [28–30]; Xie *et al*. who have used a lower temperature reaction of In and P with assistance of a reducing agent (KBH_4) and a specially designed ultrasonic generator [31–32]. Some other authors used reaction of sodium phosphide and indium chloride in TOP (trioctylphosphine) [33] or thermo-decomposition of single source precursors for both In and P constituents [34]. The four first groups reported good crystalline quality and low size dispersion of the colloidal InP NPs obtained from a route using high boiling point solvents such as TOPO (trioctylphosphine oxide)/ TOP or ODE (octadecence) using reaction temperatures around 250-300 $^{\circ}$C. In addition, the mentioned groups have synthesized InP QDs in long periods of the reaction/growth time, typically from few hours to several days; using pyrophoric and expensive chemical agents for the P source [e.g, $P(Si(CH_3)_3)_3$]. Because of the use of very pyrophoric $P(Si(CH_3)_3)_3$, all reaction were performed in severe oxygen free or airless condition. From the practical point of view, the above technological conditions have precluded development of the synthesis of InP QDs on a larger scale. During my thesis I have efficiently synthesized InP QDs in the reaction of newly created In and P in toluene [35]. Recently, we have reported the single-step one-pot synthesis of InP/ZnS QDs with a luminescence quantum yield (LQY)

exceeding 60% [36–37]. These QDs possess an alloyed internal structure in contrast to conventional core/shell InP/ZnS QDs prepared by two-step methods.

Semiconductor QDs have been considered to be good phosphors for light emitting diodes (LEDs) and wavelength converter with the goal to realize solid state white lighting in order to replace incandescent light bulbs or other fluorescence lamps. III-nitrides offer the possibility of achieving white light by combining the three fundamental colors or by combining the blue (from commercialized GaN-based LEDs) and orange emission (from QDs). In addition, red emission is required for getting a higher color rendering index (CRI) of full color devices that can be achieved by doping of suitable host materials with Eu^{3+} ions. InP QDs could be good luminophores emitting at orange color and be a good host materials for doping Eu^{3+} ions. In this case, the spectral positions from the well shielded intra 4f-transitions are nearly independent of the host material. The energy transfer between the host InP QDs and the guest Eu^{3+} dopant could be well understood by studying the optical processes related to the Eu^{3+} dopant. Thus, studies on the synthesis of InP QDs doped with Eu^{3+} trivalent ions and the excitation/de-excitation processes, as well as energy transfer between InP QDs and Eu^{3+} ions are not only interesting from the basic research point of view but also in view of the QDs potential use in lighting applications.

Other phenomena related to the nanometer size of QDs discussed in this thesis are the quantum confined Stark effect with the contributions of the electric field induced by the polarization of the QDs and the dielectric environment of the close-packed QDs with short interparticle distance. This study gives information about the influence of the electric field applied to the QDs and also about the energy transfer between excited QDs.

The experimental techniques used in realizing the thesis are as follows: (i) Various chemical methods were used for synthesis of InP QDs. (ii) Appropriate techniques were utilized for samples characterization: TEM for morphology; HRTEM, X-ray diffraction and Raman spectroscopy for determining the QDs structure; absorption and photoluminescence including time-resolved photoluminescence spectroscopy for studying the optical properties.

The thesis is divided into six chapters with appendices. Following this introduction, Chapter 2 presents a general introduction on the quantum confined nanostructures and the characteristic properties of nanocrystals and rare-earth ions.

Chapter 3 gives the general information on InP NCs and describes a novel synthetic method for the fabrication of InP NCs at low temperature by using yellow phosphorus. The obtained InP NCs of a 3-4 nm size range exhibit good crystallinity. Chapter 4 presents the general synthetic methods and the optical characterization of highly luminescent InP/ZnS core/shell and In(Zn)P alloyed core/ ZnS shell QDs. The importance of experimental key parameters such as the Zn^{2+}:In^{3+} ratio and reaction-growth temperature is discussed. In the appendices, the details of synthesis of InP, InP/ZnS and In(Zn)P/ZnS QDs using different methods and the characterization techniques are presented. Chapter 5 focuses on a three-step, one-pot method for the synthesis of Eu-doped In(Zn)P/ZnS NCs. The key factors for the successful doping process, including reaction temperature for each process, dopant concentration, and the epitaxial growth of the ZnS shell to prevent the removal of RE^{3+} ions, are discussed. The optical characteristics and the energy transfer mechanism from the NCs host to RE^{3+} ions are systematically studied. Chapter 6 will finally summarize the most important results of this thesis and give some perspectives.

The research described in the thesis was carried out in close collaboration between IMS/VAST (Vietnam 50% of time) and INAC/SPrAM/CEA Grenoble (France 50% of time) with financial support from the French Minister of Foreign Affairs (Evariste Galois program), CEA and IMS.

References

[1] P. Reiss, J. Bleuse, A. Pron, *Nano Lett.* **2**, 781 (2002).

[2] A. P. Alivisatos, *Nat. Biotech*. **22**, 47 (2004).

[3] I. L. Medintz, H. T. Uyeda, E. R. Goldman, H. Mattoussi, *Nat. Mater.* **4**, 435 (2005).

[4] N. C. Greenham, X. Peng, A. P. Alivisatos, *Phys. Rev. B* **54**, 17628 (1996).

[5] Th. Andreev, E. Monroy, B. Gayral, B. Daudin, N. Q. Liem, Y. Hori, M. Tanaka, O. Oda, L. S. Dang. *Appl. Phys. Lett*. **87**, 021906 (2005).

[6] S. Nizamoglu, T. Ozel, E. Sari, H. V. Demir, *Nanotechnology* **18**, 065709 (2007).

[7] W. U. Huynh, J. J. Dittmer, A. P. Alivisatos, *Science* **295**, 2425 (2002).

[8] T. Andreev, N. Q. Liem, Y. Hori, M. Tanaka, O. Oda, L. S. Dang, B. Daudin, B. Gayral, *Phys. Rev. B* **74**, 155310 (2006).

[9] V. L. Colvin, M. C. Schlamp, A. P. Alivisatos, *Nature* **370***,* 354–357 (1994).

[10] V. I. Klimov, S. A. Ivanov, J. Nanda, M. Achermann, I. Bezel, J. A. McGuire, A. Piryatinski, *Nature* **447***,* 441–446 (2007).

[11] D. V. Talapin, J. S. Lee, M. V. Kovalenko, E. V. Shevchenko, *Chem. Rev*., **110**, 389-458 (2010).

[12] U. T. D. Thuy, N. Q. Liem, D. X. Thanh, M. Protière, P. Reiss, *Appl. Phys. Lett.* **91**, 241908 (2007).

[13] M. Fujii, K. Nagasuna, M. Fujishima, T. Akita, H. Tada, *J. Phys. Chem. C* **113**, 16711–16716 **(**2009).

[14] M. J. Bruchez, M. Moronne, P. Gin, S. Weiss, A. P. Alivisatos, *Science* **281***,* 2013–2016 (1998).

[15] H. W. Spiess, U. Haeberlen, G. Brandt, A. Rauber, J. Schneider, *Phys. Status. Solidi.* B **62**, 183 (1974).

[16] H. Y. Ueng, H. L. Hwang, *J. Phys. Chem. Solids* **50**, 1297 (1989).

[17] K. Wakita, H. Hirooka, S. Yasuda, F. Fujita, N. Yamamoto, *J. Appl. Phys*. **83**, 443-447 (1998).

[18] J. Krustok, J. H. Schon, H. Collan, M. Yakushev, J. Madasson, E. Bucher, *J. Appl. Phys.* **86**, 365-369 (1999).

[19] K. Wakita, F. Fujita, N. Yamamoto, *J. Appl. Phys.* **90**, 1292-1296 (2001).

[20] T. T. K. Chi, L. Q. Phuong, N. Q. Liem, L. Li, P. Reiss, *J. Adv. Nat. Sci.* 1, 025007 (2010).

[21] S. Xu, J. Ziegler, T. Nann*, J. Mater. Chem.***18**, 2653 (2008).

[22] C. B. Murray, D. J. Noris, M. G. Bawendi, *J. Am. Chem. Soc*. **115**, 8706 (1993).

[23] J. Park, J. Joo, S. G. Kwon, Y. Jang, T. Hyeon, *Angew. Chem. Int. Ed.* **46**, 4630 (2007).

[24] M. Green, *Curr. Op. Sol. St. Mater. Sci.* **6**, 355 (2002).

[25] S. W. Kim, J. P. Zimmer, S. Ohnishi, J. B. Tracy, J. V. Frangioni, M. G. Bawendi, *J. Am. Chem. Soc*. **127**, 10526 (2005).

[26] L. Li, M. Protiere, P. Reiss, *Chem. Mater.* **20**, 2621 (2008).

[27] O. I. Micic, C. J. Curtis, K. M. Jones, J. R. Sprague, A. J. Nozik, *J. Phys. Chem*. **98**, 4966 (1994).

[28] O. I. Micic, S. P. Ahrenkiel, A. J. Nozik, *Appl. Phys. Lett.* **78**, 4022 (2001).

[29] M. J. Seong, O. I. Micic, A. J. Nozik, A. Mascarenhas, H. M. Cheong, *Appl. Phys. Lett*. **82**, 185 (2003).

[30] D. Battaglia, X. Peng, *Nano Lett*. **2**, 1027 (2002).

[31] P. Yan, Y. Xie, W. Wang, F. Liu, Y. Qian, *J. Mater. Chem.* **9**, 1831 (1999).

[32] B. Li, Y. Xie, J. Huang, Y. Liu, Y. Qian, *Ultrasonics Sonochemistry* **8**, 331 (2001).

[33] K. W. Jun, P.K. Khanna, K. B. Hong, J. O. Baeg, Y. D. Suh*, Mater. Chem. Phys*. **96**, 494-497 (2006).

[34] Y. Qian, *Adv. Mater*. **11**, 1101 (1999).

[35] U. T. D. Thuy, T. T. T. Huyen, N. Q. Liem, P. Reiss, *Mater. Chem. Phys*. **112**, 1120 (2008).

[36] L. Li, P. Reiss, *J. Am. Chem. Soc.* **130**, 11588 (2008).

[37] U. T. D. Thuy, P. T. Thuy, L. Li, P. Reiss, N. Q. Liem, *Appl. Phys. Lett*. **96**, 073102 (2010).

2. Theory related to the optical properties of semiconductor nanocrystals and rare-earth ions

2.1. Quantum size effect

One of the key factors associated with nanomaterials is the size dependence of their physical and chemical properties. The difference of properties between the bulk material and the isolated NPs becomes particularly pronounced in aspects related to the surface and the confinement of charge carriers. In this paragraph we present the basic knowledge on the density of states and energy levels from a QD, i.e. a NC with radius comparable to the Bohr radius of its exciton [1]. The quantum size effect not only includes the blue-shift of the absorption edge/exciton energy but also covers the increase of the exciton oscillator strength and the binding energy [2]. Both of these effects will be discussed in the following.

In atoms and molecules electrons exist in discrete localized states, while in a bulk semiconductor the large number of atomic/molecular orbitals creates a band of continuous electronic states. In semiconductors, the valence and conduction bands are separated by an energy gap or band gap, where no Bloch function solutions of the wave equation can exist. The band gap can be defined between the top of the valence band (VB), or in terms of quantum chemistry the highest occupied molecular orbital (HOMO), and the bottom of the conduction band (CB), or the lowest unoccupied molecular orbital (LUMO). The electrons can be excited to the CB and create holes in the VB by thermal or photon excitation. In this situation, a number of free electrons and holes give rise to a certain conductivity of the semiconductor. The band gap is of fundamental importance because it determines both the electrical conductivity and the optical absorption onset energy [1]. Quantization depends on the spatial confinement and can be classified in three different regimes, namely confinement in one, two or three dimensions. Confinement in one dimension produces a quantum well, in two dimensions a quantum wire and confinement in three dimensions produces a quantum dot. The basic characteristics of these three quantum structures are different, for example the density of states as a function of the energy (see Figure 2.1). For the quantum dot structure, the density of states is a delta function showing correspondingly the discrete energy levels [3].

The quantum confinement is rated into different regimes; at weak quantum confinement regime, the characteristics are still bulk-like; while at strong quantum confinement regime the quantum size effect makes QDs behave as “artificial atom” [4].

In a bulk semiconductor, the electron and hole are coupled by attractive Coulomb forces to form a so-called Mott–Wannier exciton that is assigned as a single particle in an excited state [5]. In II-VI and III-V semiconductors, excitons are considered to be similar to a hydrogen atom and can be well described by a hydrogen-like model incorporating the effective mass and the screening described by the dielectric constant. Brus et al. [6] considered that unlike in bulk semiconductors, where the electron-hole pair is free to move, in small QDs they can become physically confined. Strong confinement leads to a rising of the electronic energy in the same way as would be expected from the simple particle-in-a-box model of quantum mechanics. The effective band gap of a NC can be derived as

$$E_{\mathrm{g,eff}}(R) = E_{\mathrm{g}}(\infty) + \frac{\hbar^2\pi^2}{2R^2}\left(\frac{1}{m_{\mathrm{e}}^*} + \frac{1}{m_{\mathrm{h}}^*}\right) - \frac{1.8e^2}{\varepsilon R}$$

where $E_g(\infty)$ is the band gap of the bulk semiconductor (~1.27 eV for InP [7– 8]), m_e* and m_h* are the effective masses and ε is the bulk optical dielectric constant.

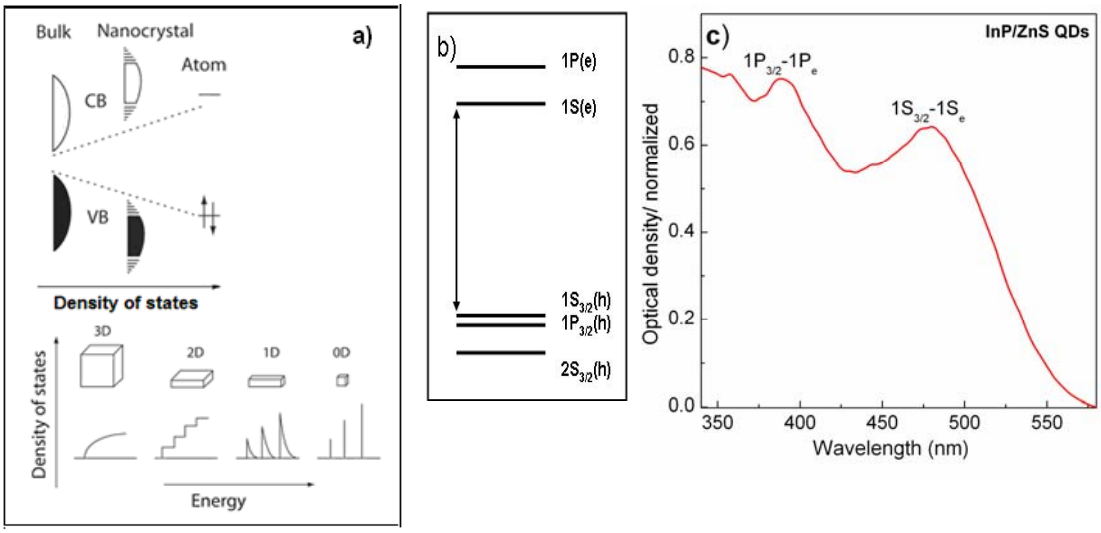

Figure 2.1: *(a) Density of states in a bulk semiconductor, a NC and an atom; and the corresponding confinement diagram illustration of them. (b) Electron and hole states in a semiconductor NC in the strong confinement regime [3]. (c) Typical absorption spectrum from a colloidal In(Zn)P/ZnS NCs.*

When R is small, the $1/R^2$ term (related to the confinement energy) is more visible and stronger contributes to the change in the final transition energy. It increases very fast with decreasing size, especially when the radius (R) is smaller than the Bohr exciton radius (α_B), which is given by

$$\alpha_{\mathrm{B}} = \frac{\hbar^2 \varepsilon}{e^2}\left(\frac{1}{m_{\mathrm{e}}^*} + \frac{1}{m_{\mathrm{h}}^*}\right)$$

where ε is the dielectric constant and m_e* and m_h* are the electron and hole effective masses, respectively.

Because of the high surface-to-volume ratio, the surfaces effect relatively weakly on the exciton energy, but have a tremendous effect on the exciton oscillator strength [4]. The exciton oscillator strength is given as follows [5]:

$$f = \frac{2m_{\mathrm{e}}}{\hbar^2}\Delta E|\mu|^2|U(0)|^2$$

where m_e is the electron mass, ΔE and μ are the transition energy and the transition dipole moment, respectively, and $|\mathrm{U}(0)|^2$ is the overlap factor between electron and hole wave functions. The confinement of electrons and holes in NCs enhances the spatial overlap between their wave function and increases the binding energy and oscillator strength. The absorption cross-section in a NC is determined by the oscillator strength per volume, f_{np}/V, where V is the volume of the NC [4,9], f_{np} is the oscillator strength of the NC. When $R >> \alpha_B$, $|\mathrm{U}(0)|^2$ is size independent and the oscillator strength is determined by the macroscopic transition dipole moment [3,9]. In the strong quantum confinement regime, where $R < \alpha_B$, the oscillator strength, f, is still only weakly size dependent, because μ follows the opposite trend, even though the overlap function $|\mathrm{U}(0)|^2$ between the electron and hole increases with decreasing size [10–13]. However, in this regime excitonic absorption becomes more intense because f_{np}/V increases with decreasing particle size and varies approximately with (α_B/R^3) [11–13].

2.2. Surface states in NCs

Atoms at the surface of NCs or bulk materials show coordinative un-saturation, leading to spatially and energetically localized electronic states (surface states or defects states) [14]. The so-called intrinsic defects reflect the aperiodic termination of the lattice on the surface of NCs. Certain adsorbates can occupy the vacant coordination sites on the surface leading in some cases to removal of the intrinsic surface states. In turn, new extrinsic surface states can be created, which arise from unsaturated coordination bonds of adsorbates, and may lie within the bandgap or in the continuum bulk states of the environment. Photooxidation is an example via oxide formation on the surface of the NC that leads to extrinsic surface states.

Another description by Brus et al. [6] explains surface defects by introducing two different kinds of trap such as deep trap and shallow trap. The deep traps are essentially localized at the lattice site defects and lie in the middle of the band gap. The shallow traps lie within a few meV of the corresponding band edge and are delocalized over several unit cells. Intrinsic surface states could be passivated by different kinds of ions including H^+ and OH^- generated from the ultraviolet light irradiation of samples in water [15].

The surface energy gap of NCs is dominated by the quantization of the energy levels in the material, thus the energy levels of the traps depend on the size of the NCs. With decreasing size produces splitting of the energy levels is more dramatic for the shallow traps than for the deep ones. Therefore, the distinction between shallow traps and the electronic states of the cluster disappears in the strong confined regime of NCs. The energy range between deep traps and delocalized states from the cluster is illustrated in Figure 2.2.

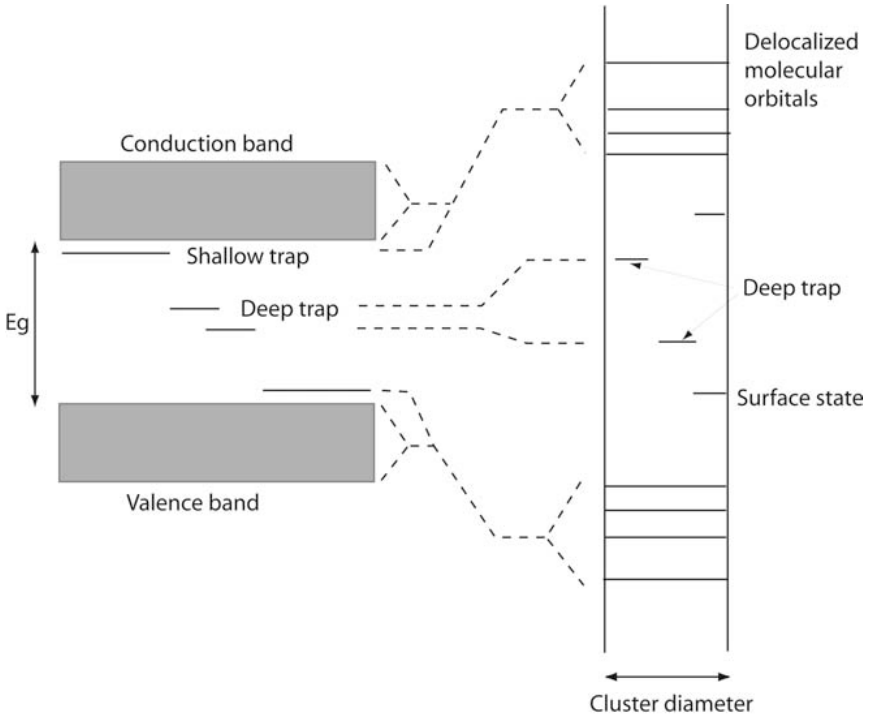

Figure 2.2: *Schematic diagram of the shallow and deep traps in the bulk (left) as well as in a semiconductor cluster/NC (right) [6].*

2.3. Luminescence spectroscopy of rare-earth (RE) ions

2.3.1. Rare earth related trap states and energy levels in semiconductors

The most interesting spectral features of RE^{3+} ions in certain host crystals are their very sharp luminescent lines much resembling the spectra of free ions. Because the 4*f* orbital of RE ions, incorporated in semiconductors, are deeply buried within the electronic shell, the energy levels of the $4f^n$ configuration are only slightly perturbed compared to free ion energy levels. Therefore, the positions of the energy levels of the 4*f* electron systems are almost unaffected by the nature of the host and the linewidths are often only slightly broadened [16].

It is well known that isoelectronic impurities in semiconductors produce bound states in the band-gap, binding an electron or a hole [17–18]. The factors affecting the intensity of binding energy potential are the electronegativity and the size difference between the impurity and the host ion which it replaces [19–20]. Also the spin-orbit coupling and the strain field in the close vicinity of the impurity, induced by size differences between the guest and the host atoms, can play an important role for creating trap levels [21]. The covalent radius and the electronegativity of RE^{3+} ions are shown in Table 2.1. If the RE^{3+} ions replace the element from column III

such as Ga and In in III-V compounds, they create isoelectronic traps due to the bigger covalent radius and the remarkably smaller electronegativity of RE^{3+} ions as compared to Ga and In ions. The RE^{3+} ions introduce electron or hole traps in III-V semiconductors. In general, most trap levels are attractive for electrons, but they can also bind in few cases a hole (GaAs:Er [22–23], InP:Bi [24–25]) or an exciton. The situation is more complicated for *n*-type and *p*-type semiconductors [20,26].

Table 2.1: *Electron configuration of selected RE atoms, RE^{3+} ions (and some elements), ionic, covalent radii, and electronegativity. The complete table can be found in [16,27].*

Element	Electron configuration	Electron configuration RE^{3+} ion	Ionic radius RE^{3+} (Å)	Covalent radius (Å)	Electro-negativity
Samarium	$..4f^6 5s^2 5p^6 6s^2$	$..4f^5 5s^2 5p^6$	0.97	1.62	1.17
Europium	$..4f^7 5s^2 5p^6 6s^2$	$..4f^6 5s^2 5p^6$	0.97	1.85	1.20
Terbium	$..4f^9 5s^2 5p^6 6s^2$	$..4f^8 5s^2 5p^6$	1.00	1.59	1.20
Erbium	$..4f^{12} 5s^2 5p^6 6s^2$	$..4f^{11} 5s^2 5p^6$	0.96	1.57	1.24
Thulium	$..4f^{13} 5s^2 5p^6 6s^2$	$..4f^{12} 5s^2 5p^6$	0.95	1.56	1.25
Ytterbium	$..4f^{14} 5s^2 5p^6 6s^2$	$..4f^{13} 5s^2 5p^6$	0.94	1.74	1.10
Gallium	$…3d^{10} 4s^2 4p$		0.62	1.26	1.81
Indium	$…4d^{10} 5s^2 5p$		0.81	1.44	1.78

The energy levels of RE^{3+} ions are shown in Figure 2.3. In many cases, one cannot observe all the corresponding transitions because the Stark splitting is not strong enough. It is clearly seen that if the optical transition from NCs is around 460 nm (~22000 cm^{-1}) it could match well the $^7F_0$ – $^5D_2$ transition of the Eu^{3+} ion to promote the resonant energy transfer between NCs and Eu^{3+} ions. Excited by the energy transferred from the host material, Eu^{3+} ions can then emit light by the 4f-electron transitions at the longer wavelength range mostly by the $^5D_0$ – $^7F_2$ transition (in this case, the transition originates from a J = 0 level that need ΔJ = 2, 4, 6).

Similarly, Tm^{3+} ions can absorb the energy to have the $^3H_6$ – $^1G_4$ transition and then to emit by the $^1G_4$ – $^3F_4$ and $^3H_4$ – $^3H_6$ transitions at 650 nm and 807 nm, respectively [36].

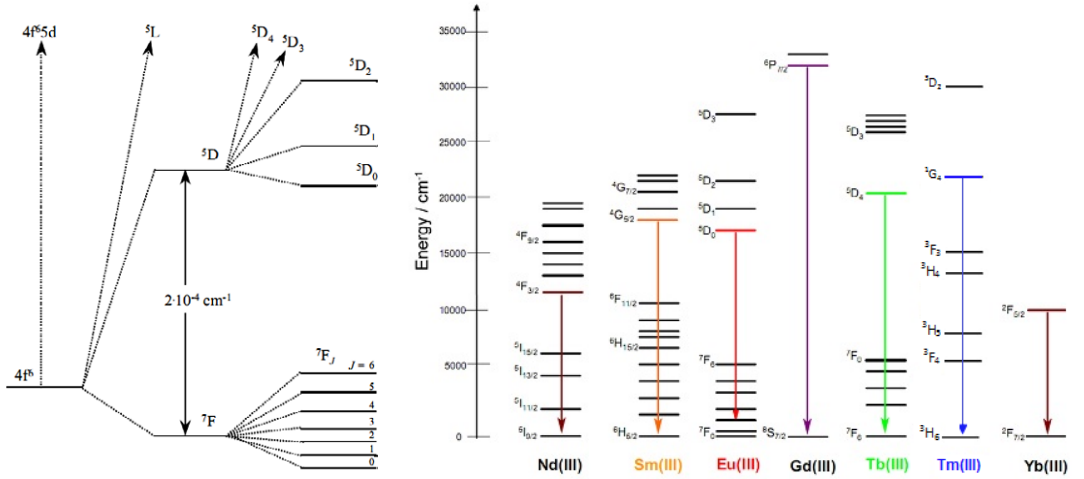

a) b)

Figure 2.3: *(a) energy levels of Eu^{3+} ions and (b) partial energy diagram of selected RE^{3+} ions. Arrows show the main transitions [28].*

The existence of trap levels can be demonstrated experimentally by measuring the lifetime of carriers, which is of course much longer when they bond to an isoelectronic trap level. If after recombination of carriers in the host the guest atom can be excited, as in the case of Eu^{3+} ions, other methods have to be used to identify trap levels, e.g. PLE or absorption spectroscopy, and thermally activated PL measurements. In the present thesis, PLE and absorption spectroscopy were used (see Section 5.3 of Chapter 5).

2.3.2. Energy transfer from the semiconductor host to the RE^{3+} ions

As mentioned above, the PL originating from the intra-4*f*-shell transitions of RE^{3+} ion is spectroscopically sharp and very weakly dependent on the surroundings. On the other hand, semiconductors doped with RE ions allow the excitation occurring *via* the host material with very large cross-section [32]. Therefore RE-doped semiconductor systems have a high potential for fabrication of optical or optoelectronic devices. A practical device requires stable and efficient room-temperature operation. To achieve this, the mechanism of energy transfer from the

host lattice to the RE ion needs to be understood and optimized. It is generally believed that the energy released from recombination of electron-hole pairs can be used to excite the RE ions into excited states, from which the radiative emission follows [16,29–30]. Yb-doped InP is commonly used as a model system to investigate these processes because Yb^{3+} ions has only one excited state and forms only one optically active center in InP [31–36]. According to this model, the energy transfer occurs between the Yb 4f-shell and an electron-hole pair at the electron trap that originates from the Yb ion substituting for In. As the Yb ion forms the electron trap, the trapped electron is located close to the 4f-shell of Yb and a strong interaction is expected between the electron-hole pair and the 4f-shell leading to an efficient energy transfer. Kinetic models from other semiconductor RE systems like Si:Er show similar characteristics [37–41].

Figure 2.4 shows a schematic model of Yb^{3+} excitation in InP bulk host. It is proposed that after band to band excitation of the semiconductor (1) the generated free electron can be quickly captured by a RE related trap (2). Then, a free hole from the valence-band is attracted to the trap by the Coulomb force (3), resulting in the formation of an electron-hole pair. The energy released from recombination of this electron-hole pair is then used to excite the Yb^{3+} ion from the $^2F_{7/2}$ ground state to the $^2F_{5/2}$ excited state in a so called Auger process involving electrons from the 4*f*-shell of the Yb atom (4). It is necessary that the energy between excited state and ground state of the RE^{3+} ions matches well the electron-hole pair recombination energy. Too low recombination energy from the recombining electron-hole pair would not yield to any excitation of the RE^{3+} ion. On the other side, the use of too wide band-gap would result in complex processes, the excess energy being released by the generations of phonons, which have been experimentally evidenced in [42].

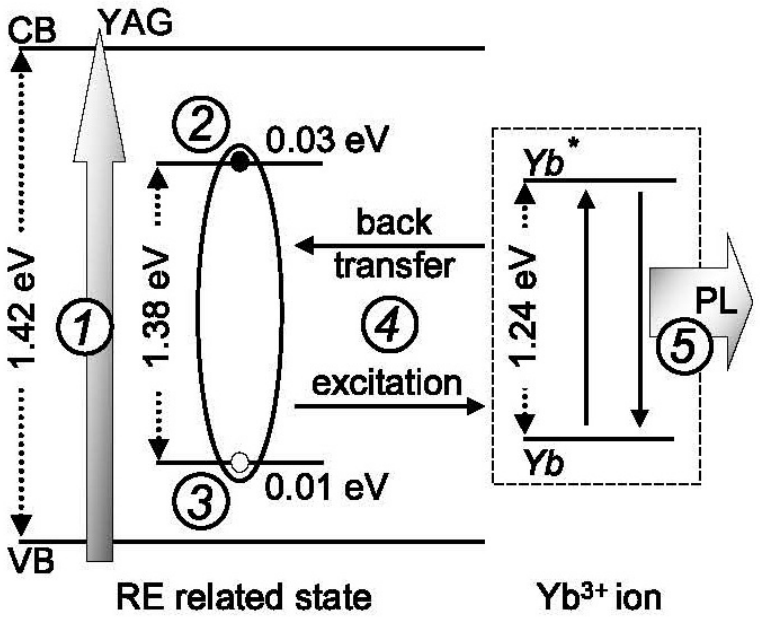

Figure 2.4: *Model of the excitation of Yb^{3+} ions in InP host. After band to band excitation **(1)** the generated free electrons can be captured at the Yb related trap **(2)**. Binding of the hole **(3)** forms an electron-hole pair on the trap. Non-radiative recombination of the pair leads to excitation of the Yb^{3+} ion **(4)**, producing the observed PL **(5)**. Energy back-transfer can cause the de-excitation of the Yb^{3+} ion without emission [31]. (Energy values at room temperature).*

The excited electron in the Yb^{3+} atom can relax to the ground state which is associated with light emission (5). However, an energy back-transfer process can also cause the de-excitation of excited Yb^{3+} ion by generation of an electron-hole pair in the host material. Then, recombination of this secondarily generated electron-hole pair can release the energy which can be used to excite again right such Yb^{3+} ion or another neighbor ion in the samples with higher content of Yb^{3+} ions. Another possibility is that an electron from the valence band can be generated with band edge related luminescence as the result. For matching the energy difference between trap level and the bottom of the conduction band or the top of the valence band, a multiphonon process is proposed [35,43]. The discussed processes occur in different time scales. The rise time of the Yb^{3+} atoms emission has been measured in the range of 1–10 μs depending on the generation rate [16,33], whereas the decay time - in the range of 7–12 μs. Note that for other RE atoms the decay time can be much longer as it strongly depends on the transition itself. Along with the above discussion the rise time must be included in the consideration of this process (1) to (3). For the decay time, only process (5) has to be considered. However

energy back-transfer with following RE ion excitation would yield much longer decay times, which is discussed in more detail in Section 5.3 for Eu-doped In(Zn)P/ZnS QDs. All other RE^{3+} ions (except Yb^{3+}) have more than one excited states so the energy transfer mechanisms are in these cases more complicated. At first the electron from the excited RE^{3+} ion can relax radiatively or with phonon emission to lower-lying excited states. Also cross relaxation processes can occur, which means that energy from an excited RE^{3+} ion is transferred, after radiative relaxation of the electron to a ground state, to another closely located RE^{3+} ion. This has of course detrimental effects on the optical output of the observed emission line as the cross excited luminescence is of the same (or lower) emission energy.

Cross relaxation processes are typically yielding long decay times. This problem will be approached in more detail in Section 5.3 using Eu-doped In(Zn)P and In(Zn)P/ZnS QDs as instructive examples. This phenomenon has been experimentally established for Eu^{3+} ions in insulators [44]. To the best of our knowledge, the energy transfer mechanism in Eu-doped In(Zn)P/ZnS QDs has not yet been investigated. This is probably caused by significant difficulties in the materials preparation, including the synthesis of high quality In(Zn)P/ZnS QDs and the doping process. In the following chapters the new results and discussion on this subject will be presented.

2.4. References

[1] Z. L. Wang et al. (Eds.), *Handbook of Nanophase and Nanostuctured Materials—Materials Synthesis and Applications (I)*, Tsinghua University Press and Kluwer Academic/Plenum Publishers, New York (2002).

[2] H. S. Nalwa (Ed.), *Handbook of Nanostructured Materials and Nanotechnology*, Optical Properties, Academic Press, San Diego, California (2000).

[3] A. P. Alivisatos, *J. Phys. Chem.* **100**, 13226 (1996).

[4] Y. Wang, N. Herron, *J. Phys. Chem.* **95**, 525 (1991).

[5] R. S. Knox, *Theory of Excitons*, Solid State Physics Supplements, Academic Press, New York, (1963).

[6] L. E. Brus, *J. Phys. Chem.* **90**, 2555 (1986).

[7] U. T. D. Thuy, T. T. T. Huyen, N. Q. Liem, P. Reiss, *Mater. Chem. Phys*. **112**, 1120 (2008).

[8] D. Lide, in *CRC handbook of chemistry and physics*, 73rd edition, CRC Press, Boca Raton, Florida (1993).

[9] Y. Wang, D. C. Neckers, D. H. Volman, G. Bunau (Eds.), *Advances in Photochemistry*, John Wiley and Sons, New York, 179 (1995).

[10] L. E. Brus, *J. Chem. Phys.* **80**, 4403 (1984).

[11] Y. Kayanuma, *Phys. Rev. B* **38**, 9797 (1998).

[12] T. Takagahara, *Phys. Rev. B* **36**, 9293 (1987).

[13] E. Hanamura, *Phys. Rev.* B **37**, 1273 (1988).

[14] F. Seker, K. Meeker, T. F. Kuech, A. B. Ellis, *Chem. Rev.* **100**, 2505 (2000).

[15] N. Q. Liem, L. Q. Phuong, T. T. K. Chi, U. T. D. Thuy, D. X. Thanh, *J. Korean Phys. Society* **53**, 1570-1574 (2008).

[16] H. J. Lozykowski, *Phys. Rev. B* **48**, 17758-17769 (1993).

[17] A. C. Aten, J. H. Haanstra, H. Vries, *Philips Res. Rep*. **20**, 395 (1965).

[18] D. C. Thomas, *J. Phys. Soc. Jpn*. **21**, 265 (1966).

[19] D. G. Thomas, J. J. Hopfield, C. J. Frosch, *Phys. Rev. Lett*. **15**, 857 (1965).

[20] R. Z. Bachrach, O. G. Lorimor, *J. Appl. Phys*. **43**, 500 (1972).

[21] A. Baldereschi, J. J. Hopfield, *Phys. Rev. Lett*. **28**, 171 (1972).

[22] P. S. Whitney, K. Uwai, H. Nakagome, K. Takahei, *Appl. Phys. Lett*. **53**, 2074, (1988).

[23] T. Benyattou, D. Seghier, G. Guillot, R. Moncorge, P. Galtier, M. N. Charasse, *Appl. Phys. Lett*. **58**, 2132 (1991).

[24] P. J. Dean, A. M. White, E. W. Williams, M. G. Astles, *Sol. St. Commun*. **9**, 1555 (1971).

[25] W. Ruhle, W. Schmid, R. Meck, N. Stath, J. U. Fischbach, I. Strottner, K. W. Benz, M. Pilkuhn, *Phys. Rev. B* **18**, 7022 (1978).

[26] P. D. Dapkus, W. H. Hackett, J. O. G. Lorimor, R. Z. Bachrach, *J. Appl. Phys*. **45**, 4920 (1974).

[27] D. R. Lide, *Handbook of Chemistry and Physics*, 74th edition, CRC Press: Boca Raton, (1993).

[28] G. H. Dieke, *Spectra and energy levels of rare earth ions in crystals*, Interscience Publishers, New York (1968).

[29] J. Palm, F. Gan, B. Zheng, J. Michel, L.C. Kimerling, *Phys. Rev. B* **54**, 17 603 (1996).

[30] S. Schmitt-Rink, C. M. Varma, A. F. J. Levi, *Phys. Rev. Lett*. **66**, 2782 (1991).

[31] M. A. J. Klik, T. Gregorkiewicz, I.V. Bradley, J. P. R. Wells, *Phys. Rev. Lett*. **89**, 227401 (2002).

[32] K. Takahei, A. Taguchi, H. Nakagome, K. Uwai, P. S. Whitney, *J. Appl. Phys*. **66**, 4941 (1989).

[33] H. J. Lozykowski, A. K. Alshawa, I. Brown, *J. Appl. Phys.* **76**, 4836 (1994).

[34] A. Taguchi, M. Taniguchi, K. Takahei, *Appl. Phys. Lett*. **60**, 965 (1992).

[35] A. Taguchi, K. Takahei, *J. Appl. Phys*. **79**, 3261 (1996).

[36] J. Wagner, J. Windscheif, H. Ennen*, Phys. Rev. B* **30**, 6230 (1984).

[37] I.Tsimperidis, T. Gregorkiewicz, H. H. P. Bekman, C. J. G. M. Langerak, *Phys. Rev. Lett*. **81**, 4748 (1998).

[38] M. Needels, M. Schlüter, M. Lannoo, *Phys. Rev. B* **47**, 15533 (1993).

[39] H. Kühne, G. Weiser, E. I. Terukov, A. N. Kusnetsov, V. Kh. Kudoyarova, *J. Appl. Phys.* **86**, 896 (1999).

[40] W. Fuhs, I. Ulber, G. Weiser, M. S. Bresler, O. B. Gusev, A. N. Kuznetsov, V. Kh. Kudoyarova, E. I. Terukov, I. N. Yassievich, *Phys. Rev. B* **56**, 9545 (1997).

[41] S. Coffa, F. Priolo, G. Franzò, V. Bellani, A. Carnera, C. Spinella, *Phys. Rev. B* **48**, 11782 (1993).

[42] A. Taguchi, K. Takahei, Y. Horikoshi, *J. Appl. Phys.* **76**, 7288 (1994).

[43] T. Andreev, PhD thesis, University of Joseph Fourier, Grenoble, France (2006).

[44] M. Dejneka, E. Snitzer, R. E. Riman, *J. Luminescence* **65**, 227 (1995).

3. InP nanocrystals

3.1. Introduction

In the past decades, NCs or QDs of various II-VI and III-V semiconductors have been synthesized and studied intensively due to their unique optical and opto-electronic properties; they are of great interest for both fundamental and applied research. Among their most promising applications their use as fluorescent probes in bio-labeling [1–3] and as light emitters or absorbers/light-converters in opto-electronic devices, such as light emitting diodes and solar cells [4–8], can be cited. Although most studies have focused on semiconductor NCs from the II-VI family (CdS, CdSe, CdTe), the synthesis and characterization of III-V semiconductor NCs such as InP(As), and GaP(As) have also received renewed interest due to their technological importance. Moreover, semiconductor NCs from the III-V family are more covalent in nature and exhibit larger excitonic Bohr diameters as compared to II-VI compounds. Therefore, one can expect that the quantum size effect is more pronounced in this class of materials, making them attractive compounds for investigations on the nanoscale and for application in optical devices. InP is especially interesting material, having a relatively large excitonic Bohr radius of 11.3 nm and a direct band gap of 1.27 eV, which enables its NCs to exhibit the photoluminescence emission in the spectral range from blue to the near infrared [9] depending on the quantum confinement regime. These InP NCs are promising alternatives to the frequently used CdSe-based NCs for applications in biolabeling, light emitting devices, photovoltaic cells, and quantum dot lasers [10–12]. Nevertheless, the synthesis of the highly luminescent III-V NCs is still challenging. While the synthesis of II-VI semiconductor QDs such as CdS, CdSe and CdTe experienced remarkable progress triggered by the seminal work of Murray *et al.* [13], the development of III-V NCs takes place on a slower time scale because of significant difficulties in the materials preparation. As a consequence only a relatively limited number of reports on InAs and InP QDs, which were synthesized by chemical methods, have been published [14–16]. Concerning the synthesis of InP NCs, the hot-injection method used for cadmium chalcogenides has been adapted by the groups of Nozik and Peng [17–20]. In these procedures, carried out in either a coordinating (TOPO/TOP, trioctylphoshpine oxide/trioctylphosphine, and various amines) [17-19] or a non-coordinating (ODE, 1-octadecene) [20] solvent at

high temperature (300-350°C), the phosphorus precursor (tris[trimethylsilyl]phosphine, $P(TMS)_3$) is quickly injected into the solution containing the indium precursor (indium chloride or indium acetate). While providing a relatively good control of the NCs size, these methods suffer from the use of stringent experimental conditions related to the injection of the pyrophoric phosphorus precursor and the high reaction temperatures, impeding the large-scale production of InP NCs. In addition, the synthesis in coordinating solvents is very time-consuming, as reaction times of several days or annealing of the isolated particles at temperature up 400°C are needed to obtain products of high crystalline quality [17–19,21]. A low temperature route enabled to obtain the well crystalline InP nanofibers at 111-203°C, however, with the use of highly toxic PH_3 gas in this process [22]. Xie *et al*. developed a different strategy, which relies on the use of indium chloride and yellow (or white) phosphorus in the presence of a reducing agent (KBH_4) [23–24]. When the reaction was carried out at 80-160°C in ethylenediamine solvent, 11-20 nm InP NCs and large-sized nanorods were obtained [23,25]. Using the same reagents in a mixed solvent of ethanol and benzene, an ultrasound-assisted reaction (25°C, 4 hrs) yielded 9 nm NCs [24]. In this case, a temperature-stabilized bath contained the reaction vessel, into which the horn tip of an ultrasonic generator was immersed to promote the production yield.

In this chapter we report on the synthesis and characterization of highly crystalline InP NCs from yellow P_4 at low temperature [26]. We used toluene as a reaction solvent in most experiments to avoid highly toxic benzene. Our method provides a number of positive features such as the use of simple precursors and experimental setup combined with a quick synthesis at low temperature that allow us to obtain the reaction yield of nearly 100% of InP NCs in the powder form after purification.

3.2. Synthesis of InP from yellow P_4 at low temperature

Recently, there have been considerable efforts to explore new solution routes to III-V group semiconductors, with the goals of searching for mild synthesis conditions, for instance, decreasing processing temperature, avoiding complex reactions and toxic precursors, and preparing on large-scale. Among them, the metathesis and solvothermal reduction routes seem to be proper choices for synthesis of III-V semiconductors especially for InP and InAs NCs. These routes use inexpensive chemicals and a simple set-up, are carried out at ambient pressure and

at low temperature. An important feature of the synthesis of spherical InP NCs, which should be mentioned here, is that yellow phosphorus dissolved in various solvents such as benzene and toluene was used as the phosphorus precursor. Xie *et al*. developed a strategy to produce InP NCs relying on the use of indium chloride and yellow (or white) phosphorus in the presence of a reducing agent KBH_4 in mixed solvents of ethanol and benzene under high-intensity ultrasonic irradiation (see reaction 3.1) [23–24].

$$4\ InCl_3 + 12\ KBH_4 + P_4 \rightarrow 4\ InP + 12\ KCl + 12\ BH_3 + 6\ H_2 \qquad (3.1)$$

In this process, KBH_4 reduces the dissolved $InCl_3$ to generate active elemental indium under ultrasonic irradiation. Ultrasonic waves that are intense enough to produce cavitations can drive high energy for the reaction between phosphorus and freshly created indium atoms to form InP NCs. The solvent also affects the reaction process and its products.The solvent also affects the reaction process and products. For instance, when the reaction was carried out at 80-160°C in 1,2-ethylenediamine solvent, 11-20 nm InP NCs and large-sized nanorods were obtained [23]. While using the same reagents in a mixed solvent of ethanol and benzene, an ultrasound-assisted reaction (25°C, 4 hrs) yielded 9 nm NCs. In this case, a temperature-stabilized bath contained the reaction vessel, into which the horn tip of an ultrasonic generator was immersed.

Herein, we used yellow phosphorus and $InCl_3$ as procursors to produce InP NCs. In fact, our method can be considered as a modification of Xie's method with some additional positive features. First, to generate active indium we used $NaBH_4$ as a reducing agent whose advantages will be discussed in Section 3.3. Another positive feature of our experiment is that we used toluene instead of benzene, a highly toxic solvent. And more importantly, by proper choice of the reaction conditions (see the experimental details in Appendix 1.2 and [26]) highly crystalline InP NCs have been successfully synthesized from the above mentioned precursors with a simple experimental setup without using ultrasounds. This combination enabled us to produce a large amount of InP NCs at low temperature with a reaction yield of nearly 100%.

We have controlled the growth regimes and the size of InP NPs by changing the $NaBH_4$ i concentration and its injection rate into the solution of indium and phosphorus precursors. The exapct procedure is described in Appendix 1.2 and in

[26]. Typically, we have checked various concentrations of $NaBH_4$ in ethanol and found that 0.2 M is appropriate to grow InP NCs in high yields without residual metallic In. The amount of $NaBH_4$ warrants the excess (two times) of reducing agent as compared to the used amount of In^{3+} ions. The freshly formed indium atoms from the reduction of the In^{3+} ions can react with available P atoms to form InP. We used two different ways for the injection of the $NaBH_4$ solution into the mixture containing indium and phosphorus precursors, which are the so-called "continuous method" (injection rate 1 mL/min) and "discontinuous method" (injection rate 5 mL/min). The reaction mixtures are maintained at temperatures of 40 or 70°C for duration of 1 to 5 hrs, depending on the desired NCs size. The produced dark precipitates are collected by centrifugation (5700 rpm, 10 min) and repeteadly washed with hot ethanol and toluene, to remove residuals and by-products such as P, NaCl and $NaBH_4$ (in some samples, CS_2 was used to wash P out). Finally, the black powder is dried in vacuum at 60°C for 1 hr. The reaction yield was close to 100%, with respect to the starting amount of the indium precursor. Concretely, after careful washing with ethanol and toluene we obtained ~2.5 mmol of InP NCs in form of a powder.

Measurement

For the structural characterization of the obtained NCs, powder X-ray diffraction (XRD, Siemens D5005) and Raman scattering spectroscopy (Jobin-Yvon Horiba Infinity spectrometer with 532 nm excitation) investigations were performed. The XRD patterns were used to identify structural phases as well as to calculate the mean crystallite sizes using Scherrer's formula. High resolution transmission electron microscopy (HRTEM JEOL 4000EX), and EDX analysis (FE-SEM Hitachi S4800) enabled us to determine directly the NCs' size and shape, as well as their stoichiometry. Samples for spectroscopic and microscopic measurements were prepared by dispersing the purified NCs in de-ionized water, followed by sonication (10 min). This treatment results in dispersions which are stable for several days without visible precipitation. For TEM, a drop of the obtained dilute NC dispersion was slowly evaporated on a holey carbon substrate (Ted Pella).

3.3. Results and discussion

The chemical reactions leading to the formation of InP in our synthetic scheme are described by equations 3.2-3.4

$$2In^{3+} + 6\ BH_4^- \rightarrow\ 2In + 3\ B_2H_6 + 3\ H_2 \quad (3.2)$$

$$4\ In + P_4 \rightarrow 4\ InP \quad (3.3)$$

$$4\ InCl_3 + 12\ NaBH_4 + P_4 \rightarrow 4\ InP + 12\ NaCl + 6\ B_2H_6 + 6\ H_2 \quad (3.4)$$

Alkali hydroborates MBH_4 undergo metathesis reactions with certain group II and group III elements; indium hydroborate, is, however unstable at room temperature [27]. Under the present reaction conditions, the redox reaction described in Equation 3.2 takes place instead, involving the oxidation of the hydroborate ions and reduction of the indium ions, accompanied by the release of gaseous hydrogen and diborane. The freshly created indium atoms react with elemental phosphorus (Equation 3.3) to form InP NCs. In Equation 3.4, the overall reaction is summarized, including the side-product NaCl, which can easily be removed by washing the NCs with de-ionized water. The resulting InP NCs precipitate as a very fine black powder. A key issue of this type of synthesis is the problem of avoiding the formation of residual metallic indium. This parameter can be controlled by adjusting the reduction rate of In^{3+} ions, which depends on the used reducing agent, the temperature and the solvent. Instead of using KBH_4 as described in [17–18], we have selected $NaBH_4$ as the reducing agent. This choice was motivated by the higher solubility of $NaBH_4$ in ethanol (due to its less ionic character), its larger commercial availability and lower price as compared to its potassium homologue. In order to control the reduction rate, we supplied the $NaBH_4$ solution in ethanol slowly by dropwise addition. Control XRD experiments performed on a series of samples prepared with varying $NaBH_4$ injection rates confirmed that this way of supplying $NaBH_4$ is of crucial importance. Using a high injection rate of $NaBH_4$ (5 mL/min), we obtained both crystalline InP NCs and metallic indium residual. Although it is in principle possible to wash out the metallic indium residual with dilute hydrochloric acid, the necessity of such additional purification steps and the reduced reaction yield are obvious drawbacks. By lowering the injection rate to 1 mL/min, InP NCs are obtained in high yield and the formation of residual metallic

indium could be significantly reduced as judged from XRD measurements. Using Scherrer's formula based on the half-widths of XRD peaks, we determined the mean size of the obtained InP NCs to be in the range of 3–6 nm for both described samples (5 mL/min and 1mL/min injection rate). Therefore it can be concluded that the reduction rate of In^{3+} does not have a strong influence on the NCs' size. In the above experiments the reaction temperature was kept at 40°C. Raising the temperature to 70°C and using the low injection rate of $NaBH_4$ (1mL/min) allowed for the complete suppression of the formation of metallic indium. Thus, in our further experiments these parameters are considered to be the "standard conditions".

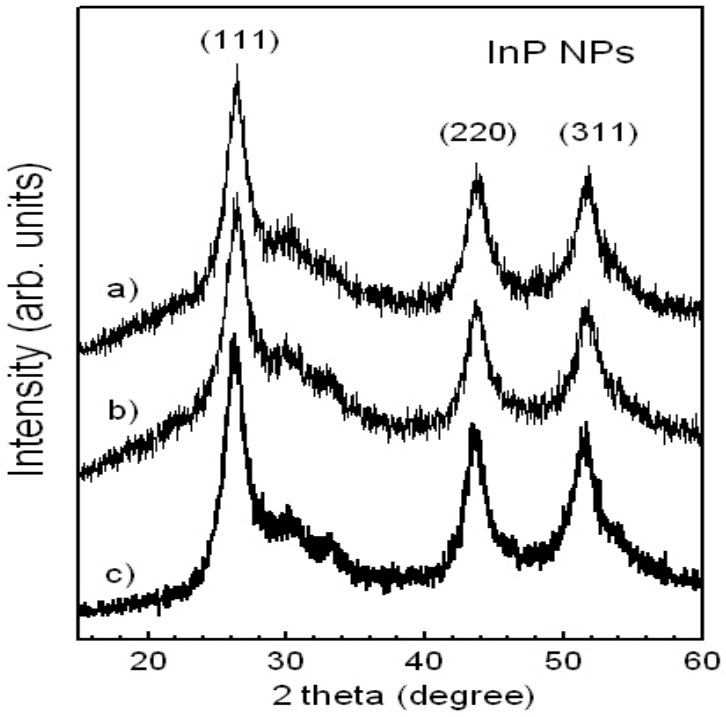

Figure 3.1: *X-ray diffraction patterns of InP NCs as a function of the reaction time (a) 1 hr, (b) 2 hrs and (c) 5 hrs (injection rate of $NaBH_4$: 1 mL/min; reaction temperature 70°C).*

Figure 3.1 shows XRD pattern of the InP NCs obtained using these conditions while varying the growth time. For all three samples, the XRD pattern is consistent with the bulk InP reflections indicating the same cubic zinc-blende lattice structure. The peak at 26.3° corresponds to the (111) lattice facet, with an atomic distance of 3.37 Å. The other peaks at 30.5°, 43.7° and 51.6° are indexed as the (200), (220) and (311) reflexions, respectively. The results reflect that the obtained InP NPs are well crystallized, which is markedly different from the previous results showing that products prepared by high intensity ultrasonic irradiation are often in amorphous form [28]. When the growth time was increased from 1 to 5 hrs, the InP NCs

became only slightly bigger, as can be seen by the almost imperceptible narrowing of the diffraction peaks. Using the peak at 43.7° to calculate the mean crystallite size resulted in ~4 nm (1 hr) and 4.2 nm (5 hrs). In the following we will demonstrate that the particle sizes determined by means of various methods are in good agreement.

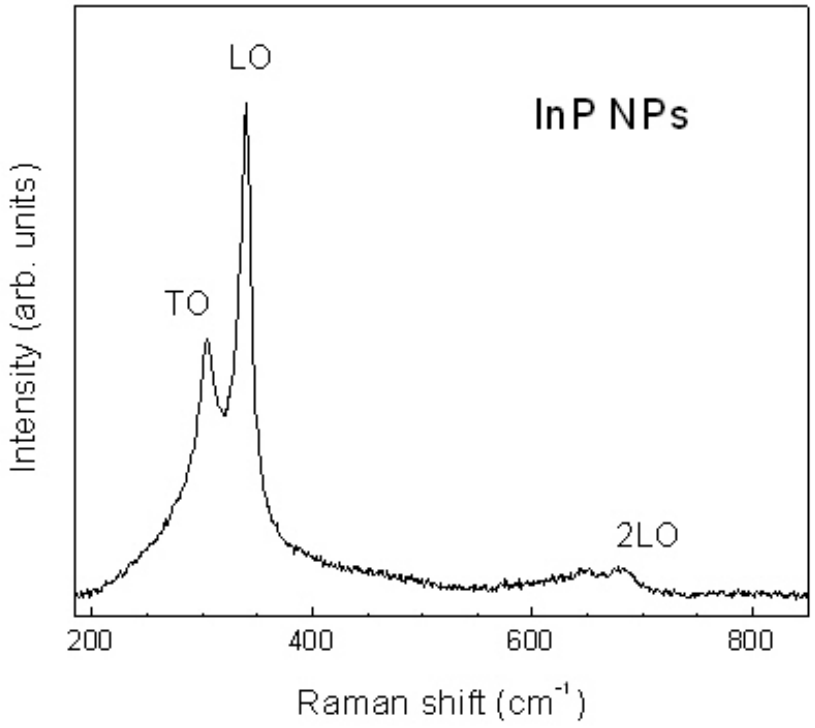

Figure 3.2: *Raman scattering spectrum of the obtained InP NCs (reaction time 2 hrs). Their mean size of 3–4 nm is estimated from the Raman shift and the intensity ratios between the 2LO and LO lines.*

Figure 3.2 shows the Raman spectrum of InP NCs obtained after a reaction time of 2 hrs, using the 532 nm light from a frequency-doubled Nd:YAG laser as the excitation source. The transverse optical (TO) and longitudinal optical (LO) phonon lines corresponding to the zinc-blende crystal structure of the InP NCs are clearly visible [19,29]. It is noteworthy that both the TO and LO Raman scattering lines could be observed because the NCs are randomly oriented; that is different from the case of oriented bulk InP, in which the recorded Raman spectra depend on the lattice facets under measurement respecting the Raman scattering selection rule. By comparing the recorded Raman spectrum to the reported size-dependent Raman spectra in Ref. 14, we estimate the size of our InP NCs to be of 3–4 nm, which is in good agreement with the crystallite size estimated from XRD measurements.

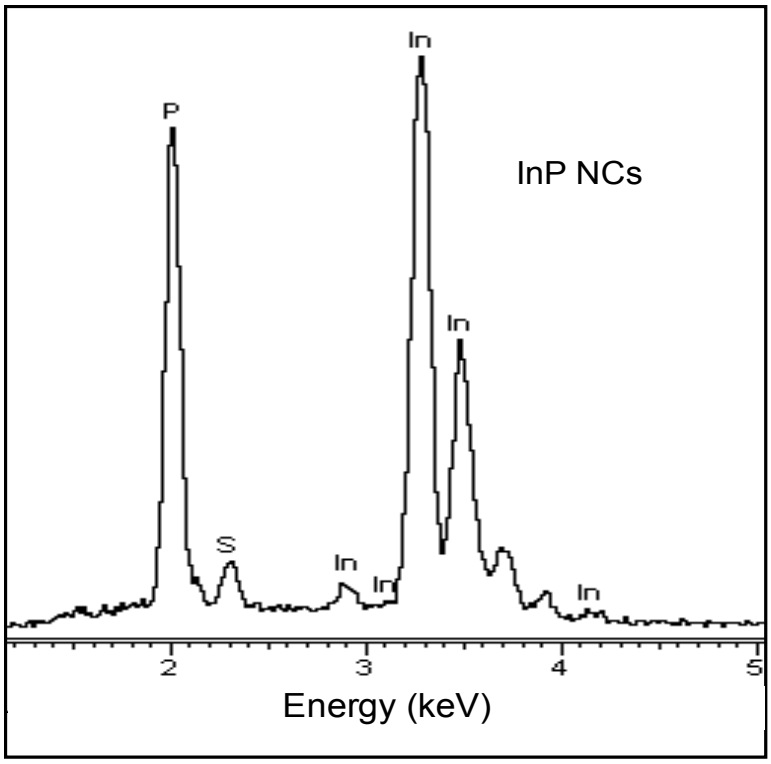

Figure 3.3: *EDX spectrum of a typical InP NCs after purification.*

An EDX spectrum of a typical sample, which was washed several times with ethanol and toluene, and then with CS_2 is shown in Figure 3.3. It reveals that the In:P atomic ratio is slightly smaller than 1 (0.96). Depending on the surface stoichiometry, a variation from equimolar composition can be expected in NCs, exhibiting a high surface to volume ratio. These deviations from stoichiometry may have effects, on the optical and electronic properties of NCs. For example, in case of a 3 nm of InP NCs, ~30% of its ~1000 atoms are located at the particle surface [30]. The observed excess of P is coherent with the higher amount of phosphorus precursor used in the synthesis, which favours a P terminated surface. The presence of sulfur is attributed to the washing of the sample with the CS_2 solution.

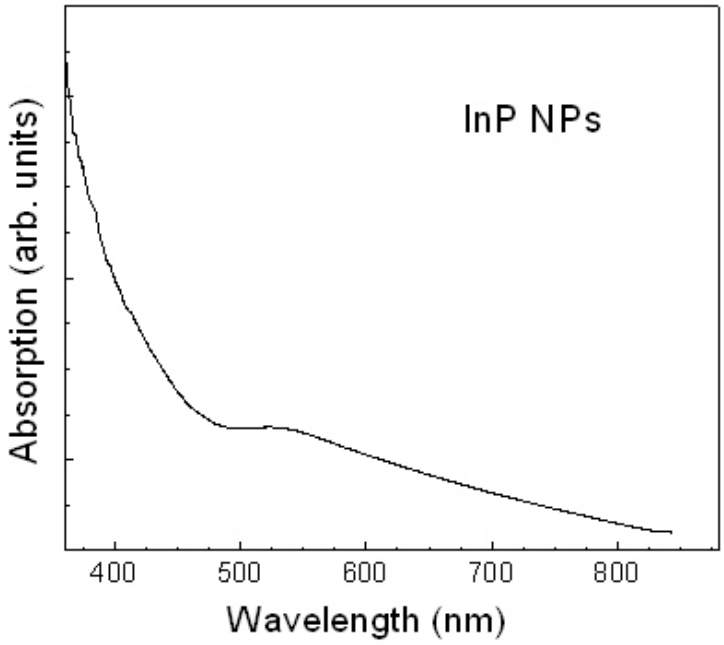

Figure 3.4: *UV-vis absorption spectrum of the obtained InP NCs (reaction time 2hrs), after purification and subsequent dispersion in de-ionized water.*

The experimental results presented so far have proved that InP NCs with a mean size around 4 nm have been synthesized with close to equimolar stoichiometry. As mentioned previously, two ways for injecting the $NaBH_4$ solution were explored, termed “continuous method” and “discontinuous method”. The results from XRD measurements and Raman spectroscopy are almost similar in the both cases. However, some differences have been detected in the UV-vis absorption spectra of both types of samples. Only when the “discontinuous method” was used, a peak corresponding to the optical transition in the near-band-edge region was distinguishable (Figure 3.4), indicating a lower size distribution than in the case of the “continuous method”. We rationalize this observation with a shorter nucleation event induced by the rapid injection of the reducing agent containing solution, and consequently a more pronounced temporal separation of nucleation and growth, necessary for the synthesis of NCs of low size dispersion. However, as mentioned before, the “discontinuous method” produces a larger amount of residual metallic indium. If we assign the spectral feature in spectrum 3.4 to the excitonic peak, its position of 540 nm corresponds to a NC size of ~2.5 nm, i.e. slightly smaller than their size determined from the results from X-ray and Raman analysis. A more detailed analysis of the spectrum is not possible due to a pronounced tail in

the longer wavelength region, which we attribute to light scattering arising from aggregates in the NCs dispersion.

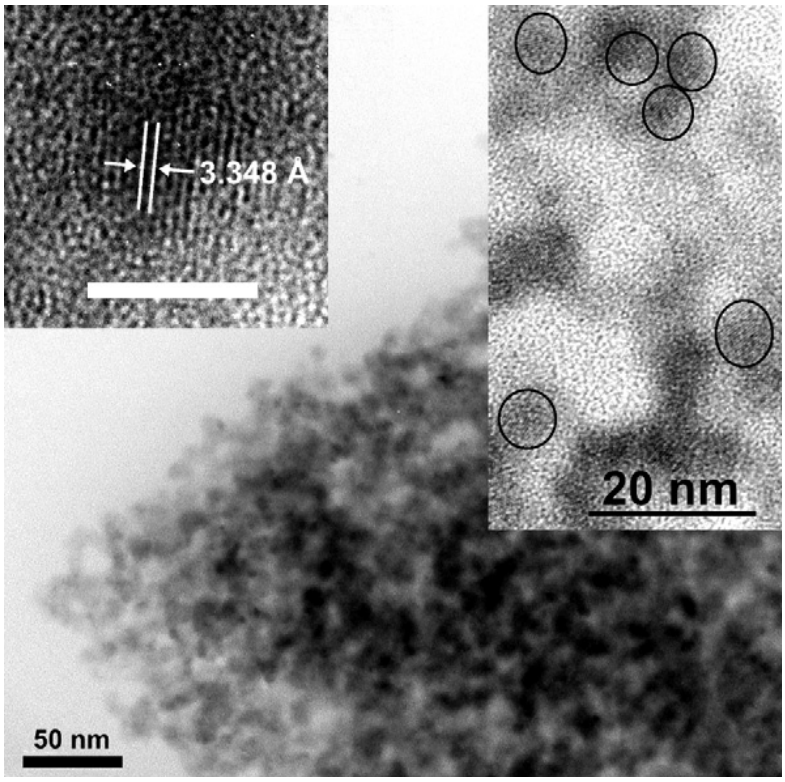

Figure 3.5: *TEM image of the obtained InP NCs. Left inset: HRTEM image of one particle showing the distance between atomic layers (scale bar: 5 nm). Right inset: overview image at higher magnification. The lattice planes of individual monocrystalline particles, highlighted with circles, are visible.*

Figure 3.5 displays the TEM images of InP NCs obtained after a reaction time of 2 hrs using the “continuous method”. Individual NCs with sizes ranging from 3–6 nm form larger aggregates. Due to the superposition of the nanocrystals, an accurate determination of the size distribution, estimated to be in range of 15–20%, is delicate. The high-resolution TEM image (inset of Figure 3.5) clearly shows the inter-reticular distance of 3.348 Å, which agrees with the lattice distances obtained from the XRD patterns (3.34 – 3.38 Å). Again a good agreement concerning the particle size with the above mentioned analysis techniques are obtained.

3.4. Conclusion

In this chapter, we have presented a novel and simple method for the synthesis of InP NCs having a mean size of 3–4 nm. The reaction temperature is 70°C, which is the lowest temperature reported to date for preparing InP NCs. Nevertheless the produced particles show high crystallinity and are obtained in high yield. Their surface is not passivated by bulky organic molecules of surfactant type, in contrast to nanoparticles synthesized *via* traditional colloid-chemical methods. Therefore charge transfer processes at the interface with their surrounding medium are facilitated. If surface oxydation could be avoided during their processing, these NCs would have a high potential for application in solar cells as broad-band light absorbers.

3.5. References

[1] M. Han, X. Gao, J. Z. Su, and S. Nie, *Nat. Biotechnol*. **19**, 631(2001).

[2] A. P. Alivisatos, *Nat. Biotech*. **22**, 47 (2004).

[3] I. L. Medintz, H. T. Uyeda, E. R. Goldman, H. Mattoussi, *Nat. Mater.* **4**, 435 (2005).

[4] N. C. Greenham, X. Peng, A. P. Alivisatos, *Phys. Rev. B* **54**, 17628 (1996).

[5] Th. Andreev, E. Monroy, B. Gayral, B. Daudin, N. Q. Liem, Y. Hori, M. Tanaka, O. Oda, and L. S. Dang. *Appl. Phys. Lett*. **87**, 021906 (2005).

[6] S. Nizamoglu, T. Ozel, E. Sari, H. V. Demir, *Nanotech*nology **18**, 065709 (2007).

[7] T. Wang, P. J. Parbrook, M. A. Whitehead, W. H. Fan, A. M. Fox, *J. Cryst. Growth* **273**, 48 (2004).

[8] T. Andreev, N. Q. Liem, Y. Hori, M. Tanaka, O. Oda, L. S. Dang, B. Daudin, B. Gayral, *Phys. Rev. B* **74**, 155310 (2006).

[9] S. Xu, J. Ziegler, T. Nann*, J. Mater. Chem.***18**, 2653 (2008).

[10] X. Michalet, F. F. Pinaud, L. A. Bentolila, J. M. Tsay, S. Doose, J. J. Li, G. Sundaresan, A. M. Wu, S. S. Gambhir, S. Weiss, *Science* **307**, 538 (2005).

[11] S. J. Pearton, C. R. Abernathy, M. E. Overberg, G. T. Thaler, D. P. Norton, N. Theodoropoulou, A. F. Hebard, Y. D. Park, F Ren, J. Kim, L. A. Boatner, *J. Appl. Phys*. **93**, 1 (2003).

[12] M. Bosi and C. Pelosi, *Prog. Photovoltaics* **15**, 51 (2007).

[13] C. B. Murray, D. J. Noris, M. G. Bawendi, *J. Am. Chem. Soc*. **115**, 8706 (1993).

[14] M. Green, *Curr. Op. Sol. St. Mater. Sci.* **6**, 355 (2002).

[15] S. W. Kim, J. P. Zimmer, S. Ohnishi, J. B. Tracy, J. V. Frangioni, and M. G. Bawendi, *J. Am. Chem. Soc*. **127**, 10526 (2005).

[16] L. Li, M. Protiere, P. Reiss, *Chem. Mater*. **20**, 2621 (2008).

[17] O. I. Micic, C. J. Curtis, K. M. Jones, J. R. Sprague, A. J. Nozik, *J. Phys. Chem*. **98**, 4966 (1994).

[18] O. I. Micic, S. P. Ahrenkiel, A. J. Nozik, *Appl. Phys. Lett.* **78**, 4022 (2001).

[19] M. J. Seong, O. I. Micic, A. J. Nozik, A. Mascarenhas, H. M. Cheong, *Appl. Phys. Lett*. **82**, 185 (2003).

[20] D. Battaglia, X. Peng, *Nano Lett*. **2**, 1027 (2002).

[21] A. A. Guzelian, J. E. B. Katari, A. V. Kadavanich, U. Banin, K. Hamad, E. Juban, A. P. Alivisatos, R. H. Wolters, C. C. Arnold, J. R. Heath, *J. Phys Chem*. **100**, 7212 (1996).

[22] T. J. Trentler, S. C. Goel, K. M. Hickman, A. M. Viano, M. Y. Chiang, A. M. Beatty, P. C. Gibbons, W. E. Buhro, *J. Am. Chem. Soc.* **119**, 2172 (1997).

[23] P. Yan, Y. Xie, W. Wang, F. Liu and Y. Qian, *J. Mater. Chem.* **9**, 1831 (1999).

[24] B. Li, Y. Xie, J. Huang, Y. Liu and Y. Qian, *Ultrasonics Sonochemistry* **8**, 331 (2001).

[25] Y. Qian, *Adv. Mater*. **11**, 1101 (1999).

[26] U. T. D. Thuy, T. T. T. Huyen, N. Q. Liem, P. Reiss, *Mater. Chem. Phys*. **112**, 1120 (2008).

[27] L. Artus, R. Cusco, J. M. Martin, G. Gonzalez-Diaz, *Phys. Rev.* B **50**, 11552 (1994).

[28] K. S. Suslick, *Ann. Rev. Mat. Sci*. **29**, 295 (1999).

[29] V. K. LaMer, R. H. Dinegar, *J. Am. Chem. Soc.* **72**, 4847 (1950).

[30] K. J. Klabunde, Nanoscale Materials in Chemistry, *Wiley-Interscience*, 23-24, New York (2001).

4. Luminescent InP/ZnS nanocrystals

4.1. Introduction

In Chapter 3 we presented the synthesis of InP NCs by means of a simple low temperature method with low cost precursors. In fact, this method, using $InCl_3$ and yellow P_4 in toluene and ethanol, enables the fabrication of large amounts of InP NCs in powder form. However, the obtained InP NCs possess a large size distribution and no luminescence could be detected. In this chapter, we present the study on the synthesis of highly luminescent InP/ZnS NCs.

Since the first successful preparation of InP NCs via an organometallic synthetic route, enormous efforts have been undertaken to prepare NPs of the technologically important III-V semiconductors [1–4]. However, the synthesis of III-V family NPs other than InP and InAs has shown to be more difficult than that of II-VI NCs. The reason is that III-V semiconductors are compounds more covalent in nature. Therefore higher temperatures and longer reaction times are usually required in the synthesis as compared to their II-VI analogues [5–7]. Consequently, only a limited number of papers discussing the synthesis and characterization of these NCs appeared in the literature [2–13]. Due to surface traps, dangling bonds and stacking faults in the crystal, a higher activation barrier of III-V compounds for de-trapping is observed as compared to the II-VI ones [7,14]. As-prepared InP NCs typically exhibit weak LQY, usually less than 1%, and broad PL linewidth (of the order of 60–100 nm) [15]. In addition, due to their large surface to volume ratio, nonradiative recombination at surface sites and surface traps competes very efficiently with luminescence [16–17]. Strategies to enhance the LQY aim to reduce nonradiative recombination by confining the wave function of the electron-hole pair to the interior of the crystallite. This is achieved either by chemically modifying the particle surface or by epitaxial growing of a shell of a largeer band gap semiconductor around each particle. In recent years, the preparation of surface-passivated III-V semiconductor NCs, including InAs, InP, GaAs core NCs, and CdSe, ZnSe and ZnS shells, was reported by Nozik et al.[18], Banin et al.[8], Peng et al.[9] and Reiss et al.[19]. Talapin et al. developped an efficient way to increase the LQY of InP NCs to values approaching of 40% by photo-assisted etching of their surface with HF [20]. Haubold et al. used organometallic precursors to grow a ZnS

shell on InP and obtained a subsequent increase of the LQY of 15% after 3 days and 23% after 3 weeks at room temperature [21]. Strategies to adjust the parameters of core and shell materials and to reduce strain-induced defects further led to strongly increased LQY of these semiconductor nanocrystals. Several lattice parameter adjusted core/shell NCs of II-VI compounds such as ($CdS/Cd(OH)_2$ [22], CdSe/ZnS(Se) [23–29] or CdS/HgS/CdS [30]) and III-V ones ($InAs(P)/CdZnSe_2$ [21,31–32]) have been reported. Among these examples, CdSe/CdS/ZnS core/shell/shell QDs showed narrow PL spectra with FWHM of 20–30 nm and high LQY of 50–85% [25,33–34]. The obtained LQY strongly depended on the shelling process for a given nanocrystal. In general, core/shell systems show a significant increase of LQY and improvement of their chemical stability and photostability that make them attractive for such applications as biomedical labeling [35–36], opto-electronic devices [37–38], and potential laser development [39].

In this chapter, the synthesis of InP core and InP/ZnS core/shell NCs is described, followed by the study of their structural and optical characteristics. Although the lattice constants of InP and ZnS differ by 8%, ZnS is expected to grow easily on small spherical InP NCs to yield core/shell particles similar to the strongly luminescent CdSe/CdS core/shell system [19,40–43]. Deposition of the ZnS is achieved in ODE by using the air-stable precursors zinc stearate ($ZnSt_2$) and zinc ethylxanthate ($Zn(EX)_2$) in the presence of InP NCs. The resulting colloidal solution in ODE is perfectly stable for months and shows a strong enhancement of the LQY. In our experiments, depending on the aim, the InP/ZnS NCs could be used in colloidal solution or in form of close-packed solid films. Details of the synthesis and processing of the InP/ZnS NCs as well as the characterization techniques used for the investigation of their structural and optical properties are presented in Appendix and at appropriate places in the following paragraphs.

4.2. Synthesis of InP and InP/ZnS core/shell nanocrystals in non-coordinating solvent

InP NCs were first synthesized by the method developed by Nozik *et al*. [1], based on Well's method of dehalosylilation [44], (see equation 4.1). The reaction was carried out in a glove box, under protective inert atmosphere using TOPO-TOP as stabilizing agents (to prevent the formation of bulk InP).

$$InCl_3 + [(CH_3)_3Si]_3P \xrightarrow{180-260\,^{\circ}C,\ \text{stabilizing agents}} InP + 3(CH_3)_3SiCl \qquad (4.1)$$

The InP particles formed after the nucleation stage are usually amorphous; annealing for 1–6 days at temperatures above 250°C is required to obtain crystalline InP NPs. Because of the long period of the annealing time, a relatively broad size distribution (~25–30%) with sizes ranging from ~2.2 to 6 nm was observed. Such size dispersion requires an appropriate post-preparative size fractionation. After using the size selective precipitation technique, up to ten size selected fractions can be obtained with a diameter distribution narrower than 8–10% of the average size [45]. Using amines as stabilizing and size-regulating agent permits to obtain smaller NCs with narrower size distribution as compared to the conventional TOPO/TOP method [45]. Although the coordinating solvents have yielded high quality II-V NCs [25,33–34,46–47], attempts to extend those approaches to other types of semiconductor NCs proved to be difficult. Evidently, not many compounds can act as the coordinating solvent [48], which makes it extremely challenging to identify a suitable reaction system for growing high quality NCs. Non-coordinating solvents, such as simple alkenes, were then introduced and the results have been very encouraging.

The most frequently used non-coordinating solvent is ODE [9,49–50]; it is a liquid at room temperature and its boiling point is at about 320°C. Fatty acids were chosen as ligands for stabilizing the NCs and the cationic precursors. This choice of solvent and stabilizing agent not only greatly shortened the reaction time to few hours, but also generated fairly monodisperse InP NCs without any size sorting. The key difference between coordinating and non-coordinating solvents is that, in the latter case, the reactivity of the monomers can easily be tuned by varying the ligand concentrations [49]. This tunable reactivity of the monomers provides a key to balancing nucleation and growth, and thus makes it possible to controllably synthesize high quality NCs. The capping of the NCs surface with the organic ligands results in

Following the above strategy for preparing InP and InP/ZnS NCs with suitable modifications in the use of chemical agents and the synthesis conditions, we have successfully synthesized highly luminescent InP and InP/ZnS NCs. In the following we present two methods used to synthesize InP and InP/ZnS NCs of low size dispersion in non-coordinating solvent, namely the “hot-injection” and the “heating-up” method.

4.2.1. Hot-injection method using PH_3 gas

The organic-phase hot-injection synthetic method has been widely used to synthesize NCs [53]. This method produces a high degree of supersaturation by the rapid injection of excess precursors into a hot organic surfactants solution, resulting in fast nucleation. The detailed synthesis of the InP/ZnS core/shell NCs and the experimental setup are described in Appendix 1.3.1. Briefly, InP NCs were formed in the high temperature (250–300°C) reaction of the indium and the phosphorus precursors in ODE solvent. The In precursor was indium myristate, formed *in situ* from indium acetate and myristic acid, while the P precursor was PH_3 gas, generated by the reaction of finely ground Ca_3P_2 or Zn_3P_2 powder with H_2SO_4 in a separate flask, connected to the synthesis flask. The PH_3 gas flow was controlled by the flux of Ar carrier gas. The size of the InP NCs was controlled by the concentration of the precursors and by the growth time. As-synthesized InP NCs could easily be dispersed in a number of solvents, including hexane, toluene, or chloroform. The ZnS shell was made by the subsequent slow addition of the air-stable ZnS precursors ($ZnSt_2$ and $Zn(EX)_2$) to the crude InP core NCs dispersion at 210-270°C. The high quality of the synthesized InP core and InP/ZnS core/shell QDs was confirmed by their UV-vis absorption and PL characteristics (Section 4.3.1).

4.2.2. Heating-up one-pot method using $P(TMS)_3$

The heating-up method is a batch process in which the precursors, reagents, and solvent are mixed at room temperature and heated up to a certain temperature to initiate the crystallization reaction and the growth. This method is very simple and particularly advantageous for large-scale synthesis. It can give a size uniformity of the QDs comparable to that obtained with the hot-injection method [51–53]. Recently, we successfully applied this method to synthesize high quality InP/ZnS NCs emitting luminescence in the visible spectral range with a quantum yield exceeding 60% [19, 54].

The detailed synthesis of the obtained InP/ZnS NCs is described in Appendix 1.3.2. Briefly, the In ($In(MA)_3$), P ($P(TMS)_3$), Zn ($ZnSt_2$) precursors were mixed at room temperature under argon atmosphere in the ODE solvent. The temperature of the reaction mixture was rapidly raised to 250–300°C and kept for several minutes to grow NCs until the desired size was reached. ZnS shell growth was subsequently

performed in the same manner as in the PH_3 method. After cooling to room temperature and purification by repeated precipitation (acetone/methanol) and redispersion (hexane) cycles, the synthesized InP/ZnS NCs could easily be dispersed in a number of solvents, including chloroform, toluene, or n-hexane. Detailed results concerning the structural and optical properties of the obtained InP/ZnS NCs are presented in Section 4.3.2.

4.3. Results and discussion

4.3.1. InP/ZnS NCs synthesized by the hot-injection method using PH_3 gas

In this Section, we discuss the optical properties of InP/ZnS core/shell NCs synthesized by the hot-injection method. The ZnS shell played a decisive role to passivate imperfections on the surface of InP QDs and to prevent from oxydation, consequently giving rise to a strong enhancement of the PL from the InP core. Under appropriate excitation conditions, not only the emission from the InP core but also that from the ZnS shell was observed. The emission peak in InP core QDs varied as a function of NCs' size, ranging in the 590–720 nm region; while the ZnS shell showed emission in the blue region around 470 nm, which is interpreted as resulting from defects in ZnS.

The formation of InP NCs is based on a two-step reaction:

$$Zn_3P_2 + 3H_2SO_4 \rightarrow 2PH_3\uparrow + 3ZnSO_4 \quad (4.2)$$

$$PH_3 + In\sim MA \rightarrow InP \quad (4.3)$$

Herein, the PH_3 gas was gradually generated *in situ* from Zn_3P_2 and H_2SO_4, similar to the case of the multiple precursor injections, to support NCs growth in the "size focusing" regime for long enough time to obtain larger crystals [9,53,55]. Therefore, the obtained InP NCs possess a narrow size distribution and a well-defined excitonic peak. These results indicate that the synthesized InP NCs have a high quality comparable to that of CdTe NCs, produced by H_2Te gas injection [50,56].

The growth of NCs depends strongly on the experimental parameters such as the reaction temperature, the ratios and the concentration of precursors in the reaction solution. The experimental results show that with increasing reaction temperature (230–300°C) the excitonic peak of NCs is red-shifted (570–650 nm) leading to the formation of bigger size InP NCs (Figure 4.1a). With increasing the P/In ratio (from 0.5:1 to 6.0:1) not only larger quantities of InP NCs are formed but also their mean size increases as indicated by a shift of their excitonic peaks in

range of 570–700 nm (Figure 4.1b). On the contrary, with increasing concentration of the In precursor, the mean sizes decrease (Figure 4.1c). This is consistent with the classical nucleation theory that the higher precursor concentrations cause the formation of a larger number of nuclei leading to NCs with smaller mean size [57]. The experimental results also show that for the 1:3 the molar ratio of In:MA in the precursor, the reaction yields InP NCs having the best size distribution and a well-distinguished excitonic absorption feature (Figure 4.1d). These results are consistent with the results reported by Peng and coworkers who synthesized InP NCs using $P(TMS)_3$ [9].

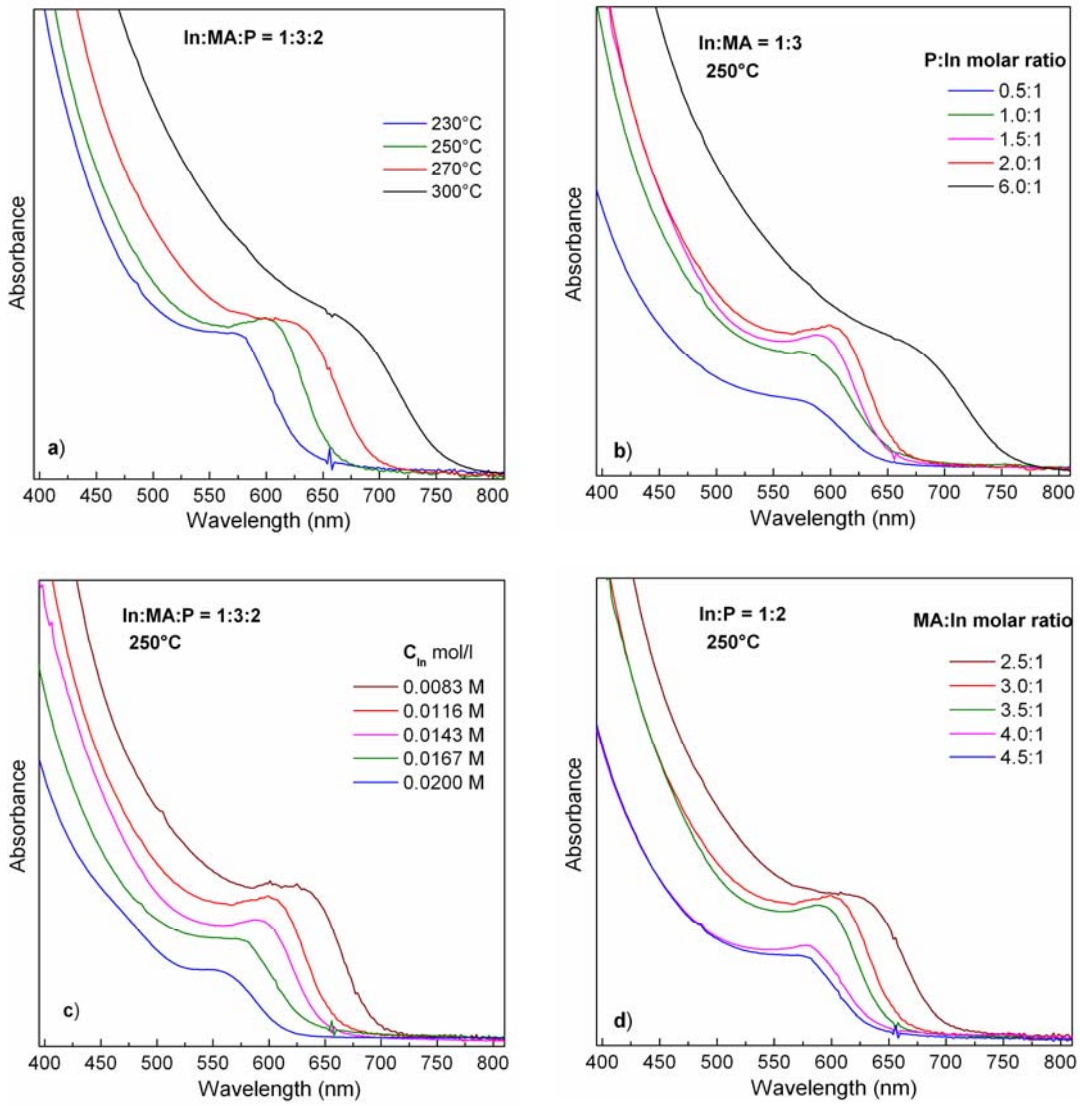

Figure 4.1: *UV–vis absorption spectra evidencing the influence of different parameters on the size evolution of InP NCs (reaction time: 30 min): (a) temperature; (b) In/P ratio; (c) indium precursor concentration; and (d) In/MA ratio.*

Our method can be tuned to obtain larger sized InP NCs having exciton and emission peak in the near-infrared region that makes them promising for application in invivo biological imaging. To the contrary for InP NCs synthesized from $P(TMS)_3$, it is difficult to obtain larger sized InP NCs with the exciton peak > 600 nm [50,58]. However, the obtained large sized InP NCs exhibited a broader size distribution. Moreover their LQY was of 0.1 % and some samples did not exhibit at all detectable photoluminescence. In this case surface states act as non-radiative channels for the relaxation of the excited charge carriers [59]. Growing a ZnS shell on the InP core resulted in a strong increase of the LQY, reaching ~20% (Figure 4.2a) due to the passivation of surface states and confinement of the photogenerated carriers inside the InP core NCs. Figure 4.2b shows the normalized PL spectra of two different-sized InP/ZnS core/shell samples investigated under 370–nm excitation. For the InP core sizes of 2.7 and 3.6 nm, strong emission bands at 620 nm and 690 nm were observed, respectively. This size-dependence is a direct consequence of the quantum size effect. For easier identification of each sample hereafter, we have named the InP/ZnS core/shell QDs emitting at 620 nm as S-QDs and the 690 nm emitting as L-QDs. Along with the PL band originating from the exciton transition in the InP QDs (core), one can see another PL band peaking at shorter wavelength around 470 nm. The latter signal is very occurs at very similar wavelengths in different InP/ZnS core/shell QD systems, regardless of the size of the core InP QDs. We attributed the 470 band to lattice defect-related emissions from the ZnS shell. In fact, ZnS single crystals emit intensive blue luminescence under excitation with the 365–nm line from a high-pressure mercury lamp [60]. The 365 nm light is below the band gap of ZnS. However it can excite defect-related self-activated centers to emit luminescence.

If we suppose that the PL spectrum taken from InP/ZnS QDs contains two spectral components, in the SSPL measurement the PL intensity of each component appears to be proportional to the product of the recombination/transition rate and its density of states (with the same absorbance). This product is much larger for the InP QDs than for the ZnS shell, giving rise to the relative intensities of the PL signal observed in Figure 4.2.

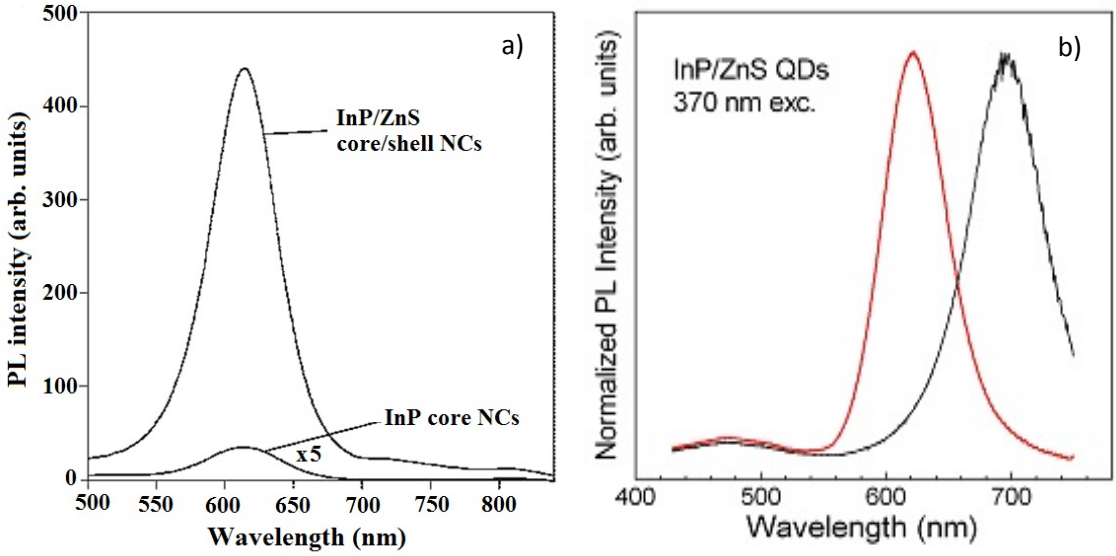

Figure 4.2: *a) SSPL spectra of the as-synthesized InP QDs (x5) and of the InP/ZnS QDs (LQY ~20%) under 450–nm excitation. b) normalized PL spectra of two different sized InP/ZnS core/shell QD samples under 370–nm excitation.*

The TRPL technique, by tracing the PL intensity at certain moments delayed from the excitation, enables us to determine exactly the instant PL intensity of each spectral component at a certain time interval after the pulsed excitation. It therefore allows us to determine the role of each relevant transition resulting in the overall emission. Figure 4.3 presents the TRPL spectra of the two InP/ZnS core/shell QDs, in which the 470 nm band was clearly observed, very prominent as compared to the proper emission from the InP core QDs. The intensity evolution of both bands as a function of the delay time (Figure 4.3a) is possibly related to the different transfer rate of carriers from the ZnS shell to the InP core.

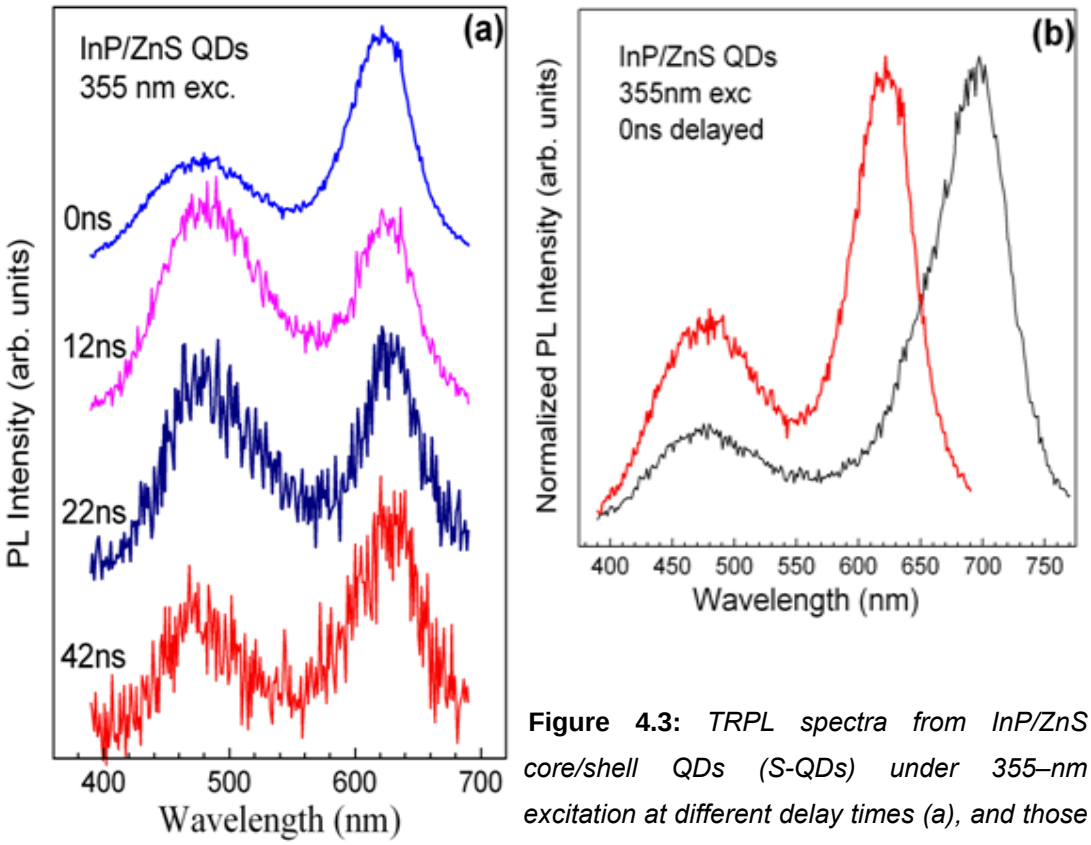

Figure 4.3: *TRPL spectra from InP/ZnS core/shell QDs (S-QDs) under 355–nm excitation at different delay times (a), and those from S-QDs (red) and L-QDs (black), at 0 ns-delay time (b) showing the two emission bands originating from the InP cores (at 620 nm and 690 nm) and the ZnS shell (at 470 nm).*

In conclusion for this kind of InP QDs, our method can be adjusted to obtain relatively large InP and InP/ZnS core/shell QDs with an excitonic absorption peak in the 570–700 nm range. The emission peak related to the InP core varied as a function of the QD size in the 590–720 nm range, while the ZnS shell showed emission in the blue region around 470 nm, arising from defect states. The results from TRPL measurements demonstrated that the ZnS shell emitted on a comparable timescale to that from the InP core, in the ten nanosecond range. The ZnS overcoating played a decisive role in the passivation of imperfections at the surface of InP QDs, consequently increasing the photoluminescence intensity related to the excitonic transition in the InP core. In addition, our study reveals that, beside the optical transitions in the InP core, the optical processes within the ZnS shell strongly influence the dynamics of carriers' population and evolution after photo-generation.

4.3.2. InP/ZnS NCs synthesized by the heating-up one-pot method using P(TMS)$_3$

In this section, we present the synthesis of high quality InP/ZnS NCs using the heating-up method with the presence of $ZnSt_2$ in the reaction solution. $ZnSt_2$ strongly contributed to the control of the nucleation and growth of InP NCs as a surfactant and to alloying with indium in the growth process. As we will demonstrate later, an alloy structure is obtained. Therefore, in the following, the studied systems are denoted In(Zn)P/ZnS instead of InP/ZnS NCs. By changing the Zn^{2+}:In^{3+} molar ratio and the reaction-growth temperature, the emission color could easily be tuned throughout a large spectral range (485-590 nm) with high LQY (~70%).

Several "optimal" experimental parameters have been reported by other groups [9,19], such as the In:MA and In:P molar ratios, which were fixed at 1:3 and 2:1, respectively. Our study thus concentrated on the influence of three parameters on the quality of the obtained In(Zn)P and In(Zn)P/ZnS NCs, namely the Zn^{2+}:In^{3+} ratio in the precursor solution, the reaction-growth/shelling temperature and time. The term "shelling temperature" means the temperature at which the ZnS shell growth was carried out.

Typically, the synthesis of In(Zn)P/ZnS NCs was performed with a Zn^{2+}:In^{3+} molar ratio of 1:1, a reaction-growth temperature for forming the core NCs of 300°C and a shelling temperature of 285°C. Figure 4.4 shows the temporal evolution of the absorption and PL spectra of In(Zn)P core and In(Zn)P/ZnS core/shell NCs as a function of the reaction-growth and shelling time. The spectra shown were taken from as-prepared samples (i.e. directly from the reaction flask) without any size selection. They were diluted with toluene to provide the optical densities appropriate for PL measurements. The In(Zn)P core NCs taken after 1 min (not shown in Figure 4.4) exhibit a relatively weak PL and a relatively large FWHM that might be explained by the existence of nonradiative channels originating from surface states. However, after 2 min of growth, a sharp excitonic absorption peak was clearly observed at 430 nm, accompanied by the narrowing of the PL peak at 493 nm (FWHM ~50 nm). These features indicate a high crystalline quality of the synthesized In(Zn)P NCs. This means the "size-focusing" growth regime has been reached [61–62]. All samples show a pronounced excitonic peak of the $1S_e$–$1S_h$

transition indicating a rather narrow size distribution of the In(Zn)P core and In(Zn)P/ZnS core/shell NCs [63]. The absorption and PL peaks of the In(Zn)P core NCs were gradually shifted to longer wavelengths with prolonging reaction time (Figure 4.4) corresponding to an increase of the mean particle size as a consequence of quantum confinement. The LQY of In(Zn)P core NCs was dramatically increased after growing the ZnS shell for 1 hr (in our experiment, the thickness of the ZnS shell was estimated from the shelling time), reaching up to 70%. We observed a red-shift of the emission peak of *ca.* 18 nm (Figure 4.4a), evidencing successful shell growth [33–34,46]. The main reason for this red-shift is the lower confinement of the charge-carrier wavefunctions of the core QDs upon shelling that leads to a lower confinement energy in the final emission. In other words, the exciton “leaks” from the core QDs into the shell, reducing the total energy of emission. In addition, with the ZnS shell, the LQY of In(Zn)P/ZnS QDs was enhanced significantly [64–66]. One more important result that we have obtained is that even though the shelling time varied from 5 to 60 minutes, the absorption and emission peaks were almost not shifted (Figure 4.4b). This means that there were correspondingly no change in size and size distribution of the shelled QDs. Note that in general with long growth time an Ostwald ripening could happen causing a change in size and broadening in size distribution of NCs. The un-changed-size characteristic of NCs with growth time is favorable for doping RE into In(Zn)P/ZnS QDs because the duration time needed to dope was usually as long as 100 minutes. This also facilitates the study of the energy transfer from the host lattice to RE^{3+} ions.

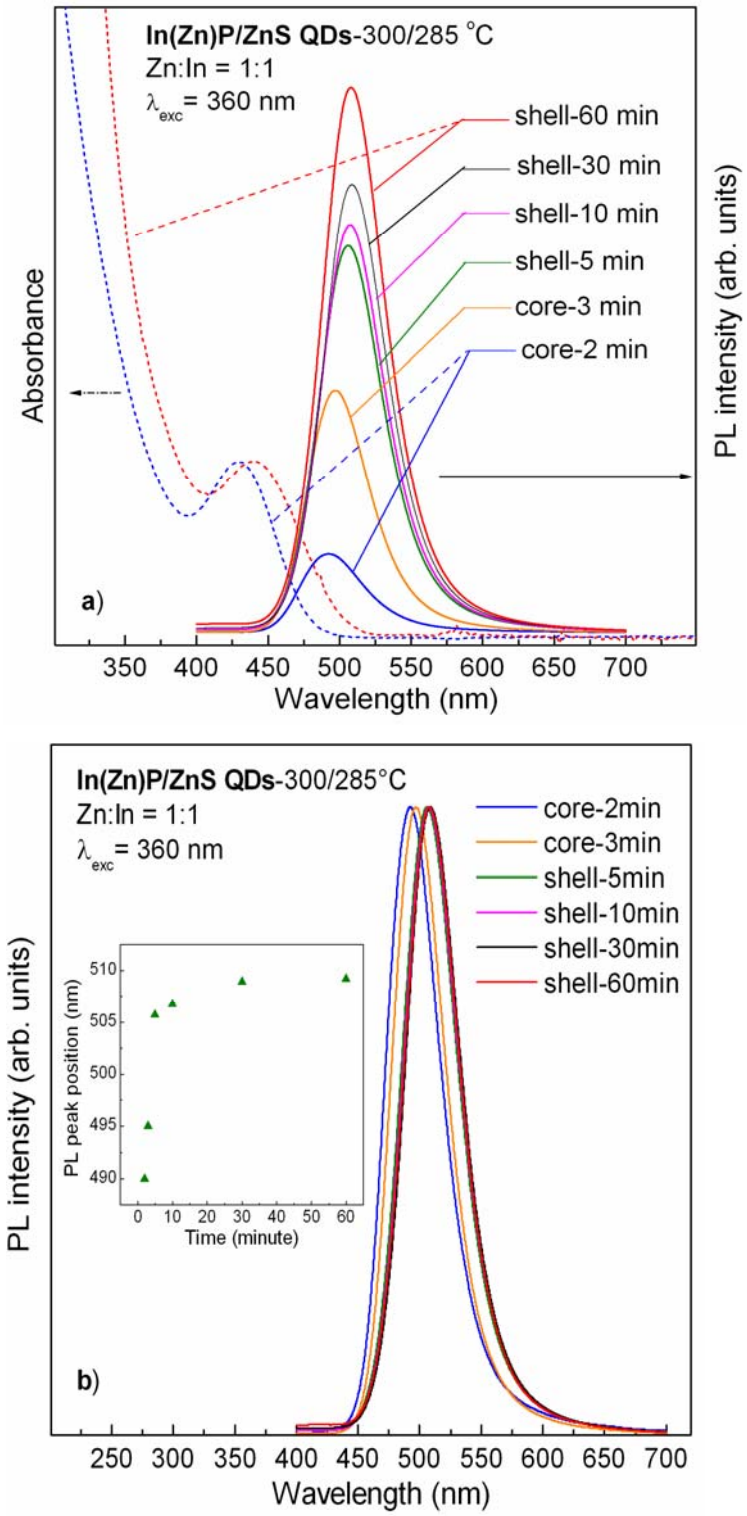

Figure 4.4: *Temporal evolution of absorption and PL spectra of In(Zn)P/ZnS core/shell QDs synthesized at the Zn^{2+}:In^{3+} molar ratio of 1:1, the reaction temperature for forming the core and the shelling temperature were fixed at and 300°C and 285°C respectively with the different reaction-growth/shelling time indicated on the figure. The inset shows the extracted PL peaks as a function of shelling times.*

While the size and size distribution do not change with shelling time, their evolution strongly depends on the reaction-growth/shelling temperature and the used precursor ratios. We now present the optical properties of InP/ZnS QDs obtained at different reaction-growth/shelling temperatures, while all other synthesis parameters were kept the same. Generally, the temperature significantly affects the nucleation and the growth rate of NCs. Higher temperature usually produces bigger particles and better quality crystals. The experimental results obtained with two different reaction-growth/shelling temperatures are shown in Figure 4.5.

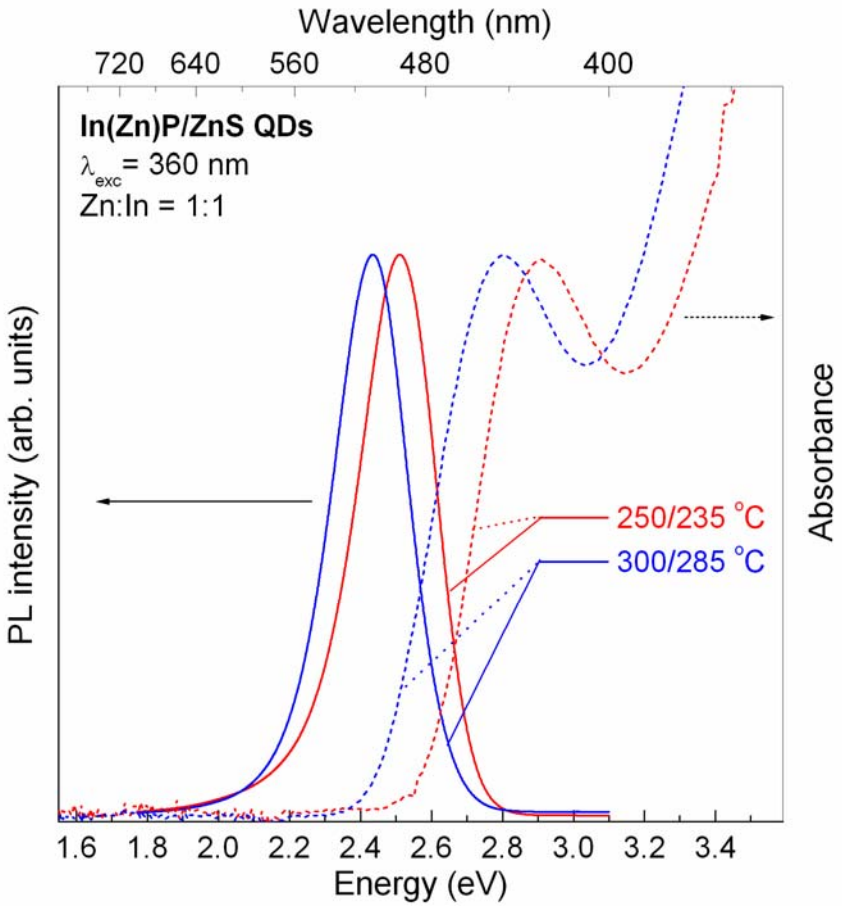

Figure 4.5: *Absorption and PL spectra of In(Zn)P/ZnS core/shell QDs synthesized at two different reaction-growth/shelling temperatures of 250°C/235°C (red) and 300°C/285°C (blue) with the Zn^{2+}:In^{3+} molar ratio of 1:1 and the shelling time of 1 hr.*

With increasing the reaction-growth temperature from 250°C to 300°C, we observed a red-shift in the PL peak of 15 nm. This observation indicates that the mean size increase from 1.6 to 1.8 nm. We notice an important feature from the In(Zn)P/ZnS QDs, i.e. QDs synthesized in the presence of $ZnSt_2$, that even for rather high temperature and long shelling time the PL spectra showed a FHWM of 50 nm for all samples. This means the size distribution did not change with reaction-growth/shelling temperature for the Zn-containing InP/ZnS QDs or In(Zn)P/ZnS QDs. For the InP/ZnS QDs synthesized without $ZnSt_2$, higher temperature not only yielded bigger particles but also promoted Ostwald ripening happened quickly giving rise to FWHM broadening: the PL spectra taken from InP/ZnS QDs, which were synthesized with reaction-growth/shelling temperatures of 300°C/285°C and 250°C/235°C, respectively possess a FWHM around 100 nm and 84 nm (see Figure 4.10 b) and d); Zn:In = 0:1). For the higher reaction-growth/shelling temperature (300°C/285°C) the InP/ZnS QDs showed a PL spectrum with a clear additional band at 470 nm beside the main one peaking at 586 nm which originates from InP QDs. The 470-nm band is known to originate from defects in the ZnS shell [59]. This result indicates that the higher temperature led to a thicker ZnS shell on the InP core QDs. We did not observe any PL band specific to the ZnS shell from the samples synthesized at low reaction-growth/shelling temperature.

To analyze their crystal structure, we studied the obtained QDs by XRD. Figure 4.6 shows a typical powder XRD pattern of In(Zn)P/ZnS NCs synthesized with the Zn^{2+}:In^{3+} molar ratio of 1:1 at a reaction-growth temperature of 300°C and a shelling temperature of 285°C for 1 hr. The diffraction patterns of bulk zinc-blende InP and ZnS are given for comparison. The clear diffraction peaks show that the In(Zn)P/ZnS QDs are well crystallized in the zinc-blende structure.

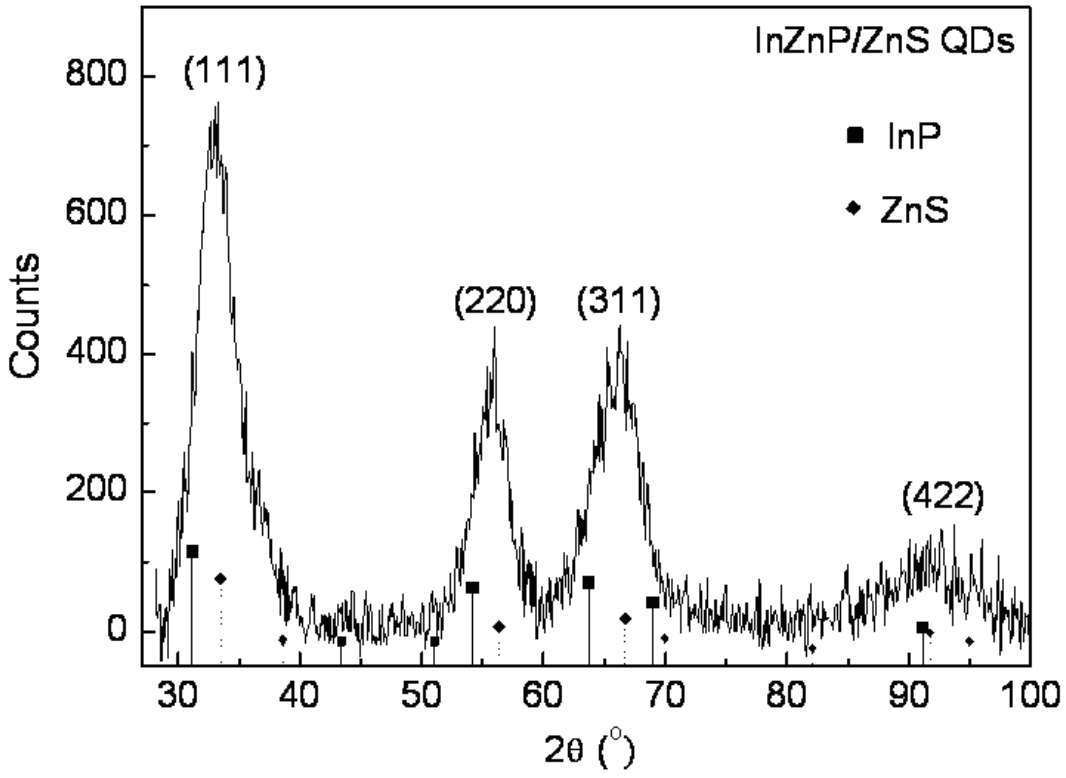

Figure 4.6: *XDR pattern of In(Zn)P/ZnS NCs synthesized with the Zn^{2+}:In^{3+} molar ratio of 1:1, the reaction-growth temperature for forming the core and the shelling temperature were fixed at 300°C and 285°C respectively, and the shelling time was 1 hr. The diffraction patterns corresponding to pure bulk InP and ZnS are also indicated for comparison.*

In order to study in more detail the influence of Zn on the structure and optical properties of the resulting QDs, we prepared a series of samples with various Zn^{2+}:In^{3+} molar ratios. With increasing Zn concentration in the reaction medium (Zn^{2+}:In^{3+} molar ratio ranging from 0:1 to 2:1), we did not observe clearly the XRD peaks shift toward larger angles. Such a shift would be expected from the smaller lattice constants caused by replacing Zn on In sites of the crystal. This is understandable because (i) the lattice constants of cubic ZnS are similar to those of InP and the peak position lie indeed in between those of InP and ZnS; (ii) the peaks are too broad due to the small crystal size. The mean size of alloying In(Zn)P/ZnS QDs calculated using the Scherrer equation for only the (111) peak is of 2.3 nm, which is close to the mean value obtained directly from the TEM image (Figure 4.7).

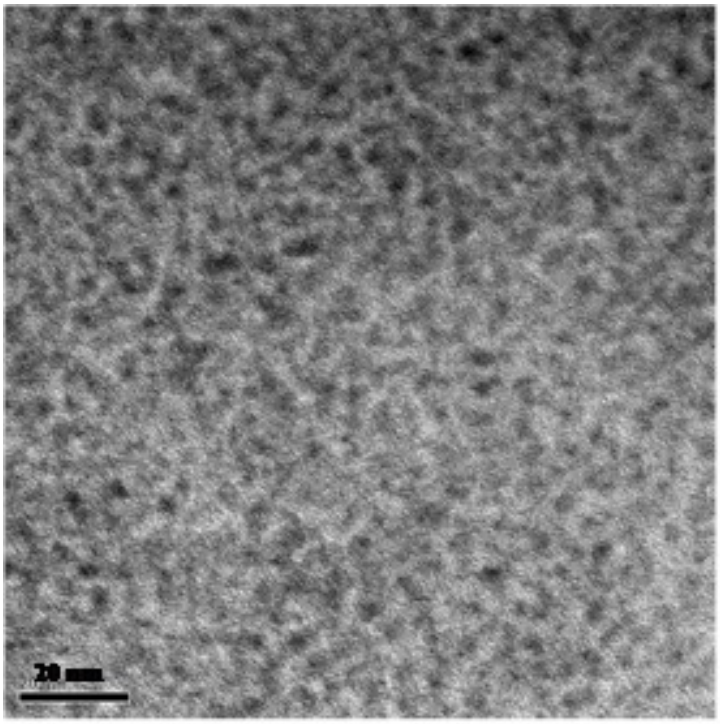

Figure 4.7: *TEM image of In(Zn)P/ZnS NCs with the Zn^{2+}:In^{3+} ratio of 1:1, the reaction-growth temperature for forming the core and the shelling temperature were fixed at 300°C and 285°C respectively, and the shelling time was 1 hr.*

Figure 4.7 shows the TEM image of the In(Zn)P/ZnS NCs in which the particles are nearly spherical in shape having a mean size of ~2.0 nm. This image is consistent with the NCs size calculated from the absorption spectra. However, the small size of NCs and the low contrast of the TEM image make further analyses difficult.

We have also performed EDX analysis of a series of samples with different Zn^{2+}:In^{3+} ratios to investigate the relationship between the composition of the reaction medium and the formation of the alloy structure in In(Zn)P/ZnS NCs. The results are shown in Figure 4.8 and Table 4.1. It should be noted that in order to remove any un-reacted compounds the samples must be very carefully purified prior to the EDX analysis experiments. The EDX data indicate that with increasing $ZnSt_2$ concentration the atom percentage (at. %) of the elements In and P decreased gradually, while the In to P ratio and the at. % of S remained almost constant of 2.0 and 32%, respectively for all InP/ZnS NCs. The number of cations (In^{3+}, Zn^{2+}) is

larger than that of anions (P^{3-}, S^{2-}) in the studied alloy NCs samples. These results suggested two underlying mechanisms involved in the synthesis of In(Zn)P/ZnS NCs: (i) the Zn^{2+} ions could passivate the surface of InP NCs by the weak Zn-P binding to reduce surface defects giving rise to an increase of the LQY. Moreover, zinc adsorbed on the surface of InP NCs favors the growth of a ZnS shell resulting in an increase of the LQY as well; (ii) the Zn^{2+} ions could replace In^{3+} ions to form an alloy structure of In(Zn)P that causes the band-edge fluctuation to enhance the confinement of the excited carriers leading to an increase of the radiative transition probability. The observed blue-shift of the excitonic absorption and PL peaks (Figure 4.10 below) with increasing molar concentration of Zn also confirms the *in situ* formation of the alloy structure. Therefore, we suppose that $ZnSt_2$ plays two different roles: a stabilizer and as a reactant which promotes the formation of the In(Zn)P core/ ZnS shell alloy-type NCs.

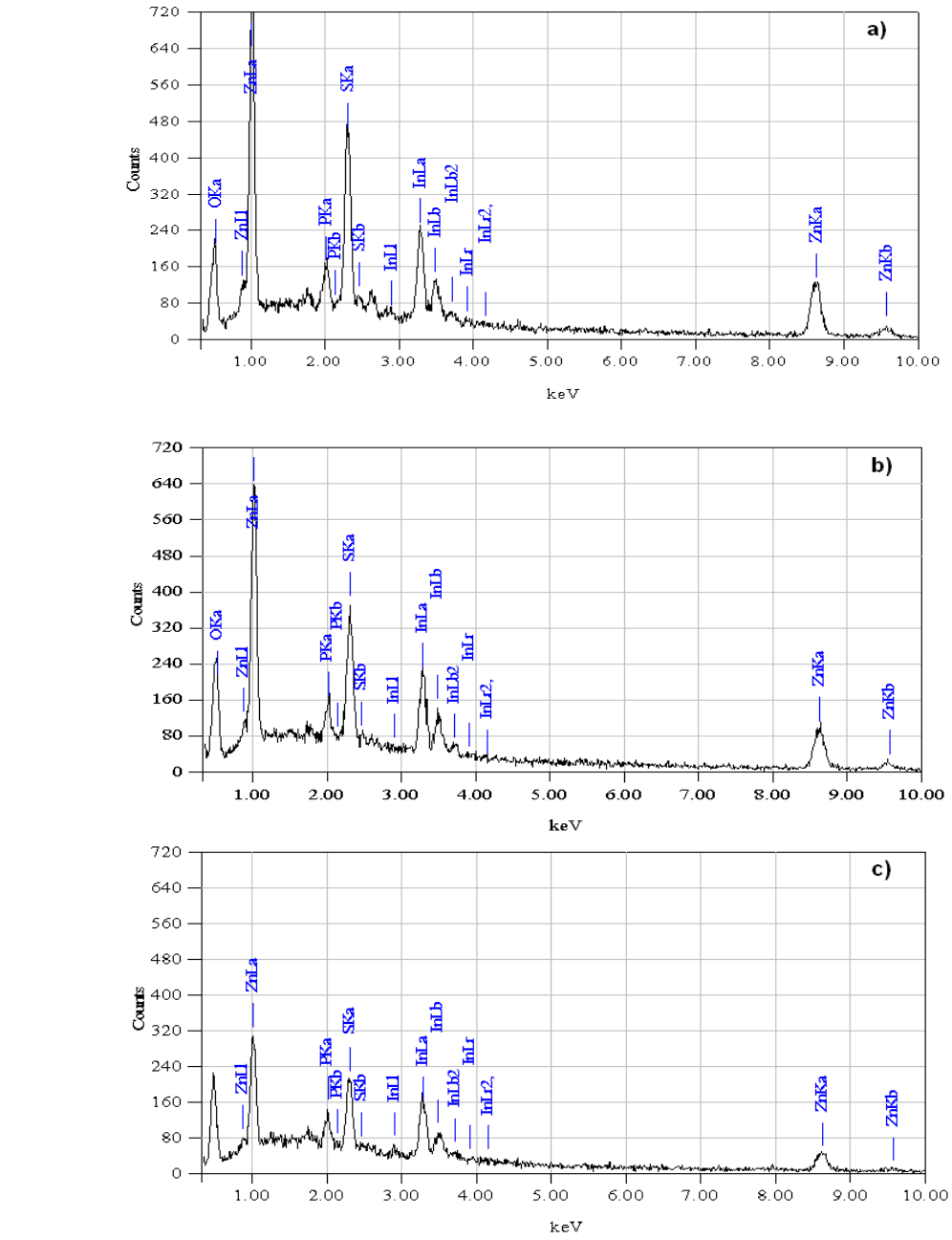

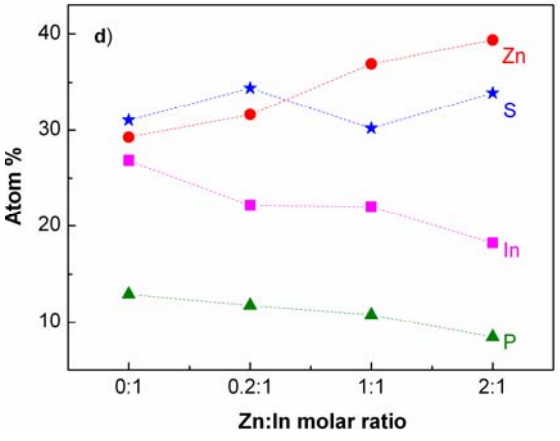

Figure 4.8: *EDX spectra of the In(Zn)P/ZnS NCs synthesized for 1 hr with the Zn^{2+}:In^{3+} ratio of (a) 2:1, (b) 1:1, and (c) 0:1. (d) Atomic percentage of the elements In, Zn, P and S as a function of the Zn^{2+}:In^{3+} ratio (dashed lines are added to guide the eye).*

Table 4.1: *Atomic percentage (at. %) of the elements determined from EDX analysis (mean values of 5 independent measurements per sample) for aliquots taken at different initial Zn^{2+}:In^{3+} ratios.*

Zn^{2+}:In^{3+} molar ratio	In (at. %)	Zn (at. %)	P (at. %)	S (at. %)
0:1	26.83	29.23	12.91	31.04
1:5	22.15	31.62	11.77	34.41
1:1	22.00	36.95	10.77	30.18
2:1	18.20	39.34	8.44	33.90

It is interesting to note that initially synthesized InP core NCs exhibit very weak fluorescence; by adding an appropriate amount of $ZnSt_2$ in the reaction solution, however, we could obtain In(Zn)P QDs which showed sharp excitonic absorption and rather bright emission (Figure 4.9). One can see a blue-shift of the excitonic peaks of 80 nm with increasing the Zn^{2+}:In^{3+} molar ratio (from 0:1 to 2:1). In the reaction solution at high temperature, $ZnSt_2$ probably acts as a surfactant which controls the deposition rate of the monomers onto the surface of the NCs. At the same time, it is possible to form the alloy In(Zn)P by replacing some Zn atoms into the In sites. Our experimental results on the structural and optical characteristics taken from series of the samples with different Zn^{2+}:In^{3+} ratios strongly support the hypothesis of an alloy structure of the synthesized In(Zn)P QDs.

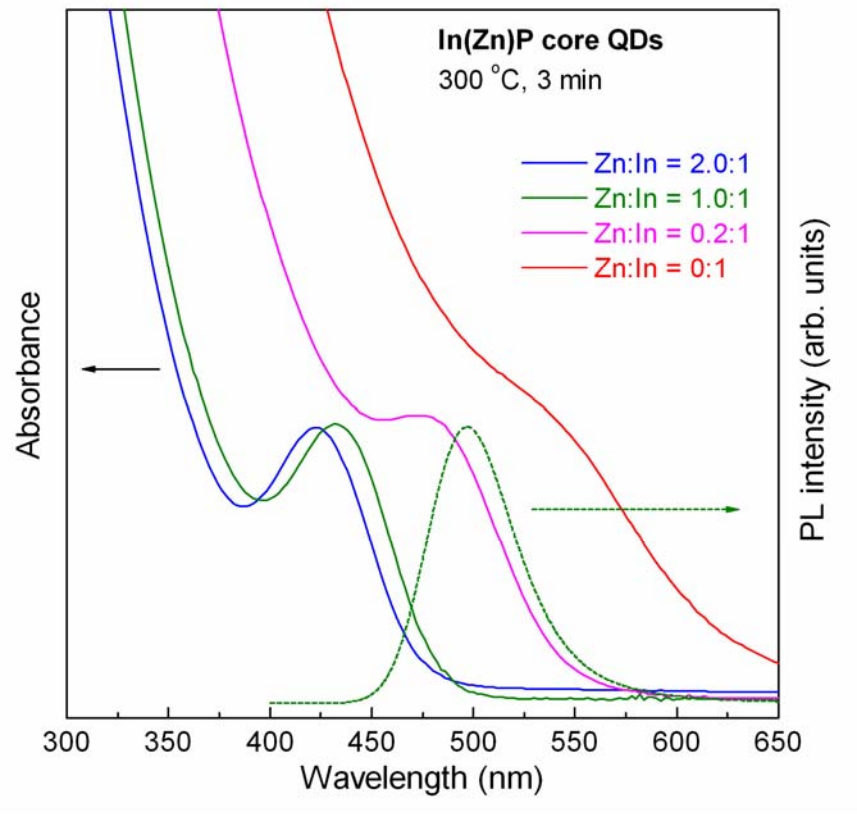

Figure 4.9: *Absorption spectra of In(Zn)P core only QDs synthesized at 300°C for 3 min as a function of the Zn^{2+}:In^{3+} molar ratio. A typical PL of In(Zn)P core QDs with the Zn^{2+}:In^{3+} molar ratio of 1:1 is also presented (dashed line).*

Figure 4.10 shows the absorption and PL spectra of In(Zn)P/ZnS QDs as a function of the Zn^{2+}:In^{3+} molar ratios and the reaction-growth/shelling temperatures. We noted that the emission spectral range could be tuned by varying the Zn^{2+}:In^{3+} molar ratio and/or the reaction-growth/shelling temperatures. More precisely, we have found that at higher temperature and higher $ZnSt_2$ concentration, the resulting In(Zn)P/ZnS NCs exhibited higher LQY. This is reasonably explained by the existence of more free and mobile Zn^{2+} ions from $ZnSt_2$ at the higher reaction-growth/shelling temperatures to contribute to the growth/alloying and passivation processes. During the shelling Ostwald ripening might occur, however, as presented in the previous paragraph, we did not observe a significant red shift of the spectral peaks with long shelling time, meaning that the In(Zn)P core size was unchanged. We will discuss in more detail the role of zinc in the improvement of the optical properties of In(Zn)P/ZnS QDs in Section 4.3.3.

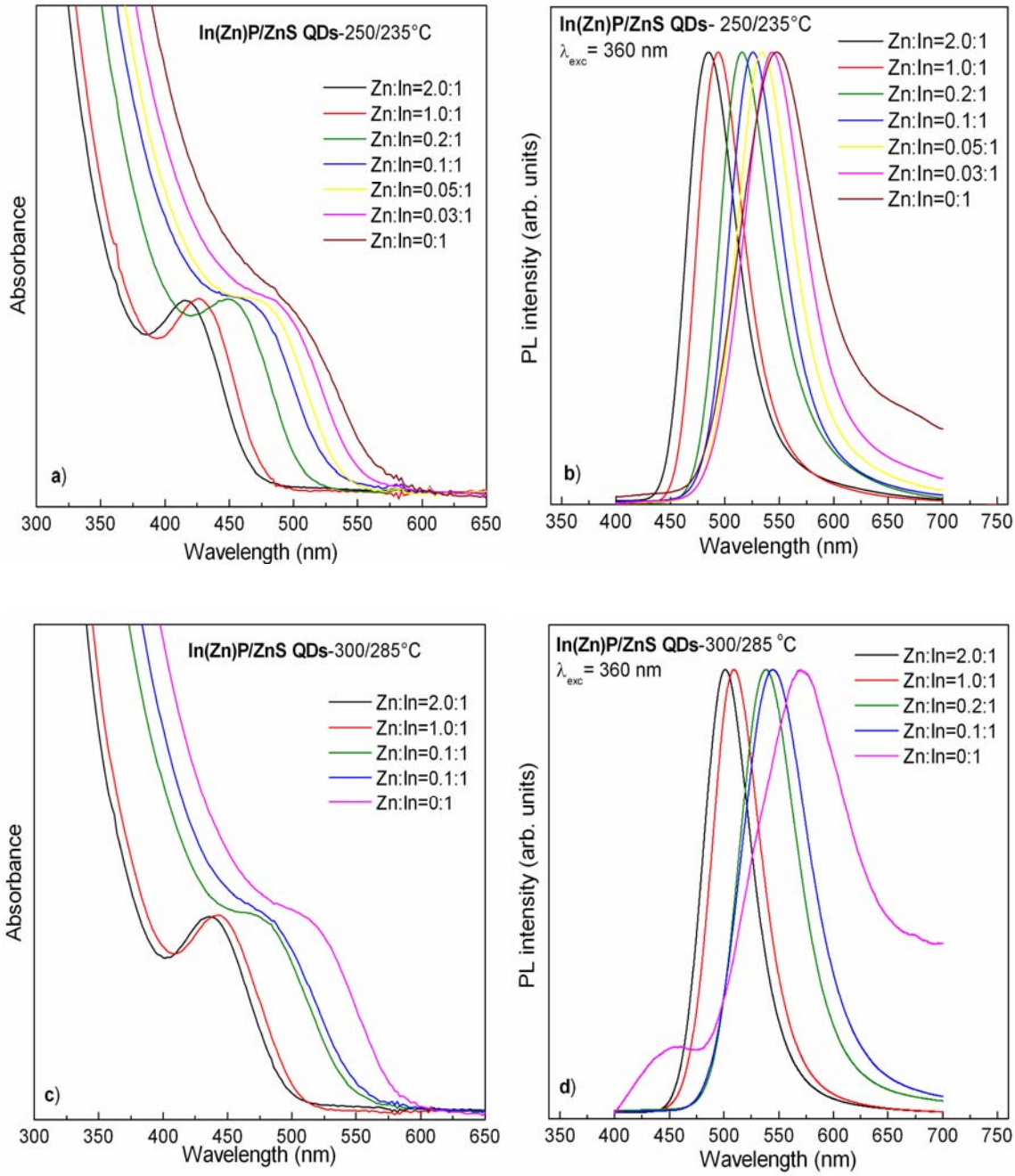

Figure 4.10: *Absorption (a, c) and PL (b, d) spectra of In(Zn)P/ZnS QDs as a function of the Zn^{2+}:In^{3+} molar ratio and the reaction-growth/shelling temperatures (indicated on the figures).*

By changing the Zn^{2+}:In^{3+} molar ratio (from 0:1 to 2:1), the emission color of In(Zn)P/ZnS core/shell NCs can be easily tuned in the wide spectral range of 485 – 590 nm as shown in Figure 4.10 and Table 4.2, corresponding to a mean size of the InP(Zn)P core of ~1.5–2.5 nm.

Table 4.2: *Optical properties of In(Zn)P/ZnS QDs synthesized at two different temperatures with various Zn:In molar ratios in the precursor solution.*

Zn^{2+}:In^{3+} molar ratio	λ_{max} [L] (nm)	FWHM [L] (nm)	LQY [L] (%)	λ_{max} [H] (nm)	FWHM [H] (nm)	LQY [H] (%)
0:1	549	84	7	586	100	-
0.03:1	543	67	-	576	100	-
0.05:1	534	61	15	-	-	-
0.10:1	526	58	20	550	73	30
0.20:1	515	58	31	538	63	37
1.00:1	494	50	45	510	50	70
2.00:1	485	50	19	500	50	59

[L] Low temperature (250°C for core and 235°C for shell)

[H] High temperature (300°C for core and 285°C for shell)

4.3.3. Role of zinc in the improvement of the luminescence properties of InP QDs

In this Section, we discuss in more detail the contribution of zinc to the improvement of the optical properties of In(Zn)P/ZnS QDs synthesized by the heating-up one-pot method as described in detail in Appendix 1.3.2. The experimental conditions were studied and presented in Section 4.3.2. Briefly, by determining the optimal synthesis conditions (i.e. the reaction-growth/shelling temperature and time, the Zn^{2+}:In^{3+} molar ratio), the LQY of the In(Zn)P/ZnS QDs was optimized to 60–70% in the best cases.

To study further the influence of zinc on the optical properties of the In(Zn)P/ZnS QDs, we performed TRPL measurement on a series of samples synthesized at optimized experimental conditions with different $ZnSt_2$ concentrations. In the TRPL measurements, the 337.1 nm pulsed light from a

nitrogen gas laser was used as the excitation source, whose excitation power density could be varied in the range from 100 W/cm^2 to 100 kW/cm^2, with pulse duration of 1 ns. The PL signals were dispersed by means of a 0.6-m grating monochromator (Jobin-Yvon HRD1) and detected using a fast photomultiplier (Hamamatsu model H733, with a rise time of 700 ps) for the TRPL measurements. Averaging the multi-pulses at each spectral point using a 1.5 GHz digital oscilloscope (LeCroy 9362) strongly improved the signal-to-noise ratio.

Figure 4.11 shows the absorption and SSPL spectra of the two In(Zn)P/ZnS QDs samples synthesized under the same conditions except the change of the Zn^{2+}:In^{3+} molar ratio being 0:1 (Figure 4.11a and b) and 1:1 (Figure 4.11c and d), respectively. The In(Zn)P core was synthesized at 300°C and then shelling with ZnS was carried out at 285°C for 1 hr. For the "pure" InP/ZnS (i.e. Zn^{2+}:In^{3+} = 0:1) QDs, the excitonic absorption appears as a shoulder and the PL spectrum is composed of two components: the one peaking at 586 nm is assigned to originate from InP QDs while that peaking near 470 nm is attributed to defect emission from the ZnS shell [59]. The FWHM of the InP PL peak is around 100 nm and the Stokes shift accounts for 280 meV. For the samples with the presence of $ZnSt_2$ in the reaction solution, a more pronounced excitonic absorption peak and strong, rather narrow (FWHM~50 nm) luminescence were observed at 443 nm and 510 nm, respectively, i.e. at much shorter wavelengths in comparison QDs without $ZnSt_2$ in the reaction solution. Note that in this case, the Stokes shift is clearly larger, namely of 370 meV, than in case without using Zn for the core NC synthesis. For various Zn contents in In(Zn)P/ZnS QDs, we observed a systematic red shift of the SSPL peak with decreasing the Zn^{2+}:In^{3+} molar ratio and with increasing reaction-growth temperature as shown in the inset of Figure 4.11.

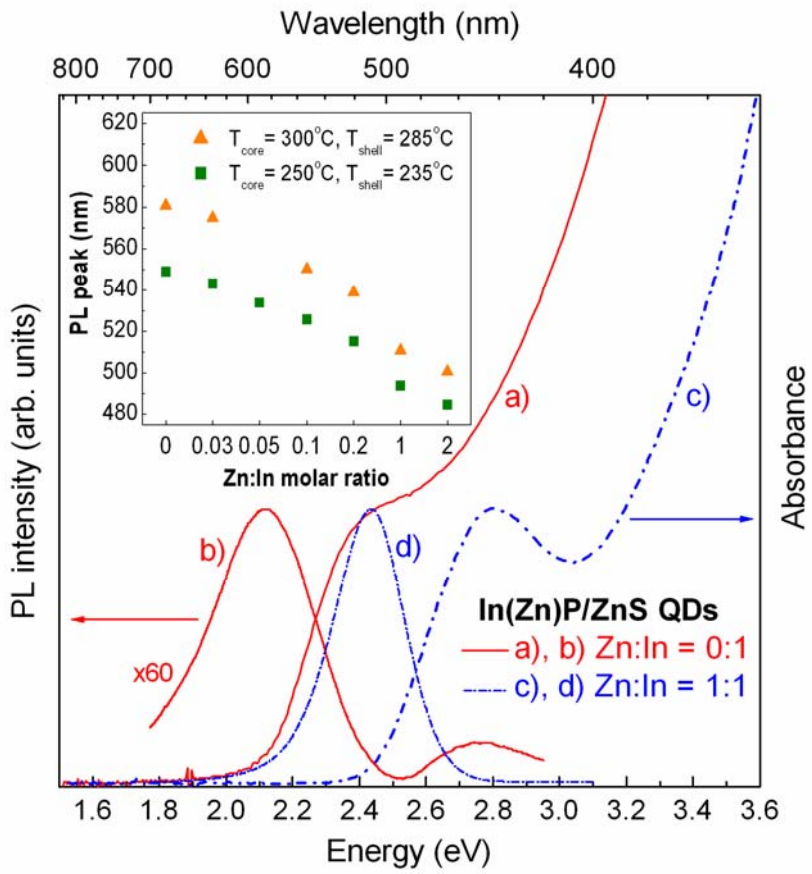

Figure 4.11: *Absorption and SSPL spectra of InP/ZnS core/shell QDs (i.e. the Zn^{2+}:In^{3+} ratio equals to 0:1) and alloy In(Zn)P/ZnS QDs (Zn^{2+}:In^{3+} ratio 1:1). The inset shows the PL peak position as a function of the Zn^{2+}:In^{3+} ratio at two different reaction-growth/shelling temperatures.*

These optical characteristics obtained from the systematical absorption and SSPL measurements indicate that alloy In(Zn)P core NCs were formed rather than InP core NCs. The larger Stokes shift is an evidence for the band fluctuation due to alloying the lattice structure by replacing Zn into In sites, as similarly observed in ZnSSe thin films and other alloy QDs [67–68]. Furthermore, if no alloying occurred despite the presence of Zn in the starting reaction solution, the emission peak should be located at a similar wavelength as in the case of crystals without Zn and show a slight red-shift with an increasing Zn concentration during the shell growth. The existence of Zn in the reaction solution provides a smooth change at the interface between the In(Zn)P core and the ZnS shell. This could contribute to a significant enhancement of the LQY up to ~70% of the alloy In(Zn)P/ZnS QDs due to suppression of surface states including P dangling bonds.

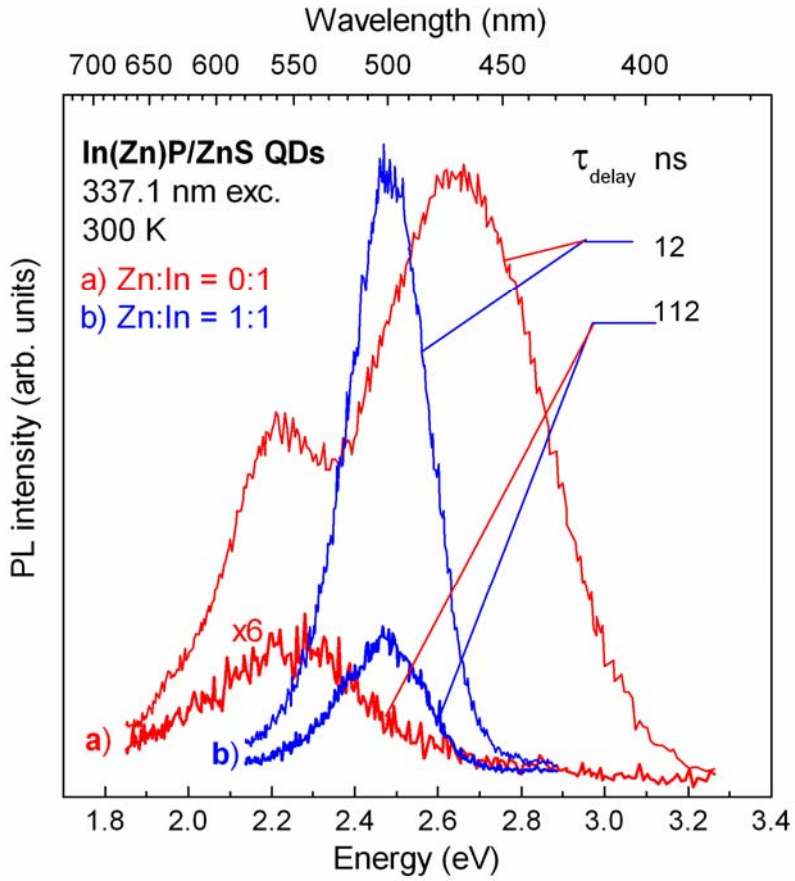

Figure 4.12: *TRPL spectra taken from two different structured samples. (a) InP/ZnS core/shell QDs, and (b) alloy In(Zn)P/ZnS QDs with the Zn^{2+}:In^{3+} ratio of 1:1 that synthesized in the same conditions.*

From TRPL measurements, it is possible to trace the PL intensity at a certain delay from the excitation moment with the goal to determine exactly the instant PL intensity of each spectral component in a complex emission. Figure 4.12 illustrates the TRPL spectra of the InP/ZnS "real" core/shell QDs (Figure 4.12a) and the alloy In(Zn)P/ZnS structure (Figure 4.12b) prepared with changing the Zn^{2+}:In^{3+} molar ratio in the precursors' solution of 0:1 and 1:1 while keeping all other experimental conditions the same. At a delay time of 12 ns, the InP/ZnS core/shell structure exhibited InP excitonic emission at 586 nm along with the one at around 470 originated from imperfections in the ZnS shell (Figure 4.12a) [59]. It has to be noted that this defect emission peak shows a higher intensity than the peak arising from InP, in contrast to the SSPL measurements (Figure 4.11). The alloy In(Zn)P/ZnS QDs only exhibits a single PL band at 510 nm. Also the evolution with the delay time from the excitation moment of these two kinds of QDs is not the same due to

differences in the decay-time corresponding to each spectral component. For the InP/ZnS core/shell QDs, PL evolution of both the 470 nm and the 586 nm bands with delay time depends on the recombination/transition rates in the ZnS shell and in the InP core, respectively. In addition, it is related to the transfer rate of charge carriers from the ZnS shell to the InP core [69].

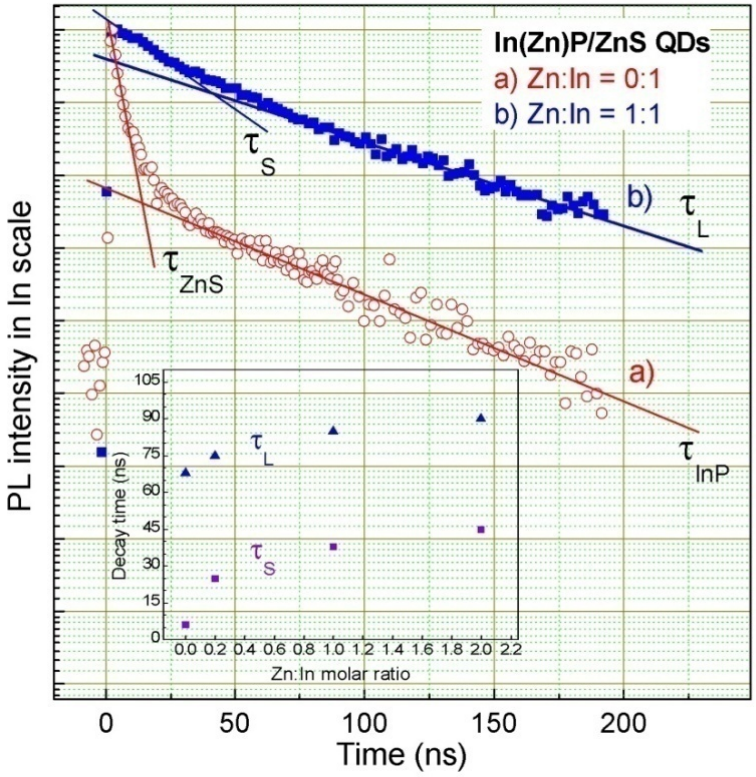

Figure 4.13: *PL decay curves for (a) InP/ZnS core/shell QDs and (b) alloy In(Zn)P/ZnS QDs measured at the emission peaks of InP and In(Zn)P QDs. The deconvolution of each PL decay curve shows two components, τ_S and τ_L, both of which are longer with higher Zn concentration as presented in the inset.*

In fact, the decay time (see Figure 4.13a) of the blue emission in ZnS is much shorter (of 6 ns) than that of InP NCs (of 68 ns). Therefore, at long delay-time we observed mainly the InP core luminescence. For the alloy In(Zn)P/ZnS QDs, the PL decays (Figure 4.13b, for the Zn:In = 1:1 case) with two decay-time constants, in which the shorter one (of 38 ns) is related to recombination at surface states and the longer one (of 85 ns) is responsible for the excitonic transition [54]. By fitting the emission of the In(Zn)P/ZnS NCs to bi-exponential functions, we can extract the decay-times as a function of the Zn:In ratio, as presented in the inset of Figure 4.13.

It is clearly seen that with increasing Zn concentration the decay-times corresponding to both emission mechanisms increase. This is again in good agreement with the enhanced confinement of the excited charge carriers due to lattice fluctuations caused by the replacement of In by Zn. In other words, the excited charge carriers are confined longer and longer by lattice fluctuations with increasing zinc concentration in alloy In(Zn)P/ZnS QDs, corresponding to the longer decay times.

In conclusion, alloy In(Zn)P/ZnS core/shell QDs synthesized in the presence of zinc during InP core NC synthesis, were studied by using XRD, absorption and SSPL/TRPL spectroscopy. The emission range of the alloy In(Zn)P/ZnS QDs could be tuned from 485 to 590 nm (FWHM 50 nm) by varying the Zn^{2+}:In^{3+} molar ratio in the reaction medium and reaction-growth/shelling temperature. Zinc stearate has a double role in the nucleation and growth process of InP QDs: i) as a surfactant influencing reaction kinetics; ii) as a zinc precursor resulting in an In(Zn)P alloy structure. The high LQY up to 60-70% is rationalized by the alloy structure of the Zn-containing InP/ZnS QDs that causes band-edge fluctuation to enhance the confinement of the excited carriers and consequently enhances the radivative transition probability.

4.3.4. Influence of surrounding environment on the optical characteristics of In(Zn)P/ZnS QDs

On the nanometer scale, the quantum confined Stark effect with the contributions of the electric field, induced by the polarization of the QDs and ligand molecules, and the polarity of the solvent causes spectral shifts [34,70–71]. Another important factor governing the dielectric environment of the QDs is the interparticle distance. In fact, in NCs of a few nanometers size, the number of the surface atoms is large as compared to the volume atoms. As a consequence of the termination and stoichiometry at the QD surface, an electric dipole moment or charge of the QD result [72–74]. Several papers reported on the permanent dipole moment of non-metallic NPs (ZnSe, CdSe) that always exists even if they crystallized in the highly symmetric zinc-blende structure [73,75]. We also reported on Stark effect induced shifts of the PL and absorption spectra as a function of the solvent's polarity. These effects occurred on CdSe QDs without inorganic shell and, to a lower extent, on those with single (CdSe/ZnSe) and double-shells (CdSe/CdS/ZnS) [34].

In this Section, we compare the optical characteristics of InP/ZnS QDs in a close-packed layer, i.e. having an interparticle distance determined by the thickness of the organic surface ligands layer, with those of QDs in colloidal solution where each QD is well-separated from the others. This study will not only give information about the influence of the solvent's polarity on the optical properties but also about the energy transfer between excited QDs. We performed UV-vis absorption, SSPL and TRPL measurements on the best sample (LQY of 70 % as presented in Section 4.3.2, Zn^{2+}:In^{3+} = 1:1, 300°C/285°C reaction-growth/shelling temperature) in the close-packed solid state and in colloidal solution. The close-packed sample (thickness ~10 µm) was prepared by evaporating a drop of the obtained In(Zn)P/ZnS QDs on a copper substrate, appropriate for temperature-dependent measurements.

The optical characteristics of close-packed and colloidal InP/ZnS alloy QDs were systematically investigated by means of SSPL and TRPL spectroscopies. In the TRPL measurements, the PL intensity corresponding to each spectral component detected at a certain moment delayed from the start of the excitation laser pulse provides a real intensity in the dynamic regime. The observed spectral shift with temperature and delay time in the case of close-packed InP/ZnS QDs gives evidence for the energy transfer by dipole-dipole interaction and/or the excited charge carrier transfer between QDs in this system.

Using the SSPL technique, the overall PL spectra generally show various spectral components originating from different recombinations/transitions. The PL intensity of each spectral component depends on the corresponding recombination/transition rate and its density of states.

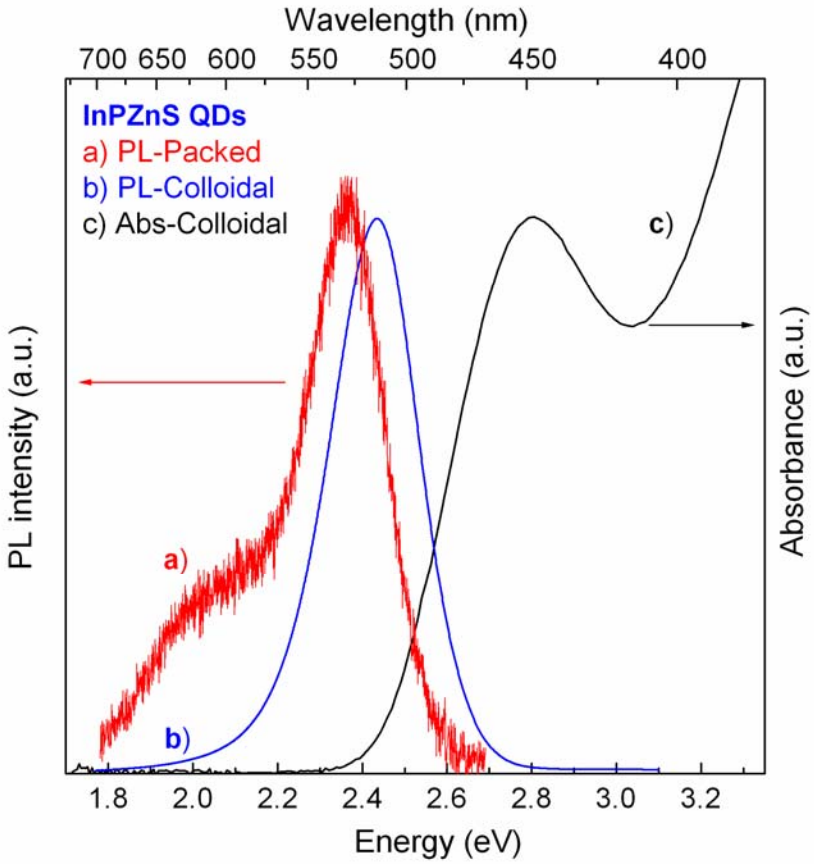

Figure 4.14: *PL spectra of InP/ZnS QDs in (a) the close-packed film and (b) in colloidal solution under 337.1–nm excitation. (c) Absorption spectrum of the colloidal QDs in chloroform.*

Figure 4.14 shows the absorption and SSPL spectra of the close-packed and colloidal InP/ZnS QDs. For the colloidal sample, the absorption and SSPL peaks are located at 443 and 510 nm, respectively. The observed Stokes shift of 370 meV and FWHM of 50 nm indicate a low density of defect states and narrow size distribution of the InP/ZnS QDs. It should be noted that the reported FWHM of the PL spectra of InP-based NCs usually lies in the range of 50–100 nm [76–80]. For close-packed InP/ZnS QDs, the SSPL peak is centered at 525 nm, about 15 nm red-shifted as compared to the colloidal sample. One explanation for this spectral shift could be the change of the effective electric field experienced by the QDs, i.e. the quantum confined Stark effect. In the colloidal phase, the polarity of the solvent partly compensates the polarization of the InP/ZnS QDs to make them emit at shorter wavelength. On the opposite, in solvent-free close-packed InP/ZnS QDs the polarization of the QDs is stronger corresponding to a higher electric field [34]. For these particles, in addition to the narrow peak at 525 nm a shoulder at lower energy

around 620 nm is visible. Generally such broad emission bands located at lower energy than the excitonic peak are related to lattice imperfections in the crystalline structure, as also observed in CdTe QDs [81]. As already mentioned before and recently confirmed by XPS measurements with variable energy synchrotron radiation [82], the In(Zn)P/ZnS QDs used in the present study possess an alloyed internal structure. The absence of a strained core/shell interface between the two crystallographically different materials InP and ZnS is at the origin the observed high LQY of this system. Accordingly, no 470 nm emission band corresponding to the ZnS shell was observed.

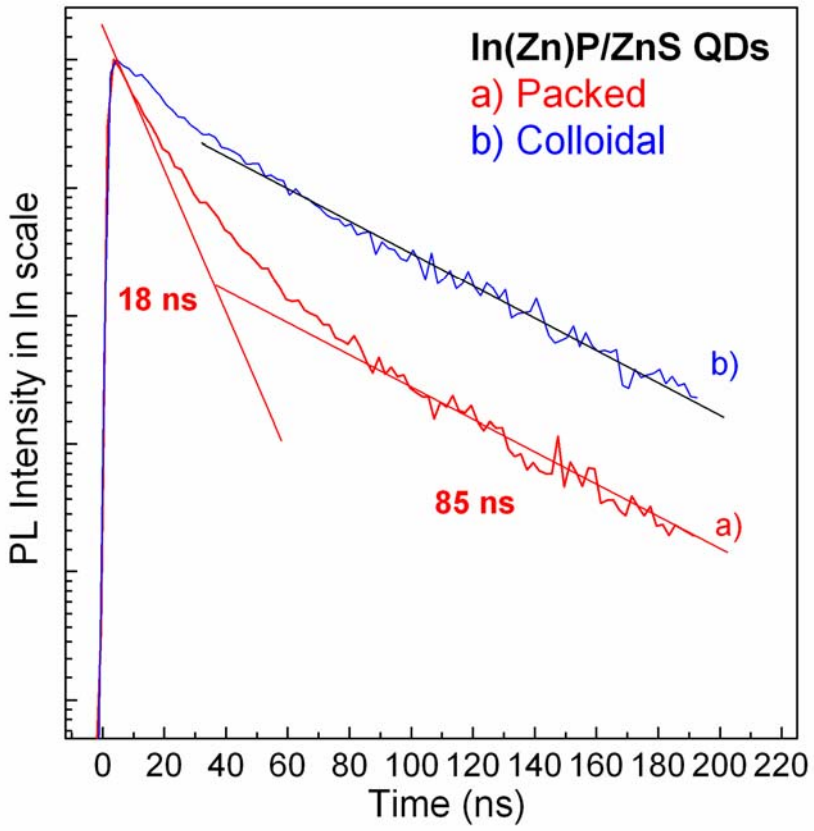

Figure 4.15: *PL decay curves for (a) close-packed and (b) colloidal In(Zn)P/ZnS QDs measured at the excitonic peak maximum. The corresponding decay times of 18 and 85 ns for the short-time decay and long-time decay components of the close-packed sample are indicated in the figure. For the colloidal sample see also Figure 4.13 and related discussion.*

Figure 4.15 presents the PL decay curves for the close-packed and colloidal InP/ZnS QDs. The decay curve is composed of two components of different decay times. The deconvolution shows that the longer decay time accounts for 85 ns for both the close-packed and the colloidal In(Zn)P/ZnS QDs. However, the shorter

decay time changes very much from the close-packed (~18 ns) sample to the colloidal one (~38 ns). As discussed in Section 4.3.3, the corresponding longer decay times of 85 ns for both samples is interpreted as the intrinsic transition of the QDs or “excitonic transition” [54]. The shorter decay time component is related to surface states of the QDs, providing additional decay channels. In the close-packed structure, due to the short interparticle distance between QDs, transfer of the excited charge carriers from larger band gap QDs to smaller band gap QDs within the size distribution competes with the radiative transition. The escape probability of the excited charge carriers contributes to the reduction of the corresponding decay time. A similar observation has been made in the case of a multilayer assembly of different-sized CdTe QDs where Förster resonance energy transfer (FRET) from the smaller to the larger particles resulted in a reduced decay time [83]. On the other hand, the probability for energy transfer *via* FRET is strongly distance dependent [84]. Therefore, in the case of the diluted colloidal solution of QDs, the large interparticle distance strongly inhibits charge carrier transfer between individual NPs. As a result, only a comparably small contribution of surface states to the total decay was observed (Figure 4.15b).

Figure 4.16 presents the TRPL spectra of both samples as a function of the delay time. It can clearly be seen that in the close-packed QDs system (Figure 4.16a) the red-shift with delay time from the excitation moment is much more pronounced than in the colloidal system (Figure 4.16b). This observation is consistent with what was observed in the case of $CuInS_2$/ZnS NCs [85]. In the close-packed QDs, the energy transfer between individual particles is possible by (i) resonance photon reabsorption (radiative energy transfer, which could also take place in the colloidal QDs), (ii) FRET-type dipole-dipole interaction between donor QD and acceptor QDs [81,86], or (iii) direct excited charge-carrier transfer from one QD to another. The latter two pathways exhibit spectral characteristics observed here, i.e., a red-shift with delay time. For the colloidal QD system, due to the spatial separation of the individual particles, the physical picture is clearly different. The dipole-dipole interactions between QDs are strongly reduced and only a small fraction of the excited charge carriers can relax to the lower energy levels, after a certain delay from the excitation moment, by cross-relaxation that causes almost no spectral shift.

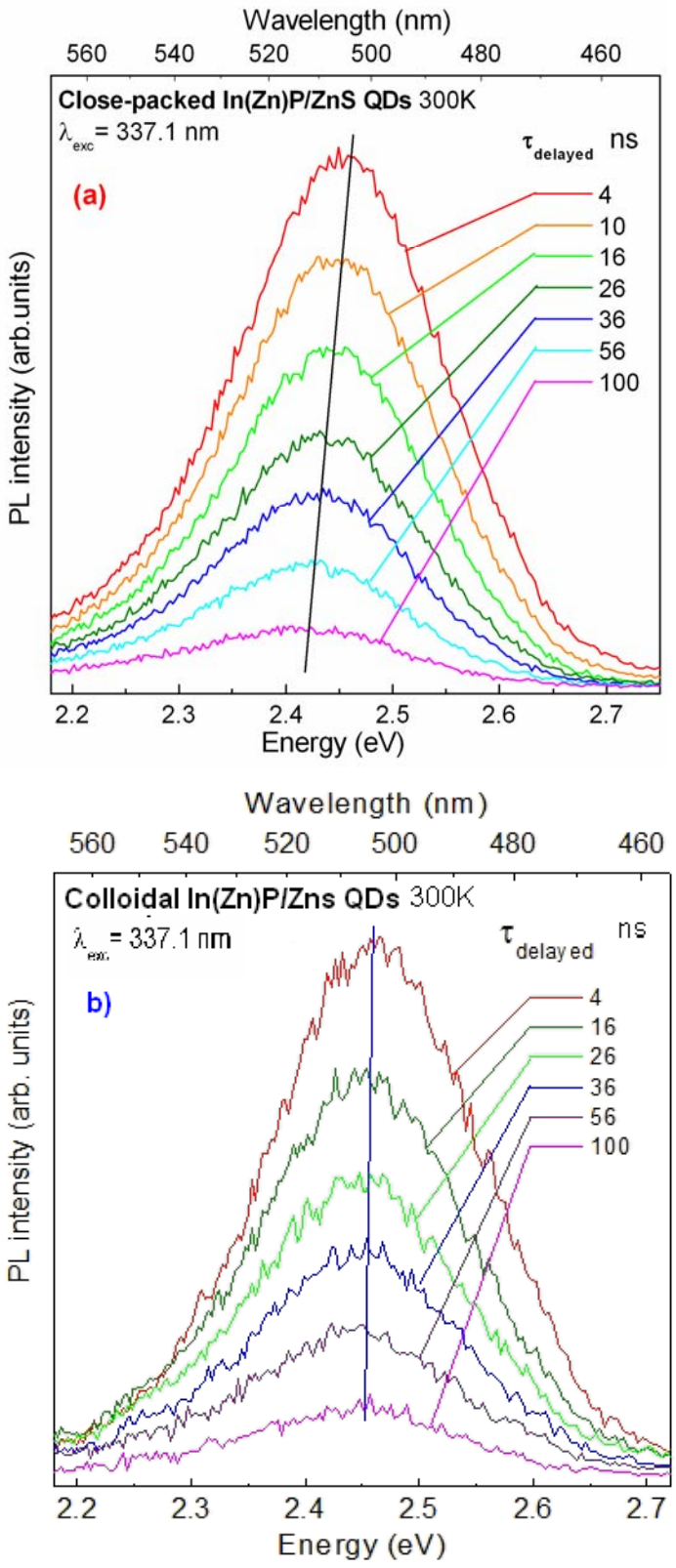

Figure 4.16: *TRPL spectra taken from (a) close-packed and (b) colloidal In(Zn)P/ZnS QDs with the indicated delay times in nanoseconds. Straight lines are added to evidence the position of the peak maximum as a function of the decay time.*

To study deeper the emission mechanism of the In(Zn)P/ZnS core/shell QDs in the close-packed solid, excitation density-dependent and temperature-dependent emission bands were analyzed. Figure 4.17 shows the zero-delay TRPL spectra of InP/ZnS QDs measured with various excitation densities changing by factors of 1 to 100, in the range of 1 kW/cm^2 to 100 kW/cm^2. We observed a slight blue-shift of the peak energy with increasing the excitation density that is attributable to the size-dependent population of the excited carriers before transition to emit light, similar to the emission originating from recombination of electrons in donor and holes in acceptor states.

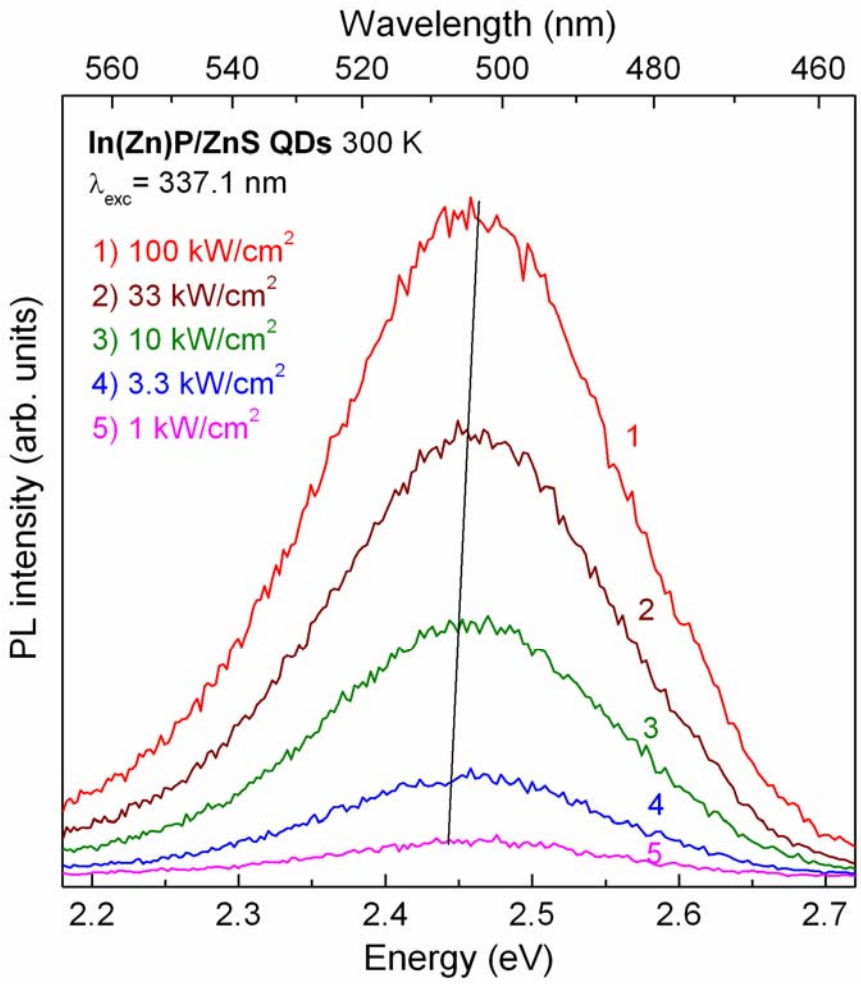

Figure 4.17: *Zero-delay TRPL spectra of close-packed In(Zn)P/ZnS QDs measured at room temperature with various excitation densities.*

Figure 4.18 shows a red-shift and an intensity increase of the PL peak of In(Zn)P/ZnS core/shell QDs with increasing temperature. This behavior is unexpected. In general, the PL intensity increases with decreasing temperature because at lower temperatures the contribution of phonons and consequently the thermally-induced microfield to scatter carriers is reduced. The red-shift of the PL spectra with increasing temperature is explained by the thermal dilatation of the lattice and the electron–phonon interaction through the thermally-induced microfield [87–90]. The former usually contributes only 10–20% to the temperature dependence of the band gap energy [25]; while the latter contributes more strongly and it arises from the different kinds of phonons involved, depending on the lattice temperature.

To explain the “abnormal” behavior of the PL intensity with temperature, we suggest the existence of surface defect energy levels located below the band-gap. Corresponding to these defects, the thermal energy (kT) is necessary for releasing trapped electrons from the defect states to recombine or transit to emit PL. Thus, the release rate, which exponentially depends on the temperature, is a main factor to contribute to the emission intensity. In other words, the integrated emission resulting from radiative recombination/transition of the excited carriers becomes weaker with decreasing temperature because less of the trapped carriers are being released. In this case, thermal energy significantly contributes to release the trapped carriers for further emission. Because of the variable activation energy of surface defect states, the trapped carriers could be gradually released with temperature to contribute to the emission, leading to the gradual increase of the PL intensity with temperature.

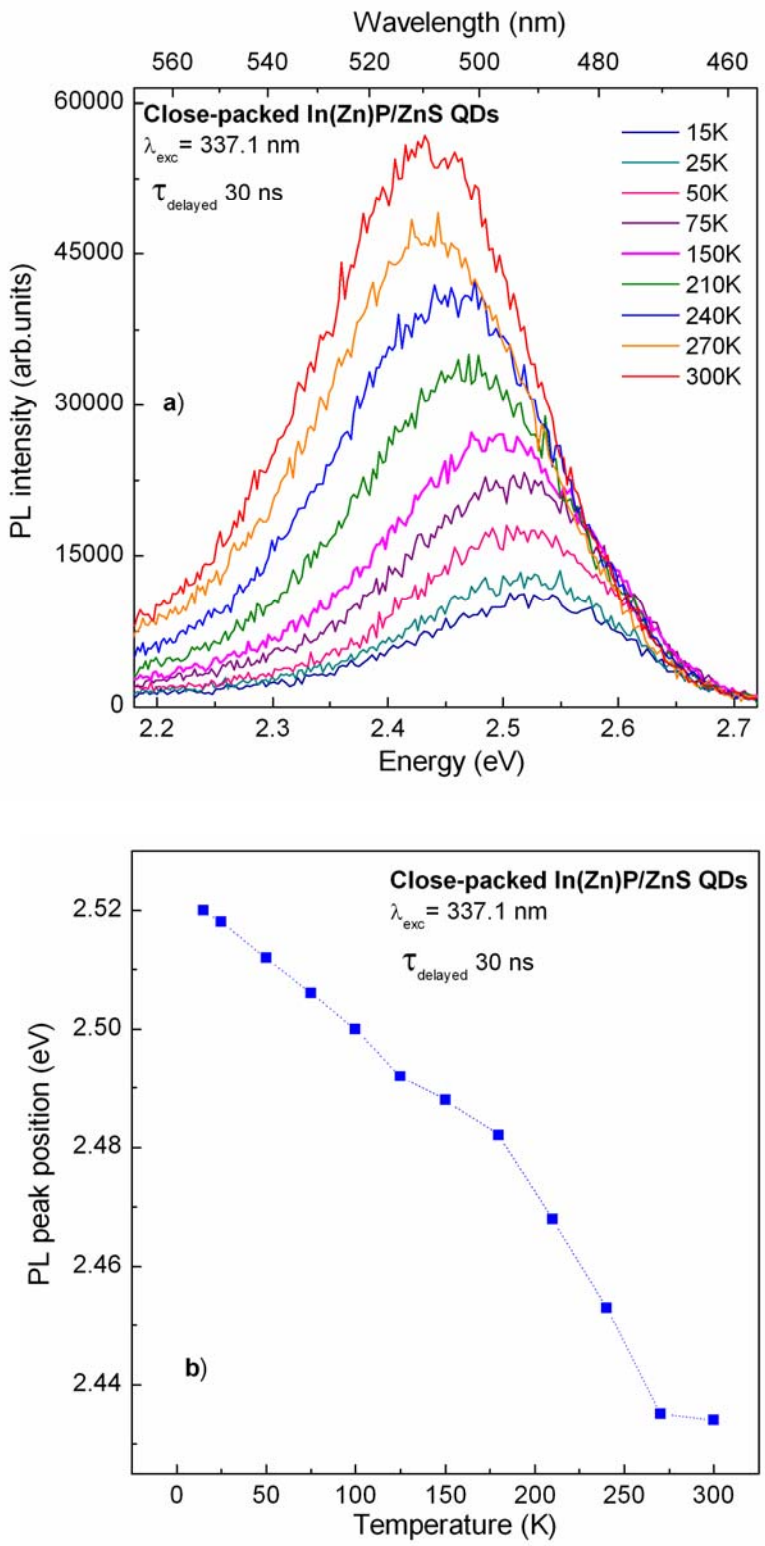

Figure 4.18: *(a) The 30-ns delay TRPL spectra of In(Zn)P/ZnS QDs and (b) the extracted emission peaks as a function of temperature.*

The hypothesis of the existence of surface defect energy levels located below the band-gap is verified by the TRPL study. Figure 4.19a shows the PL decay measured at different temperatures. It is clearly seen that each decay curve is composed of two components with different decay time constants. It is reasonable to assign the short and the long decay times to the surface-related defects and the excitonic transitions in QDs, respectively (Section 4.3.3). Deconvolution of the temperature-dependent decay curves shows that both decay times increase with decreasing temperature. The long decay time (the upper part of Figure 4.19b) is almost un-changed for temperatures higher than 100 K that is characteristic of the radiative life-time. Below 100 K, this decay time increases with decreasing temperature, due to the stronger contribution of the population time to release trapped carriers from defects for going to emission sites. Thus, at low temperature, the trapping of electrons at defects lengthens the population processes of the emissive sites causing a decrease of the PL intensity. For the shorter decay time component (the lower part of Figure 4.19b), the variation is not monotonic. Anyhow, it is shortened with increasing temperature, showing the characteristics of traps. Therefore, the TRPL results are explained in terms of charge carriers being released from traps to contribute to the emission of the In(Zn)P/ZnS QDs.

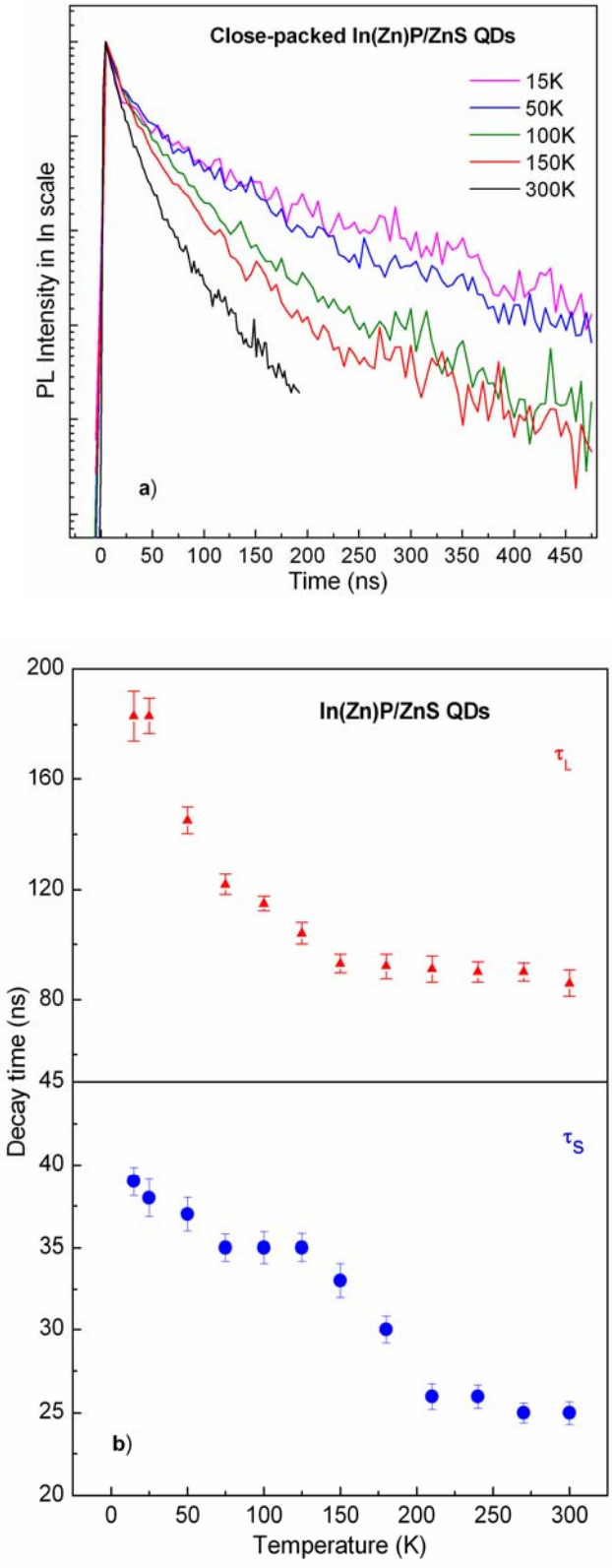

Figure 4.19: *The decay curves of alloy In(Zn)P/ZnS QDs measured with various temperatures at the emission peak of In(Zn)P QDs. Deconvolution of each PL decay curve shows two components,* τ_S *and* τ_L.

4.4. Conclusions

High quality and highly luminescent In(Zn)P core and In(Zn)P/ZnS core/shell QDs were synthesized by the hot injection and the heating-up one-pot methods. The synthesized QDs were characterized by powder XRD, TEM, EDX, UV-vis absorption and SSPL/TRPL spectroscopies.

The hot injection method using PH_3 gas as the phosphorous precursor can be adjusted to obtain bigger InP and InP/ZnS "real" core/shell QDs with an excitonic absorption peak in the 570–700 nm range. The emission peak related to the InP core varied as a function of the QD size in the 590–720 nm range, while the ZnS shell showed emission in the blue region around 470 nm, arising from defect states. The results from TRPL measurements demonstrated that the ZnS shell emitted on a comparable timescale to that of the InP core, in the ten nanosecond range. On the one hand, the ZnS overcoating played a decisive role in the passivation of imperfections at the surface of InP QDs, consequently increasing the photoluminescence intensity related to the excitonic transition in the InP core. On the other hand, our study reveals that, beside the optical transitions in the InP core, the optical processes within the ZnS shell strongly influence the dynamics of carriers' population and evolution after photo-generation.

The heating-up one-pot method using $P(TMS)_3$ and adding $ZnSt_2$ during the core NC synthesis results in In(Zn)P and In(Zn)P/ZnS QDs emitting in the range from 485 to 590 nm. The LQY reaches 70% by varying the Zn^{2+}:In^{3+} molar ratio and reaction-growth/shelling temperatures, and the typical FWHM of PL is around 50 nm. $ZnSt_2$ has an important role in the nucleation and growth process of the QDs. It is supposed to act as a surfactant and as a Zn precursor leading to alloyed In(Zn)P QDs. This alloy structure causes band-edge fluctuations which enhance the confinement of the excited carriers and increase the LQY.

Finally, we have studied the influence of the surrounding environment on the optical characteristics of the obtained alloy In(Zn)P/ZnS QDs in close-packed and colloidal phases. The SSPL spectra from the close-packed In(Zn)P/ZnS QDs are peaking at longer wavelengths in comparison with those taken from the colloidal ones. In addition, the TRPL study shows that the close-packed In(Zn)P/ZnS QDs possess a shorter luminescence decay time and a strongly increased spectral shift with the delay time from the excitation moment in comparison with the colloidal

ones. Förster resonance energy transfer and/or excited charge-carrier transfer between the In(Zn)P/ZnS QDs, favored by their alloyed internal structure, have been shown to be the main reasons for the observed behavior. The evidence for the charge-carrier transfer in close-packed layers of In(Zn)P/ZnS QDs is very important for their integration into optoelectronic devices, such as QD LEDs or light emitting field effect transistors.

4.5. References

[1] O. I. Micic, C. J. Curtis, K. M. Jones, J. R. Sprague, A. J. Nozik, H. Giessen, B. Fluegel, G. Mohs, N. Peyghambarian, *J. Phys. Chem*. **98**, 4966 - 4969 (1994).

[2] O. I. Micic, J. R. Sprague, C. J. Curtis, K. M. Jones, J. L. Machol, A. J. Nozik, *J. Phys. Chem.* **99**, 7754 - 7759 (1995).

[3] A. A. Guzelian, U. Banin, A. V. Kadavanich, X. Peng, A. P. Alivisatos, *Appl. Phys. Lett.* **69**, 1432 (1996).

[4] O. I. Micic, A. J. Nozik, *J. Lumin.* 70, 95 – 107 (1996).

[5] J. R. Heath, and J. J. Shiang, *Chem. Soc. Rev.* **9**, 2056 (1998).

[6] S. W. Kim, J. P. Zimmer, S. Ohnishi, J. B. Tracy, J. V. Frangioni, M. G. Bawendi, J. *Am. Chem. Soc.* **127**, 10526-10532 (2005).

[7] A. Narayanaswamy, L. F. Feiner, and P. J. Zagg, *J. Phys. Chem.* C 112, 6775 – 6780 (2008).

[8] Y. Cao, U. Banin, *J. Am. Chem. Soc*. **122**, 969 - 9702 (2000).

[9] D. Battaglia, X. G. Peng, *Nano Lett. **2***, 1027-1030 (2002).

[10] C. McGinley, M. Riedler, T. Möller, H. Borchert, S. Haubold, M. Haase, H. Weller, *Phys. Rev. B* **65**, 245308 (2002).

[11] D. V. Talapin, N. Gaponik, H. Borchert, A. L. Rogach, M. Haase, H. Weller, *J. Phys. Chem. B **106***, 12659-12663 (2002).

[12] S. Xu, S. Kumar, T. Nann, *J. Am. Chem. Soc. **128***, 1054-1055 (2006).

[13] D. W. Lucey, D. J. MacRae, M. Furis, Y. Sahoo, A. N. Cartwright, P. N. Prasad, *Chem. Mater. **17***, 3754-3762 (2005).

[14] S. H. Kim, R. H. Wolters, J. R. Heath, *J. Chem. Phys*. **18**, 105 (1996).

[15] A. A. Guzelian, J. E. B. Katari, A. V. Kadavanich, U. Banin, K. Hamad, E. Juban, A. P. Alivisatos, R. H. Wolters, C. C. Arnold, J. R. Heath, *J. Phys. Chem*. **100**, 7212 - 7219 (1996).

[16] A. F. van Driel, G. Allan, C. Delerue, P. Lodah, W. L. Vos, D. Vanmaekelbergh, *Phys. Rev. Lett.* **95**, 236804 (2005).

[17] E. Rabani, B. Hetenyi, B. J. Berne, *J. Chem. Phys.* **110**, 5355 (1999).

[18] O. I. Micic, H. M. Choeng, H. Fu, A. Zunger, J. R. Sprague, A. Mascarenhan, A. J. Nozik, *J. Phys. Chem.* **101**, 4904 - 4912 (1997).

[19] L. Li and P. Reiss, *J. Am. Chem. Soc.* **130**, 11588 (2008).

[20] D. V. Talapin, N. Gaponik, H. Borchert, A. L. Rogach, M. Haase, H. Weller, *J. Phys. Chem. B* **106**, 3759-3762 (2002).

[21] S. Haubold, M. Haase, A. Kornowski, H. Weller, *Chem. Phys. Chem*. **2**, 331-334 (2001).

[22] L. Spanhel, M. Haase, H. Weller, A. Henglein, *J. Am. Chem.* Soc.**109**, 5649 (1987).

[23] M. A. Hines, P. Guyot-Sionest, *J. Phys. Chem*. 100, 468 – 471 (1996).

[24] B. O. Dabbousi, J. Rodriguez-Viejo, F. V. Mikulec, J. R. Heine, H. Mattoussi, R. Ober, K. F. Jensen, M. G. Bawendi, *J. Phys. Chem. B* **101**, 9463 (1997).

[25] P. Reiss, S. Carayon, J. Bleuse, A. Pron, *Synth. Met.* **139**, 649 (2003).

[26] P. Reiss, M. Protière, L. Li, Small, **5**, 154-168 (2009).

[27] I. L. Medintz, H. T. Uyeda, E. R. Goldman, H. Mattoussi, Nature Mater., **4**, 435-446 (2005).

[28] E. Holder, N. Tessler, A. L. Rogach, *J. Mater.* Chem., **18**, 1064-1078 (2008).

[29] D. V. Talapin, J. S. Lee, M. V. Kovalenko, E. V. Shevchenko, *Chem. Rev*. **110**, 389-458 (2010).

[30] A. Mews, A. Eychmüller, M. Giersig, D. Schoos, H. Weller, *J. Phys. Chem*. **98**, 934 - 941 (1994).

[31] O. I. Micic, B. B. Smith, A. J. Nozic, *J. Phys. Chem.***104**, 12149 - 12156 (2000).

[32] D.J. Bharali, D. W. Lucey, H. Jayakumar, H. E. Pudavar, P. N. J. Prasad, *J. Am. Chem. Soc.* **127**, 11364 (2005).

[33] P. Reiss, J. Bleuse and A. Pron, *Nano Lett.* **2**, 781 (2002).

[34] U. T. D. Thuy, N. Q. Liem, D. X. Thanh, M. Protière, P. Reiss, *Appl. Phys. Lett.* **91**, 241908 (2007).

[35] M. Bruchez, M. Moronne, P. Gin, S. Weiss, A. P. Alivisatos, *Science* **281**, 933 (1998).

[36] B. Dubertret, P. Skourides, D. J. Norris, V. Noireaux, A. H. Brivanlou, A. Libchaber, *Science* **298**, 1759–1762 (2002).

[37] N. Tessler, V. Medvedev, M. Kazes, S. Kan, U. Banin, *Science* **295**, 1506 (2002).

[38] J. G. Winiarz, L. Zhang, M. Lal, C. S. Friend, P. N. J. Prasad, *J. Am. Chem. Soc.* **121**, 5287 (1999).

[39] V. I. Klimov, A. A. Mikhailovsky, S. Xu, A. Malko, J. A. Hollingsworth, C. A. Leatherdale, H. J. Eisler, M. G. Bawendi, *Science* **290**, 314 (2000).

[40] X. Peng, M. C. Schlamp, A. V. Kadavanich, A. P. Alivisatos, *J. Am. Chem. Soc.* **119**, 7019 - 7029 (1997).

[41] S. Hussain, N. Won, J. Nam, J. Bang, H. Chung, S. Kim, ChemPhysChem **10**, 1466 (2009).

[42] R. Xie, D. Battaglia, and X. Peng, *J. Am. Chem. Soc*. **129**, 15432 (2007).

[43] S. Xu, J. Ziegler, T. Nann, *J. Mater. Chem*. **18**, 2653-2656 (2008).

[44] R. L. Wells, C. G. Pitt, A. T. McPhail, A. P. Purdy, S. Schafieezad, R. B. Hallock, *Chem. Matter* **1**, 4 (1989).

[45] D. Talapin, PhD. Thesis, University of Hamburg, Germany (2002).

[46] C. B. Murray, D. J. Norris, M. G. Bawendi, J. Am. Chem. Soc. **115**, 8706 - 8715 (1993).

[47] Z. A. Peng, X. Peng, *J. Am. Chem. Soc.***123**, 183-184 (2001).

[48] L. Qu, Z. A. Peng, X. Peng, *Nano Lett*. **1**, 333 (2001).

[49] W. W. Yu, X. Peng, Angrew. Chemie. Int. Ed. **41**, 2368 (2002).

[50] L. Li, M. Protière, P. Reiss, *Chem. Mater.* **20,** 2621 (2008).

[51] W.S. Seo, H.H. Jo, K. Lee, J.T. Park, *Adv. Mater*. **15**, 795 (2003).

[52] J. Park, K. An, Y. Hwang, J.G. Park, H.J. Noh, J.Y. Kim, J.H. Park, N.M. Hwang, T. Hyeon, *Nat. Mater*. **3**, 891 (2004).

[53] J. Park, J. Joo, S.G. Kwon, Y. Jang, T. Hyeon, *Angew. Chem. Int. Ed*. **46**, 4630 (2007).

[54] U. T. D. Thuy, P. T. Thuy, L. Li, P. Reiss, N. Q. Liem, *Appl. Phys. Lett*. **96**, 073102 (2010).

[55] D.V. Talapin, A. L. Rogach, M. Haase, H. Weller, *J. Phys. Chem. B* 105, 12278-12285 (2001).

[56] N. Gaponik, D. V. Talapin, A. L. Rogach, K. Hoppe, E. V. Shevchenko, A. Kornowski, A. Eychmuller, H. Weller, *J. Phys. Chem. B* 106, 7177-7185 (2002).

[57] J. W. Mullin, *Crystallization*, Elsevier Butterworth-Heinermann, Oxford (2001).

[58] J. P. Zimmer, S. W. Kim, S. Ohnishi, E. Tanaka, J. V. Frangioni, M. G. Bawendi, *J. Am. Chem. Soc*. 128, 2526-2527 (2006).

[59] P. T. Thuy, U. T. D. Thuy, T. T. K. Chi, L. Q. Phuong, N. Q. Liem, L. Li, P. Reiss, *J. Phys: Conf. Series* **187**, 012014 (2009).

[60] N. Q. Liem, V. X. Quang, D. X. Thanh, *Acta Physica Polonica A* **89**, 717 (1996).

[61] Y. A. Yang, H. M. Wu, K. R. Williams, Y. C. Cao, *Angew. Chem., Int. Ed.* **44**, 6712–6715 (2005).

[62] X. G. Peng, J. Wickham, A. P. Alivisatos, *J. Am. Chem. Soc.* **120**, 5343–5344 (1998).

[63] S. Adam, D. V. Talapin, H. Borchert, A. Lobo, C. McGinley, A. R. B. Castro, M. Haase, H. Weller, T. Möller, *J. Chem. Phys.* ***123***, 084706 (2005).

[64] M. Protière, P. Reiss, *Small* **2**, 331-334 (2007).

[65] X. Zhong, Z. Zhang, S. Liu, M. Han, W. Knoll, *J. Phys. Chem. B* **108**, 15552 (2004).

[66] F. Liu, Y. M. Chen, W. L. Tseng, J. Coll. Interf. Sci. **337**, 414-419 (2009).

[67] E. Shin, J.I. Lee, N.Q. Liem, D. Kim, J. Son, J. Leem, S.K. Noh, D. Lee, *Solid State Commun.* **102,** 855 (1997).

[68] M. Z. Hossain, N. V. Medhekar, V. B. Shenoy, and H. T. Johnson, *Nanotechnology* **21**, 095401 (2010).

[69] R. Xie, D. Battaglia, X. Peng, *J. Am. Chem. Soc*. **129**, 15432 (2007).

[70] C. A. Leatherdale, M. G. Bawendi, *Phys. Rev. B* **63**, 165315 (2001).

[71] S. A. Empedocles, M. G. Bawendi, *Science* **278**, 2114 (1997).

[72] T. D. Krauss, L. E. Brus, *Phys. Rev. Lett*. **83**, 4840 (1999).

[73] M. Shim, P. Guyot-Sionnest, *J. Chem. Phys*. **111**, 6955 (1999).

[74] J. Müller, J. M. Lupton, A. L. Rogach, J. Feldmann, D. V. Talapin, H. Weller, *Phys. Rev. B* **72**, 205339 (2005).

[75] S. F. Wuister, C. de Mello Donega, A. Meijerink, *J. Chem. Phys.* **121**, 4310 (2004).

[76] D. W. Lucey, D. J. MacRae, M. Furis, Y. Sahoo, A. N. Cartwright, and P. N. Prasad, *Chem. Mater.* **17***,* 3754-3762 (2005).

[77] U. T. D. Thuy, T. T. T. Huyen, N. Q. Liem, P. Reiss, *Mat. Chem. Phys.* **112**, 1120 (2008).

[78] J. Zhang, Q. Li, X. Di, Z. Liu, G. Xu, *Nanotechnology* **19**, 435606 (2008).

[79] A. P. Alivisatos, *Nat. Biotech*. **22**, 47 (2004).

[80] R. Zeng, T. Zhang, J. Liu, S. Hu, Q. Wan, X. Liu, Z. Peng, B. Zou, *Nanotech.* **20**, 095102 (2009).

[81] S. F. Wuister, R. Koole, C. de Mello Donega, A. Meijerink, *J. Phys. Chem. B* **109**, 5504 (2005).

[82] K. Huang, R. Demadrille, M. G. Silly, F. Sirotti, P. Reiss, O. Renault, *ACS Nano* **4(8)**, 4799-4805 (2010).

[83] T. A. Klar, T. Franzl, A. L. Rogach, J. Feldmann, *Adv. Mater.* **17**, 769 (2005).

[84] T. Förster, *Ann. Phys.* **2**, 55 (1948).

[85] T. T. K. Chi, L. Q. Phuong, N. Q. Liem, L. Li, P. Reiss, *J. Adv. Nat. Sci*. **1**, 025007 (2010).

[86] S. A. Crooker, J. A. Hollingsworth, S. Tretiak, V. I. Klimov, *Phys. Rev. Lett*. **89**, 186802 (2002).

[87] B. G. Yacobi, *Phys. Rev. B* **22**, 1007 (1980).

[88] B. G. Yacobi, Y. Brada, U. Lachish, C. Hirsch, *Phys. Rev. B* **11**, 2990 (1975).

[89] N. Q. Liem, V. X. Quang, D. X. Thanh, J. I. Lee, D. Kim, *Solid State Commu*. **117**, 255–259 (2001).

[90] W. W. Piper, D.T. F. Marple, P. D. Johnson, *Phys. Rev.* **110**, 323 (1958).

5. In(Zn)P/ZnS NCs doped with Eu^{3+} ions

5.1. Introduction

Modern semiconductor science and technology would not exist without doping [1]. The ability to precisely control the doping of semiconductor NCs can create an opportunity for producing functional materials with new properties, which play a key role in future nanotechnology, such as doped quantum dots (d-dots) emitters for light emitting devices and bio-imaging, solar cells and spintronics [2–13]. This opportunity has stimulated research efforts to develop synthesis methods to incorporate dopants into a variety of colloidal semiconductor NCs [2–3,13–20]. The most efforts have focused on introducing Mn^{2+} ions into II-VI semiconductor host such as ZnS(Se), CdS(Se) NCs of dilute magnetic semiconductors (DMS) [2,10,13–16,21–23]. To date, semiconductor hosts have been doped with various transition metal (TM) ions (Mn^{2+}, Co^{2+}, Cu^{2+},…) [21,24–31] and rare-earth (RE) ions (Eu^{3+}, Tb^{3+}, Tm^{3+}, Er^{3+},…) [2,29–40]. A considerable effort has been made for infrared emission of InP:Yb [32, 41–44], GaAs:Er [45], Si:Er [46–50] and for visible emission of GaN:RE (RE= Tm, Tb, Eu) [51]. Through doping of QDs, one can expect an efficient energy transfer from the host to specific dopants in the resonant regime. In these d-dots therefore the advantageous characteristics of QDs such as the size-tunable emission and high LQY could be conserved while the new positive features for emission from dopants could be exploited. In general, higher self-quenching concentration and better thermal stability could be achieved [22] in d-dots. In our case, the possibility of keeping the size of the Zn-containing InP/ZnS [or In(Zn)P/ZnS] QDs for emitting in the short wavelength range (around 485–510 nm, corresponding to the absorption ~420–460 nm) provides an unique opportunity to prepare host QDs for doping Eu^{3+} ions with the goal to study the resonance energy transfer from the In(Zn)P/ZnS host to the Eu^{3+} guest. This is due to one of the main 4f-electronic transitions ($^7F_0$ – $^5D_2$) of the Eu^{3+} ion which gives rise to an emission peak around 470 nm (Section 2.3). From the energy conversion point of view, a clear benefit originating from the presence RE in doped QDs is that the semiconductor QDs hosts have a very large absorption cross-section to absorb efficiently the excitation energy and then transfer it to the Eu^{3+} ion guests to have finally the highly efficient emission from Eu^{3+} ions at the characteristic wavelengths.

The investigation of the luminescence properties of RE-doped III-V and TM-doped II-VI semiconductors is of great interest both from the fundamental and applied research point of view. The scientific interest is related to the uniqueness of the optical and electrical properties of RE dopants in semiconductors hosts; they emit sharp and temperature-stable luminescence associated with the RE intra-4*f*-shell transition. Therefore, RE-doped semiconductors can potentially be used to fabricate opto-electronic devices that are insensitive to the surrounding host environment. Luminescence is observed by photoexcitation of the host semiconductor to generate the excited charge carriers. Then due to an energy transfer from these free carriers in the host semiconductors to the RE 4*f* shell the 4f-electron are excited with subsequent emission of light [52]. However, it is not easy to dope NCs. First, doping is frequently impeded due to a “self purification” process, working against the incorporation of dopant ions into the host lattice; second, the incompatibility of dopants with the host lattice brings up difficulties in the thermodynamic or kinetic growth control [1,15,53]; third, in some cases, the “surface adsorption” of dopant atoms on the surface of NCs is hindered [20–21]. Even in the favorable case where the dopant ions have the same valence state and similar ionic radius as the corresponding host ion, successful doping is difficult to achieve in a straightforward approach by simply adding a small amount of dopant precursor during the synthesis of the host NCs [54]. Successful chemical synthesis methods for doped NCs must not only offer the commonly needed size, surface morphology and shape control, but also the control over the concentration and location of the dopants within the NC [1].

In general, two types of synthetic methods have been developed to produce doped NCs [21]. The first method is based on aqueous-phase precipitation [24,55]. This method often leads to NPs of low crystallinity and broad size distributions. The second method is an organic-phase growth, which can produce monodisperse and highly crystalline colloidal NCs [13,15,19]. In many cases, the impurity atoms exist only at the surface of the NCs but not inside the core, therefore minimizing the dopant’s effects on the NCs’ properties [15]. Gamelin *et al*. have introduced a method using isocrystalline shell growth to incorporate surface dopants into the cores [17]. Peng *et al*. and Cao *et al*. have reported that impurity-doping can be decoupled from the NC nucleation and growth stages [3] and developed a three-step synthesis to achieve radial-position-controlled doping of TM ions into II-VI, III-V semiconductor NCs [13]. For instance, they have successfully synthesized Mn-

doped CdS/ZnS NCs and Cu-doped InP/ZnSe NCs which emit the specific luminescence of Mn- and Cu-impurities with a LQY as high as 50% [4,13,56] and 40%, respectively [25]. However, for III-V d-dots, the synthesis and the relevant knowledge are rather limited [25]. The synthetic chemistry of III-V NCs is substantially different from and more difficult than that of II-VI ones. Nevertheless, the RE^{3+} ion has the same charge as the constituent III-group ion so that charge compensation is not needed for RE-doping into the III-V lattice. In addition, the RE^{3+} ionic radii are similar to the III-group ions which are favorable for doping. Therefore, beside the difficulty of synthetic chemistry of III-V NCs one can expect that the doping of RE^{3+} ions into III-V NCs is more favorable than into II-VI NCs.

Based on the success of the synthetic methods of the un-doped In(Zn)P/ZnS NCs as presented in Section 4.2.2, and literature search of the Mn-doped CdS/ZnS NCs, we have developed the synthesis of Eu-doped In(Zn)P/ZnS NCs. Experimental details are presented in Appendix 1.4. In the following sections we briefly present the synthesis of Eu-doped In(Zn)P/ZnS NCs, their PL, TRPL and PLE characteristics and discussion.

5.2. Synthesis of Eu-doped In(Zn)P/ZnS NCs

Eu-doped In(Zn)P/ZnS NCs were synthesized by using a “three-step one-pot” method. Meanings of the three steps are as follows: step 1, synthesis of the host NCs; step 2, dopant growth; and step 3, growth of the outer ZnS shell (or host-shell growth). In the syntheses, step 1 and step 3 were carried out by slightly modifying the method we presented in Section 4.2.2 [57–58], while step 2 can be considered to be a new initiative to dope RE^{3+} ions into the In(Zn)P/ZnS host QDs. The diameter of the host NCs and the thickness of the host shells determine the radial positions of Eu-dopants inside the host core/shell NCs. In step 2, the Eu doping process is achieved by the adsorption and the growth of partial EuP shells on the host NCs. Eu-doping levels are controlled mostly in this step in direct proportion to the amount of the Eu precursors added (e.g., $Eu(MA)_3$, Eu-oleate) and doping temperature. To achieve a more efficient emission as well as to further control the Eu position inside the NCs, we carried out ZnS-shell growth. The Eu^{3+} ions can diffuse during this step and the Eu content in the ZnS shell is strongly dependent on the shelling temperature.

We have carried out the syntheses of the Eu-doped In(Zn)P/ZnS core/shell d-dots exploring several key aspects of the related reactions, including temperature for

each process, dopant concentration, and the epitaxial growth of the ZnS shell to prevent the out-diffusion of RE^{3+} ions. Corresponding to the three steps mentioned above, briefly, step 1 enables to produce the In(Zn)P host NCs with the presence of $ZnSt_2$ by a quick heating-up one-pot method [57–58]. The reaction to form In(Zn)P QDs was performed under Ar with the Zn^{2+}:In^{3+} molar ratio in the precursor solution of 2:1 and the reaction–growth temperature and time fixed to 190°C and 10 min, respectively, in order to obtain In(Zn)P NCs emitting PL around 470 nm. This wavelength is nearly resonant to the $^7F_0$ – $^5D_2$ transition of the Eu^{3+} ion and therefore enables energy transfer from the excited host to the Eu dopant. After that, step 2 aims at the Eu-dopant adsorption on the surface of the In(Zn)P host NCs. In a typical reaction, this step was performed at 80°C for 100 min with adding 0.3 equivalents of Eu-oleate with respect to In^{3+} ions. Subsequently, the reaction mixture was heated to 120°C for incorporation and diffusion of Eu^{3+} ions into the In(Zn)P NCs for 20 min. In step 3, the epitaxial ZnS shell growth was carried out by slowly adding appropriate amounts of the Zn:S precursors (Zn-oleate and $(TMS)_2S$). The shelling temperature was kept at 120°C for 10 min to allow the growth of the ZnS shell, which not only improves the chemical stability of the Eu-doped In(Zn)P/ZnS core/shell d-dots as a normal passivation coating layer but also provides a diffusion barrier for preventing the dopant ions leakage out of the d-dots. We point out that shelling is carried out at comparably very low temperature to avoid the out-diffusion of Eu dopant ions. The entire shell growth process was monitored by taking aliquots for UV-vis absorption or PLE, and phosphorescence spectroscopies. After cooling down to room temperature and purification by repeated precipitation (by adding acetone/methanol) and redispersion (in hexane) cycles, the synthesized Eu-doped In(Zn)P/ZnS NCs could easily be dispersed in a number of solvents, including chloroform, toluene, or n-hexane. Their luminescence properties were studied by UV-vis absorption, PL, PLE, and TRPL (phosphorescence) spectroscopy. The obtained results are presented in detail in Section 5.3.

5.3. Results and discussion

In this section, we focus on the optical properties of the Eu-doped In(Zn)P QDs and Eu-doped In(Zn)P/ZnS QDs. Using the synthesis parameters listed in the previous section, the obtained In(Zn)P QDs possess a zinc-blende structure and sphere-like shape with the size of 1.7 nm (corresponding to the excitonic absorption at ~435 nm, and the emission at ~485 nm). Note that with the presence of Zn

reqaction medium we have successfully kept the In(Zn)P QDs size unchanged for a long duration of the doping-shelling process. Thus, we have controlled the doping level and the doping yield by control both the dopant-growth of Eu-containing layer on the surface of NCs and the ZnS-shell growth (ZnS shelling). For controlling the Eu-doping level, we used the Eu precursor with the required amount corresponding to the desired doping level. Then, the yield of the dopant incorporation into the host matrix was controlled by the temperature and duration of the Eu-precursor adsorption, the time of the diffusion of Eu^{3+} ions into the NCs, as well as by the temperature and duration of the ZnS shelling. In the Eu-doping process, two stages were applied: (i) adsorption of the Eu-containing layer on the surface of the NCs (80^{o}C) and (ii) the incorporation of Eu^{3+} ions into NCs at a higher temperature (120^{o}C). All samples were carefully purified according to the procedures described in Appendix 1.4 and then re-dispersed in toluene. The UV-vis absorption and PLE/phosphorescence spectra were performed on a HP 8452A and Carry Eclipse Fluorescence spectrometers, respectively.

In the following we present the results obtained from the systematical studies on the effects of (i) the nature of the dopant precursor on the adsorption of Eu atoms on the surface of In(Zn)P QDs, (ii) the duration and temperature of the adsorption and incorporation of Eu^{3+} ions into the In(Zn)P QDs, (iii) the temperature of the ZnS shelling, and (iv) the Eu-concentration. Figure 5.1 illustrates our view of the doping process, in which Eu^{3+} ions are adsorbed on InP NCs (stage 1 of step 2) and then they are incorporated into the InP lattice (stage 2 of step 2).

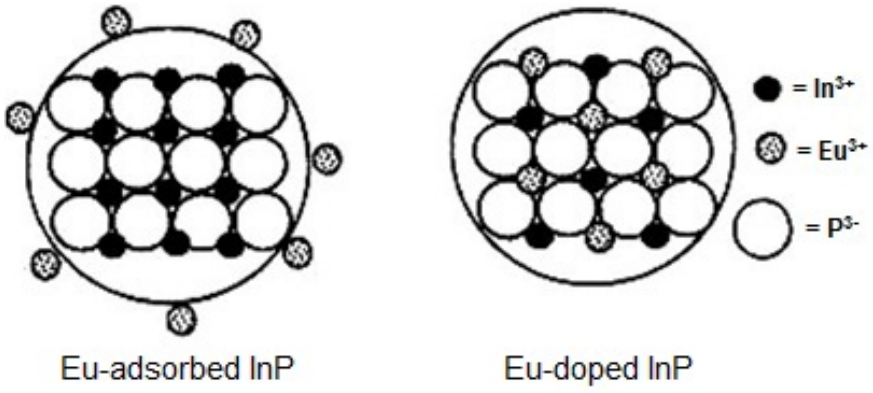

Figure 5.1: *Scheme of the Eu^{3+} ions doping into InP host NCs occurring on two stage: stage 1, adsorption of the Eu^{3+} ions onto the InP NCs surface, and stage 2, diffusion of the Eu^{3+} ions into the NC lattice.*

The effect of *the nature of the dopant precursor* on the adsorption rate of Eu atoms on the surface of the 1.7–nm In(Zn)P/ZnS NCs has been studied by performing two series of experiments with varying composition of the Eu-dopant precursors, namely Eu-oleate and Eu-myristate (Eu(MA)). All other experimental conditions were kept the same: adsorption of the Eu atoms on the surface of In(Zn)P NCs at a temperature of 80^{o}C for 100 min, Eu incorporation into the In(Zn)P QDs at 120^{o}C for 20 min, and then the ZnS shelling at 120^{o}C for 10 min. The phosphorescence (excitation at 365-nm) and PLE spectra of the In(Zn)P/ZnS QDs doped with 30% Eu from the mentioned precursors are shown in Figure 5.2. In this figure, the intrinsic PL intensity from the excitonic transition of the In(Zn)P/ZnS QDs doped with different Eu-precursors are normalized to compare the Eu-doping yield (see Figure 5.2a). Indeed, these two Eu-doped In(Zn)P/ZnS QDs exhibit a clear difference in the PL intensity ratio of the intrinsic emission from the In(Zn)P/ZnS QDs and that from the $^{5}D_{o}\rightarrow{}^{7}F_{J}$ transitions of the Eu^{3+} ions. The obtained result shows that Eu-oleate is a more favorable precursor for enhancing the Eu^{3+} ions' emission along with the proper emission from the In(Zn)P/ZnS QDs. The observation of the sharp emission lines characteristic of the Eu^{3+} ions, is however not evident for the doped In(Zn)P/ZnS NCs. Therefore, we have preformed PLE measurements at the Eu-emission for getting some evidence for the incorporation of Eu^{3+} ions into the In(Zn)P/ZnS QDs.

In Figure 5.2b, the PLE spectra were taken at the 618–nm emission line of Eu^{3+} ions; the PLE spectrum at the same wavelength for the un-doped In(Zn)P/ZnS QDs is also presented for comparison. The most prominent transition $1S_{3/2}$–$1S_{e}$ at 470 nm and another one $1P_{3/2}$–$1P_{e}$ at ~380 nm are characteristic for the excitation of the In(Zn)P/ZnS host QDs [59]. Note that for un-doped sample we have observed the PLE spectrum similar to the doped-sample, with a little bit red-shift. This is understandable because the excitation occurs even for the 618-nm emision as the red tail of the In(Zn)P QDs emission (inset of Figure 5.2a). The host absorption bands observed in the PLE spectra of the Eu^{3+} ion emission indicates that the Eu^{3+} ions are effectively excited via the In(Zn)P/ZnS QDs host, and that energy transfer from the In(Zn)P QDs to the Eu^{3+} ions occurs. This result is a direct evidence for the incorporation of the Eu^{3+} ions into the In(Zn)P/ZnS QDs.

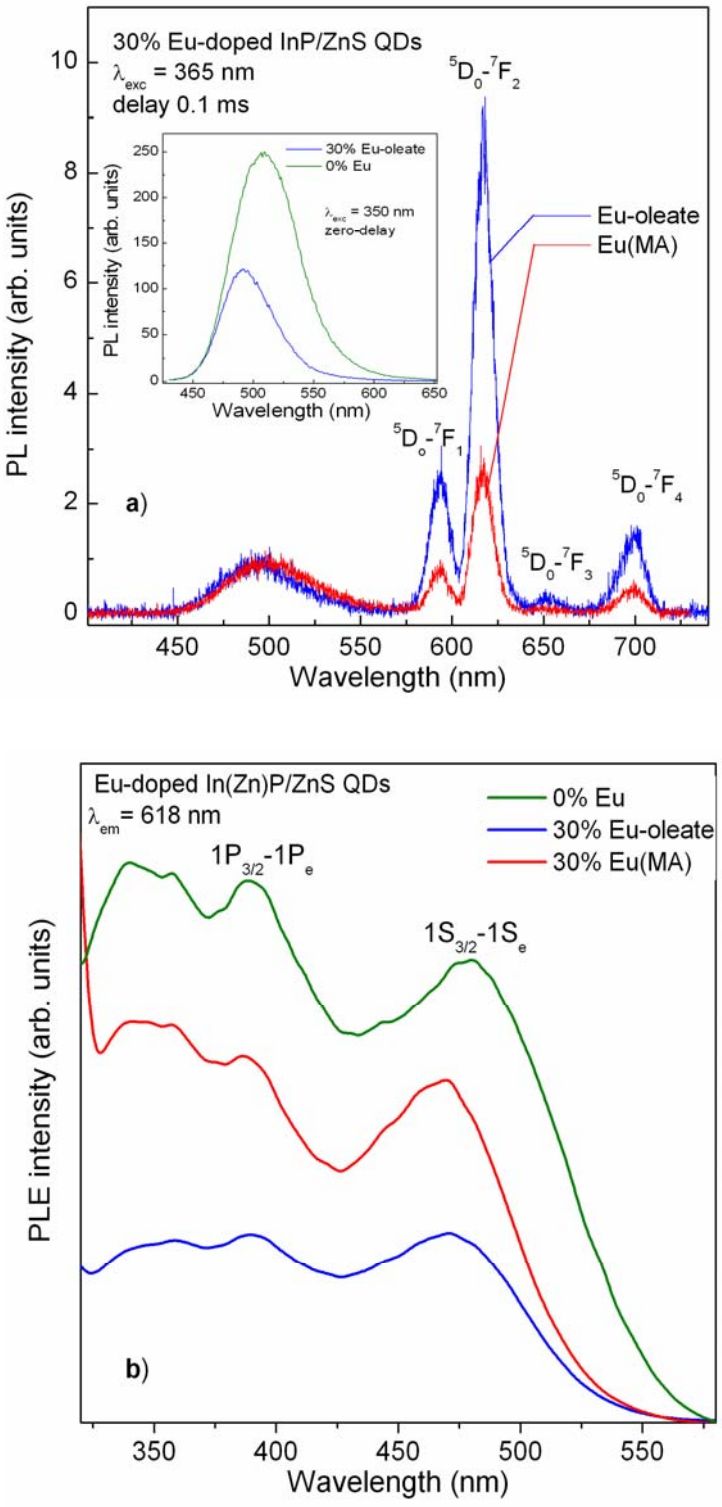

Figure 5.2: *(a) Phosphorescence (excitation wavelength: 365–nm) also 0-delay time and (b) PLE spectra for the In(Zn)P/ZnS QDs doped with 30% Eu from different precursors. The PLE spectrum was taken at the 618-nm emission of Eu^{3+} ions.*

Coming back to the results shown in Figure 5.2a, one notes a similarity of the PL spectra of the two samples, namely In(Zn)P/ZnS NCs doped with different Eu precursors, the only exception being the difference in the PL intensity. For the sample doped from Eu-oleate, the PL intensity is about three times stronger. We would explain the obtained result on the basis that Eu-oleate compound contains an unsaturated double bond hence it has a higher reactivity than Eu(MA), resulting in a lower activation energy needed to start the reaction. Therefore, Eu-oleate in the present case, could lead to the formation of strongly bound Eu at low temperature growth condition. For our next studies, we have chosen Eu-oleate compound as an active dopant precursor for doping. In addition, this is also bebeficial because we could reduce temperature for the Eu-doping process to significantly eliminate Ostwald ripening that consequently make the size distribution of NCs narrow [13].

With the three step procedure for the fabrication of Eu-doped In(Zn)P/ZnS core/shell QDs, the last step of shelling the doped In(Zn)P core is considered to be very important. One can directly imagine that at high enough temperature for shelling, already doped Eu^{3+} ions could diffuse out from the QDs. In order to determine the appropriate temperature for shelling, we performed the ZnS shelling for synthesized Eu-oleate doped In(Zn)P QDs at *different temperatures in the range from 120°C to 250°C*. We use the integrated PL ratio of the Eu^{3+} ions emission over the intrinsic In(Zn)P/ZnS QDs emission as a monitor for the existence of Eu^{3+} ions in the system. Figure 5.3 shows the integrated PL intensity ratio as a function of shelling temperature. The result indicates that the Eu doping rate strongly depends on the ZnS-shelling temperature. With increasing this temperature the integrated PL intensity ratio decreases very quickly. This means that the bound Eu can be removed from the NCs by “lattice diffusion” and/or “lattice ejection” in a cation-exchange reaction during the ZnS-shell growth at high temperatures. Note that at a temperature as high as 250°C, no emission from Eu^{3+} ions could be detected. In other words, the Eu^{3+} dopant ions could diffuse from the doped core QDs to the ZnS shell and finally to the NC surface, which facilitates their subsequent removal.

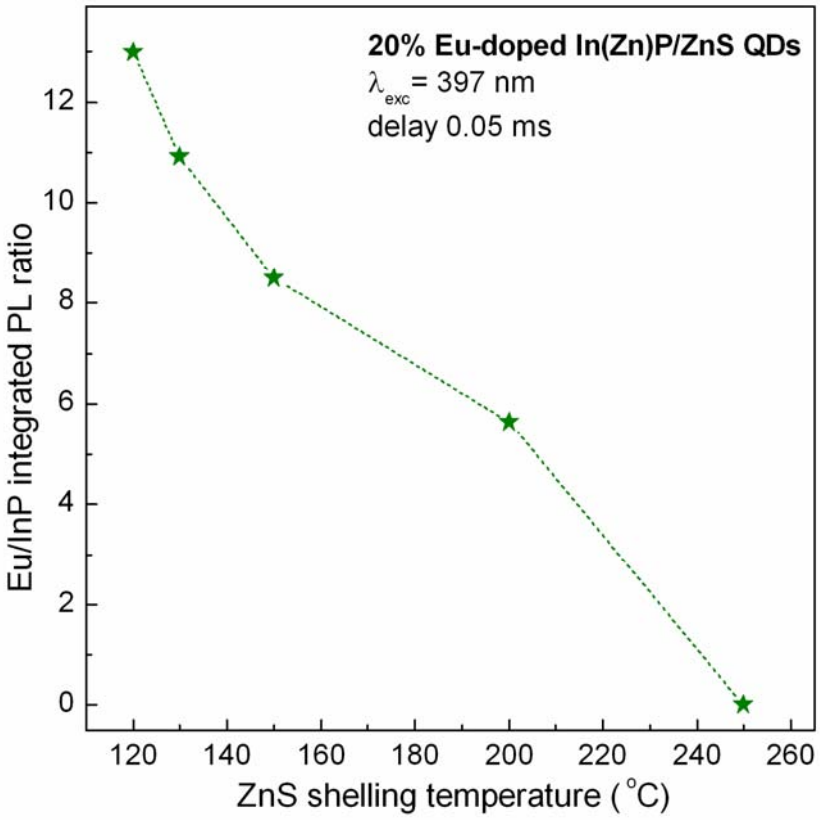

Figure 5.3: *Integrated intensity ratio of the two emission lines, I_{Eu}/I_{InP}, as a function of the ZnS shelling temperature (dashed lines are added to guide the eye). The In(Zn)P QDs reacted with 20 % of Eu-oleate at 80°C for 100 min after overcoating with the ZnS shell at different reaction temperatures between 120 and 250°C. The spectra were measured at a delay time of 0.05 ms under the 397–nm excitation.*

We now present the effect of the *duration and temperature on the adsorption and incorporation* of Eu^{3+} ions into the In(Zn)P QDs. These parameters are likely to act as key factors in the doping process. It is well known that this process actually includes multiple elementary steps, such as surface adsorption/desorption, lattice incorporation/ejection, and lattice diffusion as demonstrated in Cu:ZnSe and Mn:ZnSe d-dot systems [25]. In order to determine an optimized temperature profile for the formation of high quality Eu-doped In(Zn)P/ZnS QDs, a systematic study has been carried out. In principle, the increase of the reaction temperature could lead to the increase in the reaction rate for all processes. Therefore, to achieve a successful synthesis of d-dots, we have chosen a low ZnS shelling temperature (120°C) to study the influence of the duration of this process on the optical properties of the d-dots. For convenience, we have also chosen the same temperature for the

incorporation of the Eu^{3+} ions into the In(Zn)P QDs. In order to determined the proper temperature for adsorbing the Eu-oleate onto the surface of In(Zn)P QDs, we have checked several temperatures in between 60°C and 190°C and found that 80°C is the most suitable.

Figure 5.4 shows the phosphorescence spectra taken from In(Zn)P NCs after Eu^{3+} ions adsorption at 80°C. The solvent used is ODE. The spectra show a change in the integrated intensity ratio of the Eu^{3+} ions emission over the intrinsic In(Zn)P/ZnS QDs emission with adsorption time. At the 0.05-ms delay time, the spectra are dominated by the strongest line resulting from the $^5D_o \rightarrow {}^7F_2$ transition (around 618 nm) of the Eu^{3+} ions. We notice that the excitonic PL intensity decreased substantially; however, the contour of the spectrum is still retained. Quenching of the excitonic PL of In(Zn)P QDs with doping suggests the adsorption of Eu^{3+} ions onto the surface of the host NCs. Similarly, the brightening of the Eu^{3+} emission is considered as a spectroscopic manifestation of the binding of the Eu^{3+} ions onto the surface lattice. From Figure 5.4, one can see that the relative intensity of the Eu^{3+} ions emission with the adsorption duration of 100 min is the highest. This observation can be explained by the fact that with shorter adsorption times (60 min) a smaller number of Eu^{3+} ions binds. However, for longer adsorption durations (150 min) two effects occur: First, a saturation effect, when all surface sites are covered taking into account the steric hindrance of the Eu complex; second, the interaction of closely bound Eu ions leading to a decrease of their PL intensity [25]. Optimally, the adsorption duration is of 100 min. These results are in agreement with the results reported on Cu-doped InP NCs [25]. Thus, from the observation of the change of the integrated PL intensity ratio of the Eu^{3+} ions emission over the intrinsic In(Zn)P/ZnS QDs emission, we determine that 100 min is the best adsorption time for our experiments.

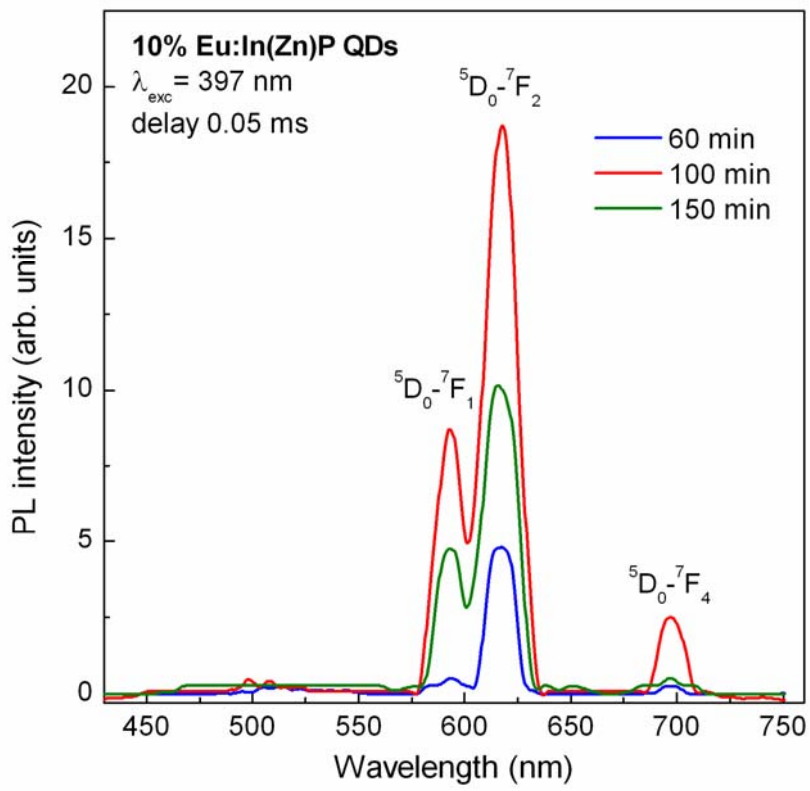

Figure 5.4: *Phosphorescence spectra measured at the 0.05-ms delay time under the 397–nm excitation from the In(Zn)P QDs adsorbed with 10% of Eu-oleate at 80°C. The adsorption duration times are indicated in the figure.*

In an attempt to determine the optimum *duration for the incorporation* (at 120°C) of Eu^{3+} ions into the In(Zn)P QDs, we performed experiments with different times between 5 min and 30 min. Using the same approach as before, we have found that a duration of 20 min is the best for the incorporation of Eu^{3+} ions into the In(Zn)P QDs.

We now present the effects of *the Eu-dopant concentration* on the optical properties of the doped In(Zn)P core QDs and In(Zn)P/ZnS core/shell QDs. These results have been obtained in a systematical study of samples synthesized under the same experimental conditions except the change in the Eu-oleate concentration. Briefly, the used conditions for the In(Zn)P QDs synthesis were 190°C for 10 min; Eu adsorption was carried out at 80°C for 100 min; Eu incorporation at 120°C for 20 min; and finally the ZnS shelling was performed at 120°C for 10 min.

Figure 5.5 shows the phosphorescence spectra taken at the 0.05–ms delay and the PLE spectra at the 618-nm Eu^{3+} ions emission for typical samples of In(Zn)P core QDs doped with Eu-oleate at different concentrations. As in Figure 5.5b, it is clearly seen that the PLE spectra look similar to the one registered for the un-doped In(Zn)P QDs, with the typical excitonic absorption from the In(Zn)P QDs host. The characteristic $1P_{3/2}$–$1P_e$ (~380 nm) and $1S_{3/2}$–$1S_e$ (~470 nm) transitions for the excitation of the In(Zn)P host QDs were observed. The observation of the absorption characteristic to the In(Zn)P QDs host in the PLE spectra of Eu^{3+} ions guests along with no characteristic transition of the Eu^{3+} ion itself means that the Eu^{3+} ions are effectively excited via the In(Zn)P QDs host, and also means that an energy transfer from the In(Zn)P QDs to the Eu^{3+} ions has occurred. At the same time, the intrinsic excitonic emission of the QDs was almost entirely quenched so that the Eu^{3+} ions emission was prominent (Figure 5.5a). This implies that the adsorption of Eu^{3+} ions on the surface and their subsequent incorporation into the In(Zn)P QDs was efficient. At a concentration of 30% Eu-oleate, the integrated luminescence intensity of the Eu-doped In(Zn)P QDs reached a maximum and above this concentration it fell off rapidly. Thus, 30% Eu-oleate seems to be the critical concentration for getting the maximum LQY of the Eu-doped In(Zn)P system. At higher doping levels PL quenching due to the interaction between the closer coming Eu^{3+} ions occurs. Though we have successfully synthesized Eu-doped In(Zn)P core QDs which give clearly the Eu^{3+} ions emission, we recognize that these core QDs are vulnerable toward chemical oxidation. Moreover the dopants can easily diffuse out, and nonradiative decays upon photoexcitation increase fast. These problems could be solved by the growth of a ZnS shell as a diffusion barrier for preventing the dopant leakage out of the system. In the following, we will discuss in more detail the Eu-concentration dependent PL/phosphorescence of Eu-doped In(Zn)P/ZnS QDs.

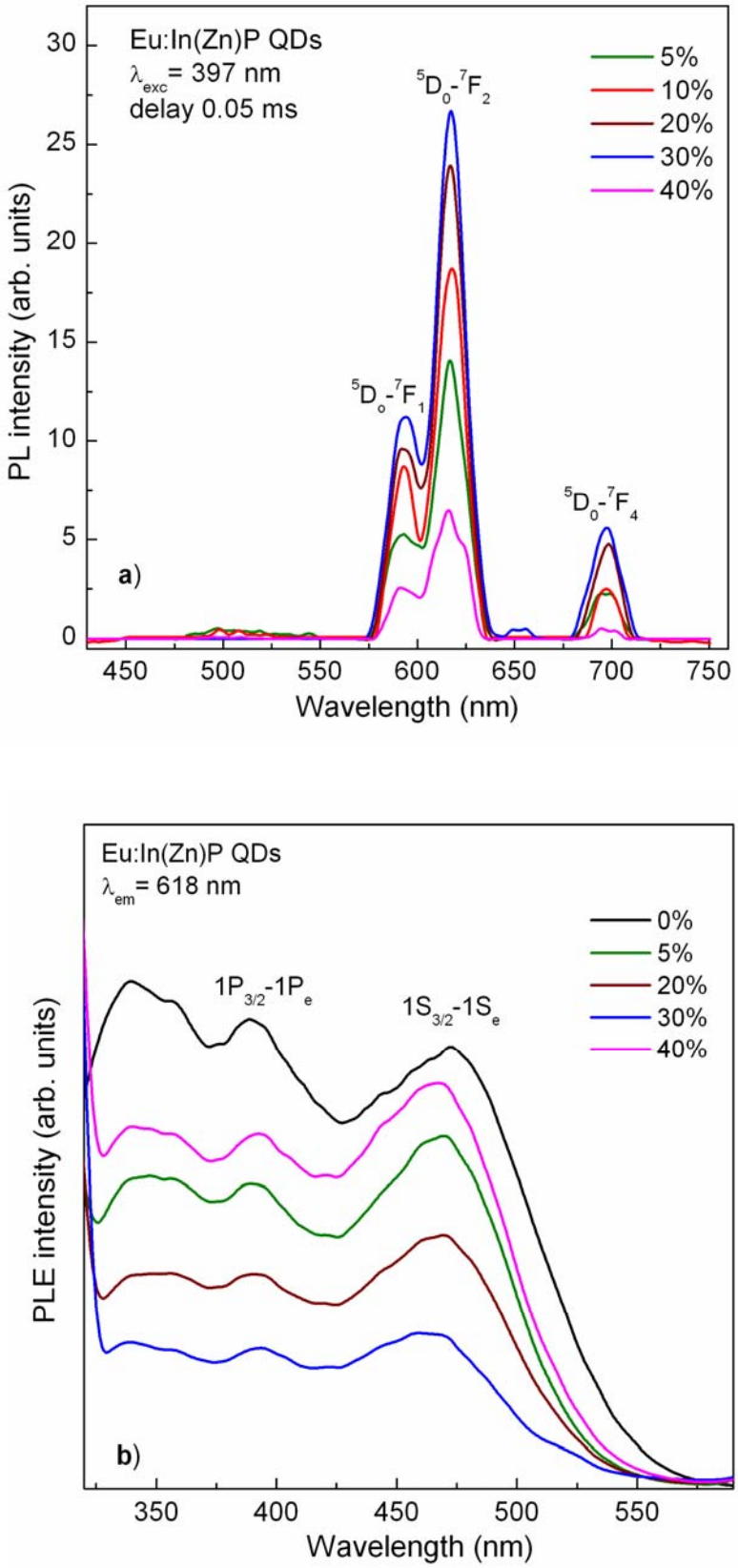

Figure 5.5: *(a) Phosphorescence (b) and PLE spectra for typical Eu-doped In(Zn)P core QDs versus the Eu-oleate concentration.*

After ZnS shelling, the obtained Eu-doped In(Zn)P/ZnS QDs showed improved photo-stability. Figure 5.6 shows that the PLE spectra of the Eu-doped In(Zn)P/ZnS core/shell QDs look similar to those taken from the Eu-doped In(Zn)P core only QDs. Once again, the important role of Zn in the synthesis In(Zn)P QDs to keep the NCs size unchanged for a long duration of the doping-shelling process is demonstrated.

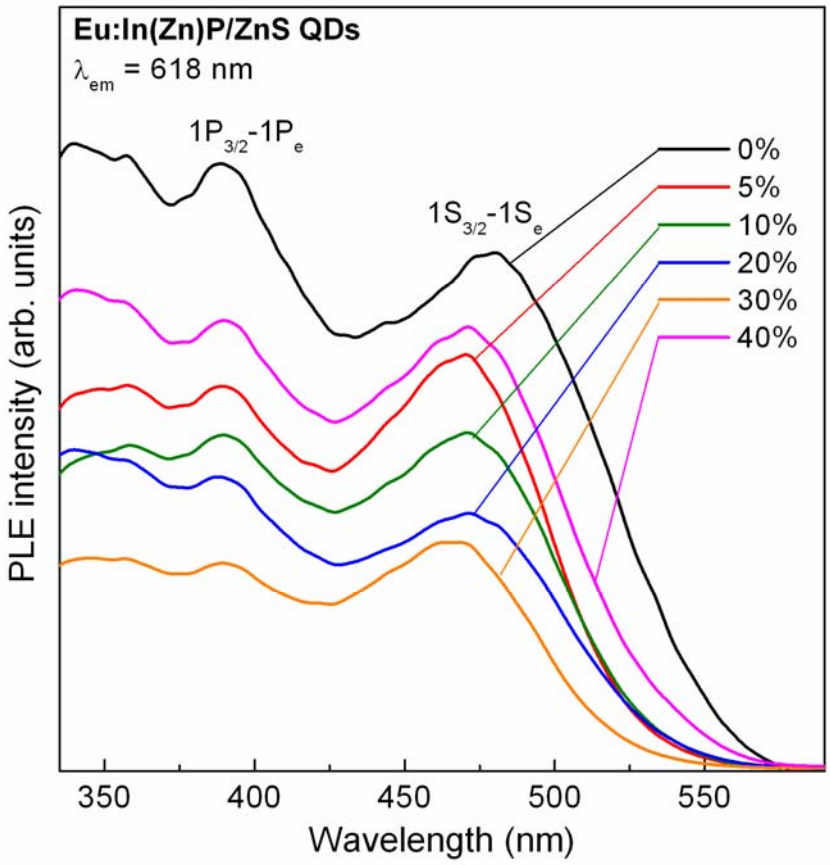

Figure 5.6: *PLE spectra of typical Eu-doped In(Zn)P/ZnS core/shell QDs for the 618-nm Eu^{3+} ions emission. The Eu-oleate concentrations are indicated in the figure.*

Figure 5.7a shows the phosphorescence spectra measured on a typical series of Eu-doped In(Zn)P/ZnS QDs synthesized at optimized experimental conditions (i.e., reaction-growth temperature of In(Zn)P core QDs at 190°C for 10 min; Eu adsorption at 80°C for 100 min; Eu incorporation at 120 °C for 20 min; and the ZnS shelling at 120°C for 10 min) with different Eu-oleate concentrations. As in the

previous cases, in order to facilitate comparison of the Eu^{3+} ions emission as a function of the Eu-concentration, we present the spectra with the normalized intensity of In(Zn)P/ZnS QDs. The PL peak position and FWHM from the In(Zn)P/ZnS QDs were found to be independent of the Eu-concentration. Figure 5.7b shows the integrated intensity ratio of the two emission lines, I_{Eu}/I_{InP}, as a function of the Eu-oleate concentration. It is visible that for Eu-oleate concentration in the range of 5–30%, the PL intensity of Eu^{3+} ions increases. This is a direct result showing that the optical output is proportional to the number of Eu atoms. At Eu-oleate concentrations higher than 30%, the Eu^{3+} ions emission intensity decreases quickly. As in the case of the In(Zn)P core NCs, we explain this phenomenon by a concentration quenching effect, in which the high Eu-oleate concentration induces strong Eu-Eu interactions. The interactions finally give rise to the release of the excited energy in a form of heat without emission. The concentration quenching effect is generally observed in doped materials. Depending on the specific materials and dopants, the critical concentrations are different. For most of bulk materials doped with RE^{3+} ions the critical concentration is of 5–10% [60]. The quenching effect occurs in NCs at a much higher concentration because each NC is separated from the others limiting the nonradiative energy transfer between the RE^{3+} ions inside one NC. A critical dopant concentration of 25-30% has been determined in several kinds of NCs doped with RE^{3+} ions [61–62]. In addition, due to the high Eu-oleate concentration it is probable to create larger crystal-field strain in the ZnS shell resulting in an increase of the nonradiative decay of the Eu^{3+} ions consequently decreasing the Eu^{3+} ions emission. Our experiments show a maximum LQY of the samples doped with around 30% of Eu with respect to In, for both Eu-doped In(Zn)P core and Eu-doped In(Zn)P/ZnS core/shell QDs.

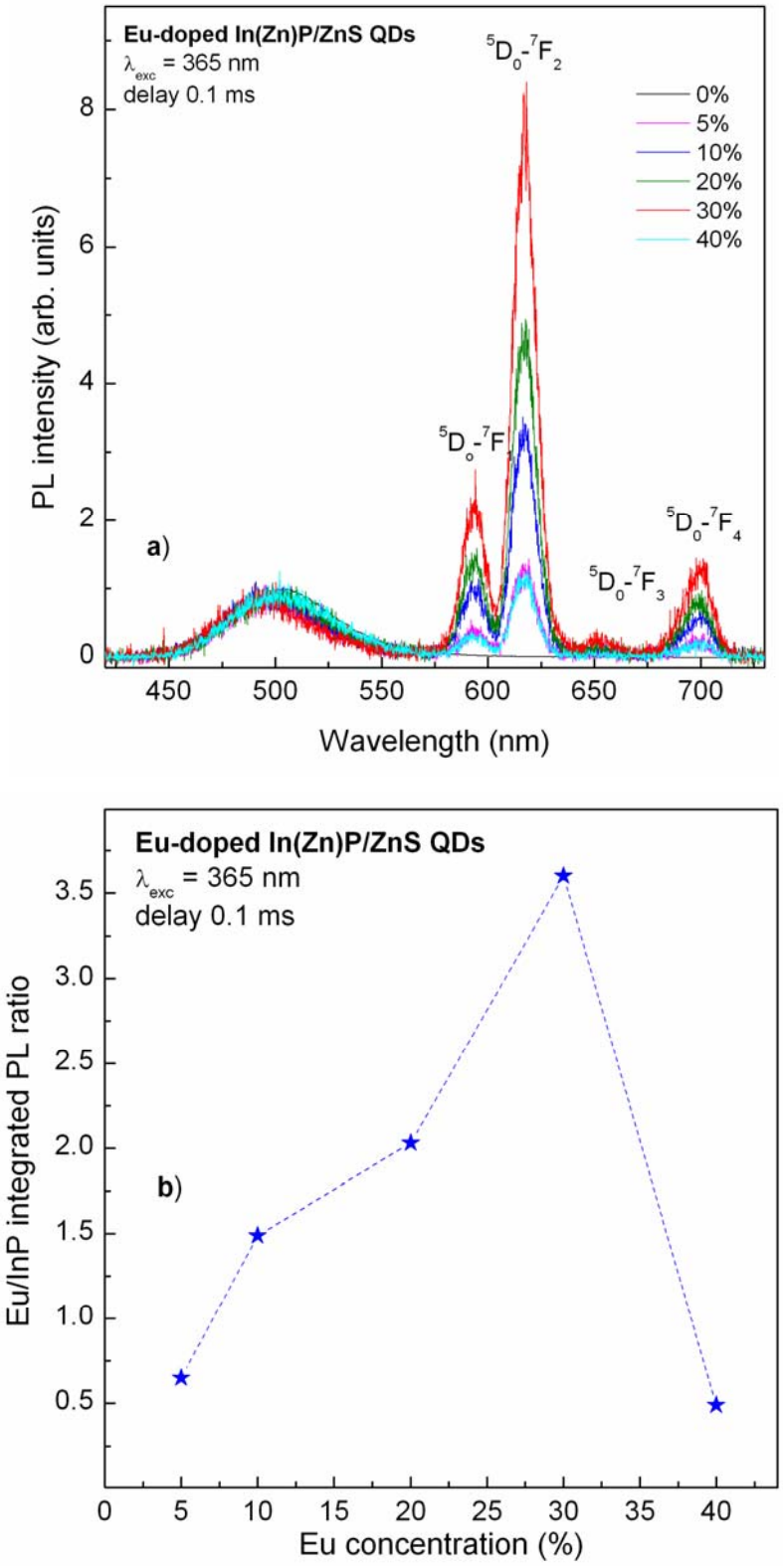

Figure 5.7: *(a) Phosphorescence spectra for a typical series of Eu-doped In(Zn)P/ZnS QDs measured at a 0.1-ms delay time. The corresponding Eu-oleate concentrations are indicated in the figure. (b) Integrated intensity ratio of the two emission lines, I_{Eu}/I_{InP}, as a function of the Eu-oleate concentration (dashed lines are added to guide the eye).*

To check if the Eu-concentration in doped QDs corresponds to the amount of the used Eu-oleate precursor, we analyzed the samples by using X-rays fluorescence spectroscopy (XRF) technique. In our experiments, all samples were carefully washed before any measurement to be sure of eliminating all by-products. Figure 5.8 shows the XRF spectrum and the Eu(Lα) and In(Lα) ratio. The analysis results are consistent with those obtained from optical measurements, showing that the Eu-doped content increases in accordance with the increase of the Eu-oleate precursor. However, at Eu-oleate precursor concentrations higher than 30% we observe a decrease in the final content of the dopant. Although the reasons for this dopant concentration decrease are not clear, this effect is of course another reason for the decrease of the PL intensity ratio, along with the concentration quenching effect.

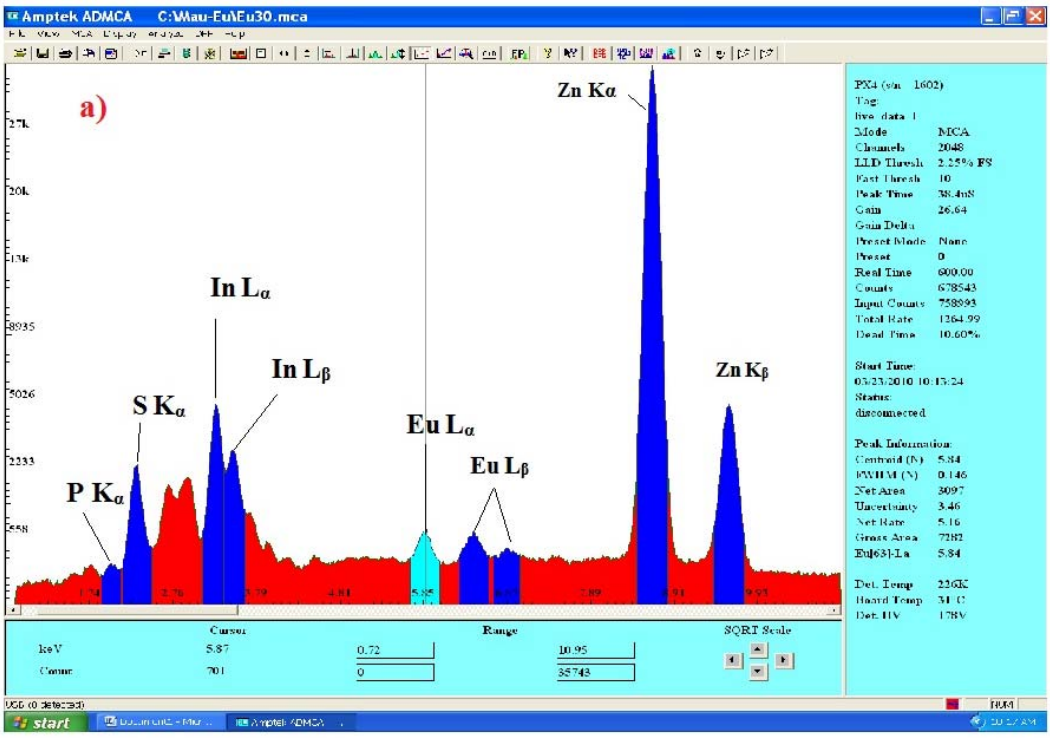

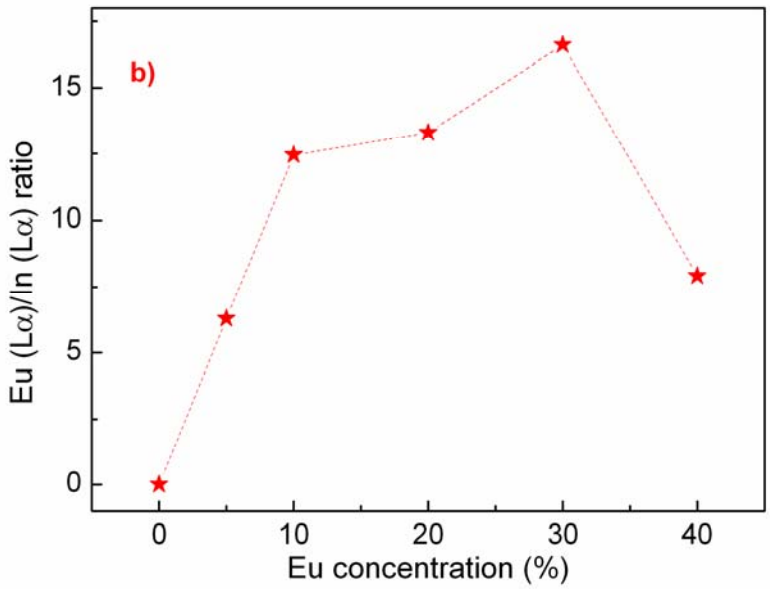

Figure 5.8: *Representative XRF spectra of Eu-doped In(Zn)P/ZnS NCs; (a) 30% of Eu-oleate; (b) Eu(Lα) and In(Lα) ratio as a function of the initial Eu-oleate concentration (dashed lines are added to guide the eye).*

To study in more detail the energy transfer from In(Zn)P QDs host to Eu^{3+} dopant, we measured the phosphorescence spectra with various delay times (TRPL) on a typical sample of In(Zn)P/ZnS QDs doped with 30% of Eu-oleate. The results are shown in Figure 5.9. One can see that no Eu^{3+} ions emission is detected just after the excitation moment, i.e. the spectrum is dominated by the intrinsic emission of the In(Zn)P/ZnS QDs. With increasing delay time the intrinsic emission from In(Zn)P/ZnS QDs is gradually quenched and the Eu^{3+} ions emission is getting more and more pronounced. This is because the Eu^{3+} ions possess much longer decay-time than In(Zn)P/ZnS host QDs. In addition, a part of the released energy from In(Zn)P/ZnS host QDs is transferred to Eu^{3+} ions to contribute to the total emission of the latter. This means that the Eu^{3+} ions are effectively excited *via* the In(Zn)P/ZnS QDs host. Figure 5.9b shows the integrated intensity ratio of the two emission lines from Eu^{3+} ions, I_{Eu}, and from In(Zn)P/ZnS QDs, I_{InP} as a function of delay time. The result indicates that after *ca.* 0.2 ms delay the ratio is almost saturated because from that delay time on the change of the two emissions is nearly the same. In principle, at very long delays, one can still observe the Eu^{3+} ions emission but very small In(Zn)P/ZnS QDs emission because of the long decay time of Eu^{3+} ions.

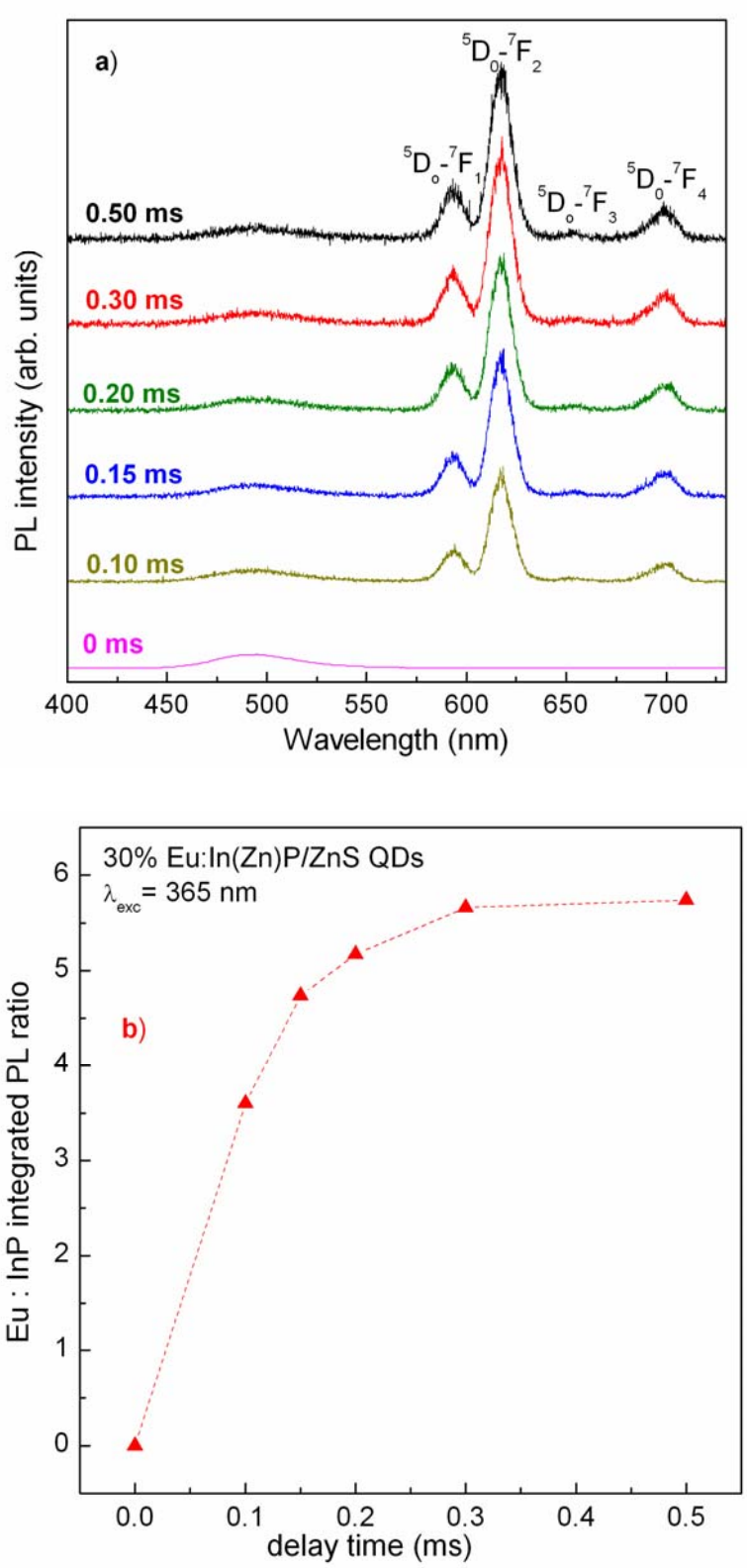

Figure 5.9: *(a) Phosphorescence spectra of 30% Eu-oleate doped In(Zn)P/ZnS QDs versus delay time. (b) Integrated intensity ratio of the two emission lines, I_{Eu}/I_{InP}, as a function of the delay time (dashed lines are added to guide the eye).*

5.4. Conclusion

In conclusion, high quality Eu-doped In(Zn)P and Eu-doped In(Zn)P/ZnS core/shell d-dots were successfully synthesized using a three-step one-pot method, namely step 1, synthesis of the In(Zn)P host NCs; step 2, Eu-dopant growth; and step 3, growth the outer ZnS shell. A high doping yield could be achieved by choosing Eu-oleate as the precursor and optimizing several synthetics parameters: (i) reaction-growth of the In(Zn)P core QDs at a temperature of 190°C for 10 min; (ii) Eu adsorption at 80°C for 100 min and Eu incorporation at 120°C for 20 min; (iii) ZnS shelling at 120°C for 10 min. In addition, the critical dopant concentration has been determined to be of 30%. Our optical measurements such as absorption, PL, PLE, phosphorescence and TRPL spectroscopies clearly support the conclusion of the successful doping of In(Zn)P and In(Zn)P/ZnS QDs, as well as of the resonant energy transfer between the In(Zn)P QDs host and Eu^{3+} guest ions.

5.5. References

[1] D. Chen, R. Viswanatha, G. L. Ong, R. Xie, M. Balasubramaninan, X. Peng, *J. Am. Chem. Soc*. **131**, 9333–9339 (2009).

[2] R. N. Bhargava, D. Gallagher, X. Hong, A. Nurmikko, *Phys. Rev. Lett.* **72**, 416–419, (1994).

[3] N. Pradhan, D. Goorskey, J. Thessing, X. Peng, *J. Am. Chem. Soc.* **127**, 17586–17587 (2005).

[4] Pradhan, N.; Peng, X. *J. Am. Chem. Soc.* **129**, 3339–3347 (2007).

[5] V. L. Colvin, M. C. Schlamp, A. P. Alivisatos, *Nature* **370***,* 354–357 (1994).

[6] V. I. Klimov, S. A. Ivanov, J. Nanda, M. Achermann, I. Bezel, J. A. McGuire, A. Piryatinski, *Nature* **447***,* 441–446 (2007).

[7] W. C. W. Chan, S. Nie, *Science* **281***,* 2016–2018 (1998).

[8] M. J. Bruchez, M. Moronne, P. Gin, S. Weiss, A. P. Alivisatos, *Science* **281***,* 2013–2016 (1998).

[9] N. C. Greenham, X. Peng, A. P. Alivisatos, *Phys. Rev. B* **54**, 17628–17637 (1996).

[10] D. M. Hoffman, B. K. Meyer, A. I. Ekimov, I. A. Merkulov, A. L. Efros, M. Rosen, G. Couino, T. Gacoin, J. P. Boilot, *Solid State Commun.* **114**, 547–550 (2000).

[11] P. V. Radovanovic, D. R. Gamelin, *Phys. Rev. Lett.* **91**, 157202 (2003).

[12] K. M. Hanif, R. W. Meulenberg, G. F. Strouse, *J. Am. Chem. Soc.* **124**, 11495–11502 (2002).

[13] Y. Yang,O. Chen, A. Angerhofer,Y. C. Cao, *J. Am. Chem. Soc.* **128**, 12428–12429 (2006).

[14] M. Shim, P. Guyot-Sionnest, *Nature* **407**, 981-983 (2000).

[15] F. V. Mikulec, M. Kuno, M. Bennati, D. A. Hall, R. G. Griffin, M. G. Bawendi, *J. Am. Chem. Soc.* **122**, 2532-2540 (2000).

[16] D. J. Norris, N. Yao, F. T. Charnock, T. A. Kennedy, *Nano Lett.* **1**, 3-7 (2001).

[17] P. Radovanovic, D. R. Gamelin, *J. Am. Chem. Soc.* **123**, 12207 (2001).

[18] W. Chen, A. G. Joly, J. O. Bovin, *J. Appl. Phys.* ***95***, 667 (2004).

[19] H. Yang, P. H. Holloway, *Appl. Phys. Lett.* **82**, 1965 (2003).

[20] D. J. Norris, A. L. Efros, S. C. Erwin, *Science* **319**, 1776 (2008).

[21] S. C. Erwin,L. Zu, M. I. Haftel, A. L. Efros,T. A. Kennedy, D. J. Norris, *Nature* **436**, 91–94 (2005).

[22] Y. Oka, K. Yanata, *J. Lumin.* **70**, 35 (1996).

[23] N. Feltin, L. Levy, D. Ingert, E. Vincent, M. P. Pileni*, J. Appl. Phys.* **87**, 1415 (2000).

[24] Y. Yang, O. Chen, A. Angerhofer, Y. C. Cao, *J. Am. Chem. Soc***. 130**, 15649–15661, (2008).

[25] R. Xie, X. Peng, *J. Am. Chem. Soc*. **131**, 10645-10651 (2009).

[26] S. J. Xu, S. J. Chua, B. Liu, L. M. Gan, C. H. Chew, G. Q. Xu, *Appl. Phys. Lett*. **73**, 478-480 (1998).

[27] A.S. Ethiraj, N. Hebalkar, S.K. Kulkarni, R. Pasricha, J. Urban, *J. Chem. Phys*. **118**, 8945 (2003).

[28] A.D. Dinsmore, D.S. Hsu, S.B. Qadri, J.O. Cross, T.A. Kenndey, H.F. Gray, B.R. Datna, *J. Appl. Phys*. **88**, 4985 (2000).

[29] L.X. Cao, J.H. Zhang, S.L. Ren, S.H. Huang, *Appl. Phys. Lett*. **80**, 4300 (2002).

[30] H. Hu, W. Zhang, *Opt. Mat.* **28**, 536-550 (2006).

[31] M. Godlewski, S. Yatsunenko, A. Nadolska, A. Opalin´ska, W. Łojkowski, K. D. Tomsia, E. M. Goldys, *Opt. Mat.* **31**, 490–495 (2009).

[32] M. A. J. Klik, T. Gregorkiewicz, I.V. Bradley, J. P. R. Wells, *Phys. Rev. Lett*. **89**, 227401 (2002).

[33] S. Malik, M. Zalewska, M. Grinberg, A. Konkowski, M. Godlewski, *J. Lumin*. **128**, 921-923, (2008).

[34] D. A. Chengelis, A. M. Yingling, P. D. Badger, C. M. Shade, S. Petoud, *J. Am. Chem. Soc***. 127**, 16752-16753 (2005).

[35] A. A. Bol, R. V. Beek, A. Meijerink, *Chem. Mater.* **14***,* 1121-1126 (2002).

[36] T. Andreev, N. Q. Liem, Y. Hori, M. Tanaka, O. Oda, D. L. S. Dang, B. Daudin, B. Gayral, *Phys. Rev. B* **74**, 155310 (2006).

[37] T. Andreev, N. Q. Liem, Y. Hori, M. Tanaka, O. Oda, D. L. S. Dang, B. Daudin, B. Gayral, *Phys. Rev. B* **73**, 195203 (2006).

[38] T. Andreev, N. Q. Liem, Y.Hori, M. Tanaka, O. Oda, B. Daudin, D. L. S. Dang, *Optical Materials* **28**, 775-779 (2006).

[39] H. J. Lozykowski, *Phys. Rev. B* **48**, 17758-17769 (1993).

[40] M. Dejneka, E. Snitzer, R. E. Riman, *J. Luminescence* **65**, 227 (1995).

[41] K. Takahei, A. Taguchi, H. Nakagome, K. Uwai, P. S. Whitney, *J. Appl. Phys*. **66**, 4941 (1989).

[42] H. J. Lozykowski, A. K. Alshawa, I. Brown, *J. Appl. Phys.* **76**, 4836 (1994).

[43] A. Taguchi, M. Taniguchi, K. Takahei, *Appl. Phys. Lett*. **60**, 965 (1992).

[44] A. Taguchi, K. Takahei, *J. Appl. Phys*. **79**, 3261 (1996).

[45] T. D. Culp, J. G. Cederberg, B. Bieg, T. F. Kuech, K. L. Bray, D. Pfeiffer, C. H. Winter, *J. Appl Phys*. **83**, 4918 (1998).

[46] M. Needels, M. Schlüter, M. Lannoo, *Phys. Rev. B* **47**, 15533 (1993).

[47] H. Kühne, G. Weiser, E. I. Terukov, A. N. Kusnetsov, V. K. Kudoyarova, *J. Appl. Phys.* **86**, 896 (1999).

[48] W. Fuhs, I. Ulber, G. Weiser, M. S. Bresler, O. B. Gusev, A. N. Kuznetsov, V. Kh. Kudoyarova, E. I. Terukov, I. N. Yassievich, *Phys. Rev. B* **56**, 9545 (1997).

[49] S. Coffa, F. Priolo, G. Franzò, V. Bellani, A. Carnera, C. Spinella, *Phys. Rev. B* **48**, 11782 (1993).

[50] I. Tsimperidis, T. Gregorkiewicz, H. H. P. Bekman, C. J. G. M. Langerak*, Phys. Rev. Lett.* **81**, 4748 (1998).

[51] T. Andreev, PhD thesis, University of Joseph Fourier, Grenoble, France (2006).

[52] A. Taguchi, K. Takahei, *J. Appl. Phys*. **79**, 4330-4334 (1996).

[53] G. M. Dalpian, J. R. Chelikowsky, *Phys. Rev. Lett.* **96***,*226802 (2006).

[54] P. Reiss in *Semiconductor Nanocrystal Quantum Dots: Synthesis, Assembly, Spectroscopy and Applications*, Springer Wien New York, 52 (2008).

[55] H. S. Yang, P. H. Holloway, B. B. Ratna, *J. Appl. Phys***. 93**, 586–592 (2003).

[56] N. Pradhan, D. M. Battaglia, Y. Liu, X. Peng, *Nano Lett. 7*, 312–317 (2007).

[57] U. T. D. Thuy, P. T. Thuy, N. Q. Liem, L. Li, P. Reiss, *Appl. Phys. Lett.* **96**, 073102 (2010).

[58] U. T. D. Thuy, P. Reiss, N. Q. Liem, *Appl. Phys. Lett.* (2010) doi:10.1063/1.3515417.

[59] J. Li, J. B. Xia, *Phys. Rev. B* **61**, 15880-15886 (2000).

[60] E. Zych, *J. Phys.: Condens. Matter* **14**, 5637 (2002).

[61] M. Ito, G. Boulon, A. Bensalah, Y. Guyot, C. Goutaudier, H. Sato, *J. Opt. Soc. Am. B* **24**, 3023 – 3033 (2007).

[62] H. Hai, PhD thesis, National University of Singapore (2005).

Conclusion

This thesis focused on the synthesis and study of the optical properties of InP colloidal semiconductor NCs and on their doping with rare earth ions. For the first time, the synthesis of InP and alloyed In(Zn)P core NCs as well as InP/ZnS and In(Zn)P/ZnS core/shell NCs was developed using novel approaches based on the reaction of indium acetate or indium chloride with different phosphorous precursors such as yellow phosphorus, PH_3 gas and $P(TMS)_3$. Based on this knowledge, for the first time Eu-doped In(Zn)P and In(Zn)P/ZnS core/shell “d-dots” were successfully synthesized. The emission of the dopant ions has been optimized by identifying the appropriate synthesis parameters, nature of the dopant precursor and its concentration. The prepared NCs were characterized by powder XRD, TEM, EDX, X-ray fluorescence, UV-vis absorption, photoluminescence excitation and steady-state as well as time-resolved photoluminescence spectroscopy.

InP NCs were first synthesized in a *low temperature reaction* using a novel and simple method in the solvent mixture of toluene and ethanol. The reaction temperature of 70°C is the lowest temperature reported for preparing InP NCs up to date. Nevertheless the synthesized particles show good crystallinity with a mean size of 3–4 nm, relatively low polydispersity and are obtained in high yields. Their surface is not passivated by bulky organic molecules of surfactant type, in contrast to nanoparticles synthesized *via* traditional colloid-chemical methods. As a consequence, these NCs do not show detectable photoluminescence. On the other hand, charge transfer processes at the interface with their surrounding medium are facilitated opening the way for their application in solar cells and photodetectors as broad-band light absorbers and electron acceptors.

Using *high temperature synthesis*, namely by means of the hot injection and the heating-up methods allowed the synthesis of highly luminescent QDs. The hot injection method can be adjusted to obtain bigger InP and InP/ZnS core/shell QDs with an excitonic absorption peak in the 570–700 nm range, corresponding to the PL in the 590–720 nm range. In addition, the ZnS shell showed emission in the blue region around 470 nm, arising from defect states. The results from TRPL measurements demonstrated that the ZnS shell emitted on a comparable timescale to that from the InP core, in the nanosecond range. The ZnS overcoating plays a decisive role in the passivation of imperfections at the surface of InP QDs,

consequently increasing the photoluminescence intensity related to the excitonic transition in the InP core. In addition, our study reveals that, beside the optical transitions in the InP core, the optical processes within the ZnS shell strongly influence the dynamics of carriers' population and evolution after photo-generation.

The alloy In(Zn)P and In(Zn)P/ZnS QDs were successfully synthesized by using a heating-up one-pot method. The role of zinc stearate added to the initial reaction mixture was elucidated, showing that it acts as: i) a surfactant controlling the NCs formation and growth kintetics, and ii) a Zn precursor resulting in an alloyed In(Zn)P core NC structure. After growth of an outer ZnS shell, the alloy In(Zn)P/ZnS core/shell QDs showed excellent optical properties such as a LQY reaching 70%, tunable emission in the range from 485 to 590 nm (by varying the Zn^{2+}:In^{3+} molar ratio and reaction temperature), and a typical PL FWHM of 50 nm. We explain the high LQY by the alloy structure of the In(Zn)P QDs that causes band-edge fluctuations to enhance the confinement of the excited carriers, which in turn increases the radiative recombination probability.

In the next part, we have studied the influence of the surrounding environment on the optical characteristics of the alloy In(Zn)P/ZnS QDs in close-packed films and in colloidal solutions. The SSPL spectra from the close-packed In(Zn)P/ZnS QDs are peaking at longer wavelengths in comparison with those taken from the colloidal ones. In addition, the TRPL study shows that the close-packed In(Zn)P/ZnS QDs possess a shorter luminescence decay time and a strongly increased spectral shift with the delay time from the excitation moment in comparison with the colloidal ones. Förster resonance energy transfer and/or excited charge-carrier transfer between the In(Zn)P/ZnS QDs, favored by their alloyed internal structure, have been shown to be the main reasons for the observed behavior. The evidence for the charge-carrier transfer in close-packed layers of In(Zn)P/ZnS QDs is very important for their integration into optoelectronic devices, such as QD LEDs or light emitting field effect transistors (LEFETs).

Eu-doped In(Zn)P and Eu-doped In(Zn)P/ZnS core/shell "d-dots" were successfully synthesized using a three-step one-pot method: step 1, synthesis of the In(Zn)P host NCs; step 2, Eu-dopant; incorporation and step 3, growing the outer ZnS shell preventing from dopant out-diffusion and providing high photostability. A high doping yield could be achieved by choosing Eu-oleate as the appropriate precursor and controlling several key parameters of the synthesis such as (i)

reaction-growth of In(Zn)P core QDs at a temperature of 190°C for 10 min; (ii) Eu adsorption at 80°C for 100 min and Eu incorporation at 120°C for 20 min; and (iii) finally the ZnS shelling at 120°C for 10 min. In addition, the critical dopant concentration has been determined to be of 30%. All optical measurements such as absorption, PL, PLE, phosphorescence and TRPL have unambiguously supported the fact of the successful Eu-doped In(Zn)P and In(Zn)P/ZnS QDs, as well as the resonant energy transfer from the In(Zn)P host to the Eu^{3+} guest ions.

Due to the similar ionic radius of several RE ions as compared to Eu^{3+} (or In^{3+}), our approach should be easily extendable to other systems. We are currently investigating the doping of In(Zn)P and In(Zn)P/ZnS QDs with Thulium (emission at ~807 nm) and Erbium (emission at ~1300 nm). Emission in these wavelength ranges is important for biological *in vivo* imaging and in emitters used in telecommunication with optical fibres. Further issues under current investigation which could not be accomplished before submission of the thesis manuscript are the determination of the atomic percentages of the different elements in the Eu:In(Zn)P and Eu:In(Zn)P/ZnS NCs as a function of the used dopant concentration and the measurement of the RE dopant emission quantum yield.

Appendix 1

Experimental section

A1.1. Chemicals and apparatus

Chemicals

All reagents and solvents were used as received without purifying: indium acetate (99.99%), indium chloride (99.9%), myristic acid (>99%), tris(trimethylsilyl) phosphine ($(PTM)_3S$, 95%), bis(trimethylsilyl)sulfide ($(TMS)_2S$, 90%), 1-dodecanethiol (DDT, 97%), 1-octadecene (ODE, 90%), sodium hydroboride (99.0%), zinc phosphide, europium chloride (99.999%), europium acetate (99.999%), sodium oleate (99%), oleic acid (>99%), zinc oxide (>99%), zinc chloride (>99.9%), potassium ethylxanthate (>98%), dimethyl formamide (DMF), acetone, methanol, ethanol, chloroform, toluene, n-hexane (all anhydrous) were purchased from Sigma-Aldrich. While zinc stearate ($ZnSt_2$, 90%), yellow phosphorus (P_4) were purchased from Riedel de Haën and Merck, respectively. Note that P_4 is stored in water to avoid its ignition.

Apparatus

Figure A1.1: *Photos of experimental setup for synthesis of core and core/shell NCs.*

A1.2. Synthesis of InP using yellow P_4 at low temperature [1]

Chemicals

All reagents and solvents were used directly without further purification: indium chloride (99.9%) was purchased from Wako Chemicals Co. Sodium hydroboride (99.0%), yellow phosphorus (P_4, stored under water to avoid its ignition) were purchased from Merck. The methanol, ethanol, toluene solvents were purchased from Sigma-Aldrich.

Experimentals

In a typical synthesis, 2.5 mmol of $InCl_3$ are dissolved in 25 mL of ethanol; separately 5 mmol of yellow phosphorus are dissolved in 25 mL of toluene. The In:P molar ratio of 1:2 used is to assure the quantitative conversion of the In precursor to InP. Both separated clear solutions become after immersion in an ultrasound bath for 15 minutes. Then, the mixture of these two solutions (hereafter called the solution MS) is put into a three-neck flask equipped with a condenser under nitrogen atmosphere. The solution MS is heated under magnetic stirring to temperatures between 40 and 70°C, yielding a translucent, light yellow mixture. A 0.2 M solution

of $NaBH_4$ is prepared by dissolving 15 mmol in 75 mL of ethanol for the purpose of its subsequent injection into the solution MS. Note that the amount of $NaBH_4$ warrants the excess (two times) of reducing agent as compared to the used amount of In^{3+} ions. The freshly created In atoms from the reduction of the In^{3+} ions can react with available P atoms in the solution MS to form InP. We used two different ways for the injection of the $NaBH_4$ solution into the solution MS: (i) the "continuous method", in which the whole amount (75 mL) of the $NaBH_4$ solution is dropwise added to the solution MS with an injection rate of ~1 mL/min. Practically, ca.12 minutes after adding the first drops, the reaction mixture turns to dark-yellow indicating that the InP NCs has been formed; (ii) the "discontinuous method", in which 10 mL of the $NaBH_4$ solution are swiftly injected into the solution MS with injection rate of 5 mL/min. After a few minutes, the reaction mixture changes its color to yellow. The remaining 65 mL of the $NaBH_4$ solution are added dropwise to the solution MS in order to assure a sufficient degree of supersaturation during the growth of the InP NCs. The reactions are maintained at a temperature of 40 or 70°C for duration of 1 to 5 hrs depending on the desired size. The produced dark precipitates are collected by centrifugation (5700 rpm, 10 min) and washed several times with hot ethanol and toluene to remove residuals and by-products such as P_4, NaCl and $NaBH_4$ (in some samples, CS_2 was used to wash P out). Finally, the black powder is dried in vacuum at 60°C for 1 hr. The reaction yield has been determined to be close to 100% with respect to the starting amount of the In precursor.

A1.3. Synthesis of InP and InP/ZnS core/shell NCs in non-coordinating solvent

A1.3.1. Hot-injection method using PH_3 gas [2]

Chemicals

All reagents and solvents with the analytical grade or with the high purity were used directly without further purification: indium acetate (99.99%), myristic acid (>99%), 1-octadecene (ODE, 90%), zinc phosphide, zinc chloride (>99.9%), potassium ethylxanthate (>98%), dimethyl formamide (DMF), acetone, methanol, ethanol, chloroform, toluene, n-hexane (all anhydrous) were purchased from Sigma-Aldrich. Zinc stearate ($ZnSt_2$, 90%) and H_2SO_4 were purchased from Riedel de Haën and Merck, respectively.

Apparatus

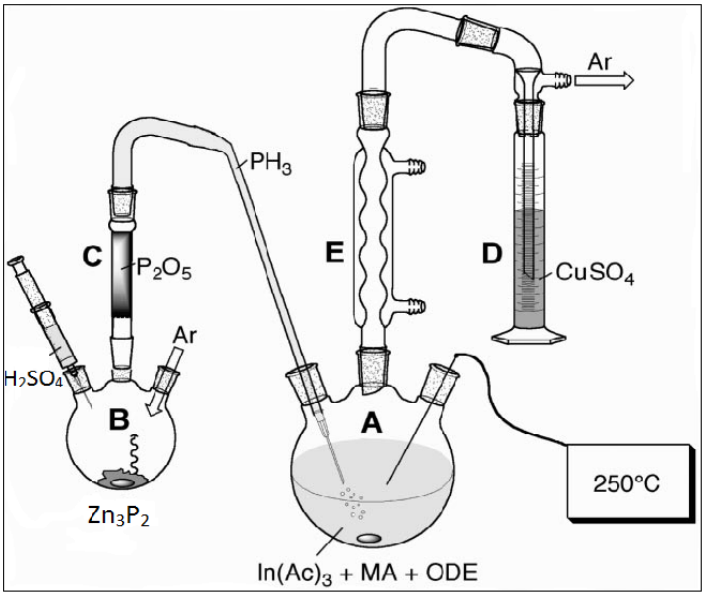

Figure A1.2: *Schematic of experimental setup for synthesis of InP NCs using PH_3 gas.*

Synthesis of InP core NCs

The InP core NCs was formed from the reaction of In precursor and PH_3 gas, which was generated *in situ* from Zn_3P_2 and H_2SO_4. Typically, 0.1 mmol of indimum acetate was mixed with 0.3 mmol of myristic acid and 6.8 g of ODE in a 50 mL three-neck flask (A) equipped with a condenser (E) under inert atmosphere. In a drybox, 75 mg (0.3 mmol) of finely ground Zn_3P_2 powder was loaded into another flask (B), which was then connected to flask A by means of column C, containing P_2O_5 for the elimination of traces of water in the subsequently produced PH_3 gas. Next, the indium precursor was heated to 100–120°C to obtain an optically clear solution, and both flasks were degassed for 1 hr and backfilled with Ar. Reaction flask A was then heated to 250°C, followed by the injection of 2 mL of 1M H_2SO_4 into flask B, initiating the production of the PH_3 gas. Carried by a flow of Ar gas, PH_3 gas was bubbled into flask A and reacted with the indium precursor to form InP NCs. In the first two minutes after H_2SO_4 injection, the observed PH_3 production was the strongest. With the goal to induce a short nucleation burst via precursor supersaturation, a stronger Ar flow was used during this period. The color of the reaction mixture quickly changed from colorless to deep red during the first 5–10 min of the reaction. The excitonic peak in the absorption spectra of the prepared InP NCs underwent a red shift from 570 nm (5 min) to around 600 nm (20 min). An

extension of the reaction time did not result in a further spectral evolution because of the consumption of the Zn_3P_2 precursor. After cooling to room temperature, the NCs were isolated by adding 1 volume equivalent of acetone and 10 equivalents of a $CHCl_3$/methanol (1/1) mixture, followed by centrifugation. The precipitated product could easily be redispersed in a number of solvents, including hexanes, toluene, or chloroform. No size sorting procedures were performed for any of the samples presented here.

Synthesis of InP/ZnS core/shell NCs

In a typical synthesis of InP/ZnS core/shell NCs, 2.5 mL of the crude solution of InP NCs prepared as above described was mixed with 5.5 g of ODE and heated up to 230°C. The amount of Zn:S stock solution (see below) was calculated from the ratio between core and shell volumes using bulk lattice parameters of InP and ZnS to obtain the desired shell thickness. This amount was gradually added with dropwise rate of 3 mL/min to the vigorously stirred solution of InP NCs under inert environment. After adding ZnS shell precursors, the growth temperature was decreased to 30°C and the heating was maintained for few hours until the expected shell thickness. The core/shell NCs can be isolated *via* the same procedure that was applied to InP-based NCs. No size sorting procedures were performed for any of the samples presented here. This method can be adjusted to obtain bigger InP and InP/ZnS core/shell QDs with an excitonic absorption peak in the 570–700 nm range, corresponding to the PL in the 590–720 nm range.

Preparation of Zn:S stock solution is as follows: 1 mmol of $ZnSt_2$ and 0.25 mmol of zinc ethylxanthate ($Zn(EX)_2$) were dissolved in the mixture of 2 mL of ODE, 1 mL of toluene, and 100 μL of DMF. $Zn(EX)_2$ was formed from reaction of zinc chloride (5 mmol, in 20 mL of distilled water) and potassium ethyl xanthogenate (10 mmol, in 20 mL of distilled water) under constant stirring. The white precipate of $Zn(EX)_2$ was filtered, washed with distilled water and dried in vacuum.

A1.3.2. Heating-up one-pot method using $P(TMS)_3$ [3-5]

Chemicals

All reagents and solvents with the analytical grade or with the high purity were used directly without further purification: indium acetate (99.99%), myristic acid (>99%), tris(trimethylsilyl) phosphine ($(PTM)_3S$, 95%), 1-octadecene (ODE, 90%),

zinc chloride (>99.9%), potassium ethyl xanthate (>98%), dimethyl formamide (DMF), acetone, methanol, ethanol, chloroform, toluene, n-hexane (all anhydrous) were purchased from Sigma-Aldrich. Zinc stearate ($ZnSt_2$, 90%) was purchased from Riedel de Haën.

Apparatus

Figure A1.3: *Photo of experimental setup for synthesis of In(Zn)P/ZnS core/shell NCs using $P(TMS)_3$*

Synthesis of In(Zn)P core NCs

For a typical synthesis of In(Zn)P QDs, 7 mL of 1-octadecene (ODE) were degassed for 1 hr at 100–120°C in a 50 ml three neck flask equipped with a condenser, backfilled with Ar and then cooled to room temperature. Next, a mixture of 0.1 mmol of indium myristate, which was formed *in situ* from indium acetate and myristic acid, a certain quantity of zinc stearate (0–0.2 mmol), and 0.05 mmol of $P(TMS)_3$ were prepared in a glove-box and injected into the ODE solution at room temperature. Finally, this reaction mixture was heated quickly to 250–300°C with a rate of approximately 2–3°C/s by means of a molten salt bath and kept for several

minutes to grow the QDs to the desired size. Subsequently, the temperature of reaction flask was decreased to perform the next step for overcoating ZnS shell.

Synthesis of In(Zn)P/ZnS core/shell NCs

The epitaxial growth of ZnS shell was carried out as follows: 0.4 mmol of $ZnSt_2$ and 0.1 mmol of $Zn(EX)_2$ were dissolved in a mixture of 3 mL of ODE, 1 mL of toluene and 0.3 mL of DMF at 100°C in a glove-box. The obtained clear solution became cloudy at room temperature. It was slowly added into the flask containing the In(Zn)P NCs at 235–285°C with dropping rate of 10 mL/hr. The reaction mixture was maintained at the shell growth temperature for 1 hr and then cooled down to room temperature. For purification, the NCs were isolated by adding 1 volume equivalent of acetone and 10 equivalents of a $CHCl_3$/methanol (1/1) mixture, followed by centrifugation and decantation. Finally, the In(Zn)P/ZnS NCs can easily be redispersed in organic solvents such as n-hexane, toluene and chloroform. No size-sorting procedures were performed for any of the samples used in the present study.

The emission could be easily tuned in range of 485–590 nm with a typical LQY reaching 60–70% by varying the Zn^{2+}:In^{3+} molar ratio and the reaction-growth/shelling temperature.

Preparation of indium myristate was as follows: 2 mmol of indimum acetate were mixed with 6 mmol of myristic acid and 20 mL of ODE in a 50 mL three-neck flask equipped with a condenser. The mixture was degassed at 100–120°C for 1 hr to obtain an optically clear solution, backfilled with Ar, and then cooled down to room temperature. This stock solution was stored in a glove-box.

A1.4. In(Zn)P/ZnS NCs doped with Eu^{3+} ions

Chemicals

All reagents and solvents with the analytical grade or with the high purity were used directly without further purification: indium acetate (99.99%), myristic acid (>99%), tris(trimethylsilyl) phosphine ($(PTM)_3S$, 95%), 1-octadecene (ODE, 90%), europium chloride (99.999%), europium acetate (99.999%), sodium oleate (99%), oleic acid (>99%), zinc oxide (>99%), acetone, methanol, ethanol, chloroform,

toluene, n-hexane (all anhydrous) were purchased from Sigma-Aldrich. Zinc stearate ($ZnSt_2$, 90%) was purchased from Riedel de Haën.

Experimentals

- *Step 1: Synthesis of In(Zn)P host QDs*

Synthesis of the In(Zn)P core QDs was described detail in Section A1.3.2. In brief, the Zn^{2+}:In^{3+} molar ratio of 2:1 and the reaction-growth temperature and time of 190°C and 10 min, respectively, were used in these studies. For the purpose of the obtained In(Zn)P QDs emitting PL at around 470 nm, which is nearly resonant to the $^7F_0 - {}^5D_2$ transition of the Eu^{3+} ions and therefore the resonant energy transfer from the In(Zn)P host to the Eu^{3+} guest ions can occur.

- *Step 2: Eu dopant growth*

In this process, two stages were applied: (i) adsorption of Eu-containing layer on surface of the In(Zn)P host QDs; (ii) incorporation of the Eu^{3+} ions into the In(Zn)P host QDs. Typically, a certain quantity of Eu-precursor (0-0.04 mmol) was dissolved in 1 mL of ODE at ~100°C in glove-box. This solution was slowly added into the flask containing In(Zn)P QDs with dropping rate of 2.0 mL/hr at 80°C. Adsorption of the Eu^{3+} ions was performed at 80°C for 100 min. Subsequently, this reaction solution was heated to 120°C for incorporation of the Eu^{3+} ions into the In(Zn)P QDs for 20 min. Their optical characteristics were studied by absorption, PLE, PL and TRPL spectroscopies.

- Step 3: *Growing the outer ZnS shell*

The ZnS shelling was carried out as description in Section A1.3.2. However, the traditional Zn:S precursors, which formed from $ZnSt_2$ and $Zn(EX)_2$), were replace by the higher activity Zn:S precursors such as Zn-oleate and $(TMS)_2S$. For a typical synthesis, a certain quantity of Zn:S precursor solution of 0.025M (see below) in ODE was injected with the dropping rate of 10 mL/hr into the flask containing Eu:In(Zn)P QDs at 120°C. The entire shell growth process was controlled by taking aliquots for UV-vis absorption, PLE, PL, TRPL and X-ray fluorescence spectroscopies. After completed shell growth, the reaction solution was cooled down to room temperature. For purification, the NCs were isolated by adding 1 volume equivalent of acetone and 10 equivalents of a $CHCl_3$/methanol (1/1) mixture, followed by centrifugation and decantation. Finally, Eu-doped In(Zn)P/ZnS NCs could be redispersed in organic solvents, such as n-hexane, toluene and chloroform.

Preparation of europium oleate (Eu-oleate) was as follows [6]: The mixture of Eu(III) chloride hexahydrate (2 mmol), sodium oleate (6 mmol), ethanol (4 mL), de-ionized water (3 mL), and n-hexane (7 mL) were vigorously stirred at 60°C for 4 hr. The top hexane layer, which containing the Eu-oleate, was isolated using a separator funnel and washed four times with de-ionized water. Affter that, the hexane was evaporated and therefore Eu-oleate obtained in waxy solid form. Finally, this Eu-oleate was kept in glove-box and used as a standard precursor for furthermore studies of Eu-doped NCs.

Preparation of Zn:S precursor solution (0.025 M) was as follows [7]: The mixture of 1 mmol of ZnO and 4 mmol of oleic acid was dissolved in 40 mL of ODE at ~300°C for 15 min in glove-box. Next, 4 mL of the obtained Zn-oleate clear solution was mixed with 0.1 mmol of $(TMS)_2S$ at around 80°C.

A1.5. Structural characterizations

For the structural characterization of the samples resulting from each specific synthesis, powder X-ray diffraction (XRD, Siemens D5005 and Phillips X'pert) and Raman scattering spectroscopy (Jobin-Yvon Horiba Infinity spectrometer with 532 nm excitation) were performed. The XRD patterns were used to identify structural phases as well as to calculate the mean crystallite sizes using Scherrer's formula. Transmission electron microscopy (TEM JEOL 4000EX), EDX analysis (FE-SEM Hitachi S4800) and XRF analysis (XRF5006-HQ02) enable us to determine directly the NCs' size and shape, as well as their stoichiometry.

A1.6. Optical characterizations

A1.6.1. Absorption spectroscopy [8]

From the point of view of photo-physics, the absorption and emission spectra could provide information on the electronic subsystem of the matter. One could consider absorption and emission to be two complementary methods, which being applied together, allow extracting additional information on the subject under study. Also one should keep in mind that not all transitions observed in absorption spectroscopy can be observed in emission spectra.

A simplified scheme of the setup absorption spectroscopy system is shown in Figure A1.4.

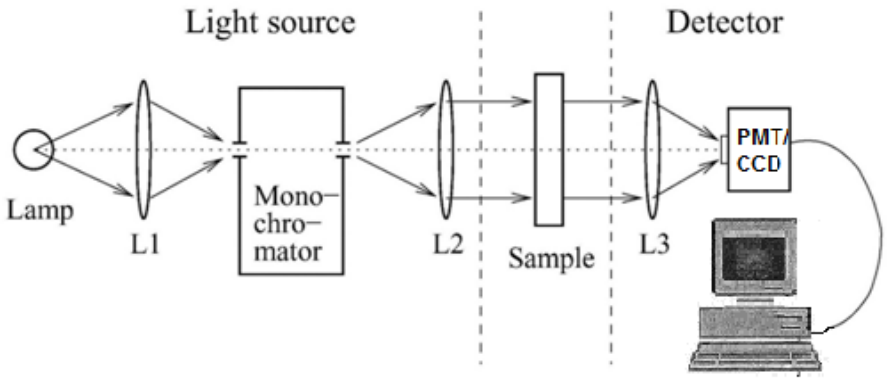

Figure A1.4: *Schematic diagram of the absorption spectroscopy system.*

The lamp emission from a tungsten halogen lamp is collected by the lens L1 and focused onto the input slit of the monochromator, which can be tuned easily in a wide spectral range. The lens L2 collects the light from the monochromator output slit and forms the monitoring beam. After the sample, the light is collected by the lens L3 and focused onto the photomultiplier detector (PMT) or CCD camera, which is required to measure the intensities before, I_{in}, and after, I_{out}, the sample placed in the measurements. Typically, at first the whole spectrum is measured without the sample, which is commonly called base line, thus giving the spectrum $I_{in}(\lambda)$. And then the spectrum is measured with the sample to obtain $I_{out}(\lambda)$. Finally, the absorbance is calculated out of these two spectra as follows:

$$A(\lambda) = -\log\left(\frac{I_{out}(\lambda)}{I_{in}(\lambda)}\right)$$

Furthermore, the absorption spectroscopy is very useful in determination of the concentration and the size of compounds. As a consequence, the concentration of a dispersion containing NCs of these materials can easily be determined by UV/Vis spectroscopy using the Beer–Lambert law:

$$A = \varepsilon * C * L$$

where A, ε, C, and L are absorbance, molar absorbtivity (L mol^{-1} cm^{-1}), NC concentration (mol L^{-1}), and path length of the cuvette in which the sample is contained (cm), respectively.

As the NC size is directly related to the excitonic peak in the UV/Vis absorption spectrum, the size-dependent molar extinction coefficient ε can be determined at the same time. The empirical functions correlating the size of InP NCs

with the position of excitonic peak in their absorption spectra as well as with the molar extinction coefficient ε can be described in good approximation [10]:

$$D = (-3.7707 \times 10^{-12})\lambda^5 + (1.0262 \times 10^{-8})\lambda^4 - (1.0781 \times 10^{-5})\lambda^3 + (5.4550 \times 10^{-3})\lambda^2 - (1.3122)\lambda + 119.9$$

and $\varepsilon = 3046.1(D)^3 - 76532(D)^2 + (5.5137 \times 10^5)(D) - (8.9839 \times 10^5)$

where D, λ and ε are NC diameter (nm), excitonic peak (nm) and molar extinction coefficient (L mol^{-1} cm^{-1}), respectively.

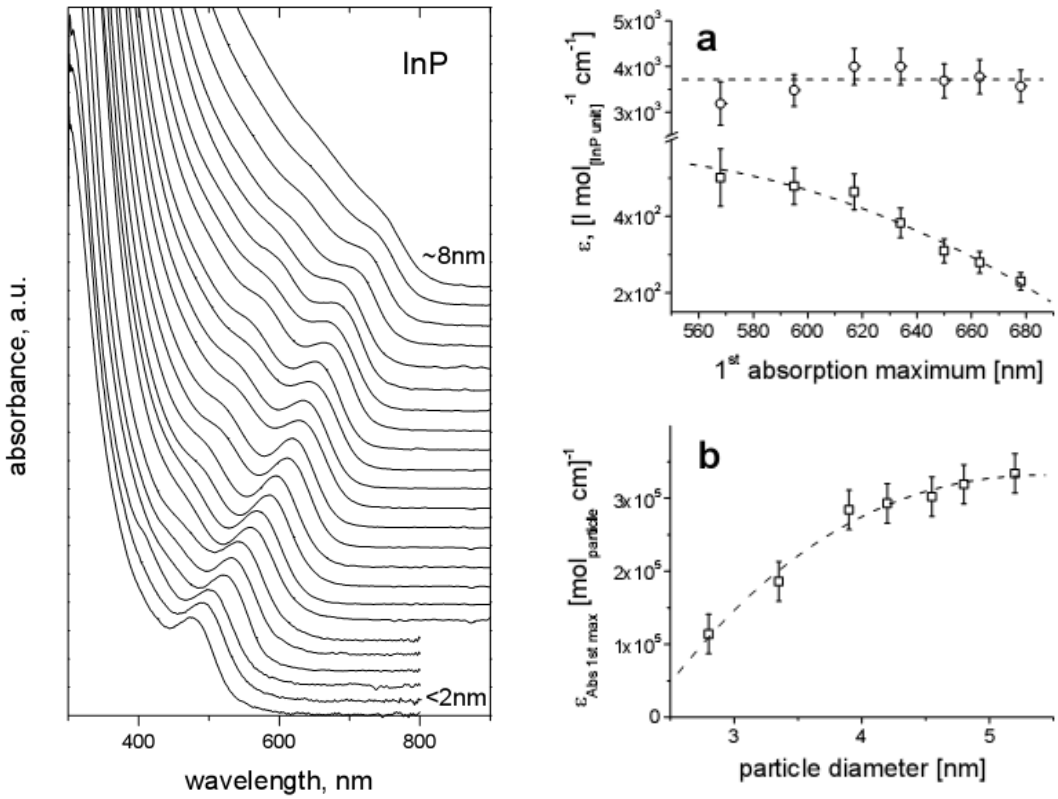

Size-dependent evolution of absorption spectra of TOPO-TOP capped InP NCs (left). (a) the extinction coefficients referred to the concentration of InP units measured at 350 nm (□) and at the first absorption maximum (□) for different nanocrystal sizes; (b) molar extinction coefficient of InP nanocrystals at the first absorption maximum referred to the particle concentration [11].

A1.6.2. Photoluminescence spectroscopy

Luminescence is a physical phenomenon when an electron and a hole are created and then recombined radiatively to generate a photon. The term luminescence includes all types of light emission (especially fluorescence and phosphorescence) appearing as a consequence of some input energy into the sample. There are many ways to excite luminescence, for example, the case of optical excitation resulting in photoluminescence. Typically, an electron from the valence band is raised up to the conduction band by absorbing a photon with energy higher than E_g. Thus it leaves a hole with positive charge (+) in the valence band. The light emission is created by recombining this electron-hole pair, is called PL. Therefore, the simplest PL setup consists of an excitation source and a detector for measuring the intensity of the luminescence (Figure A1.5).

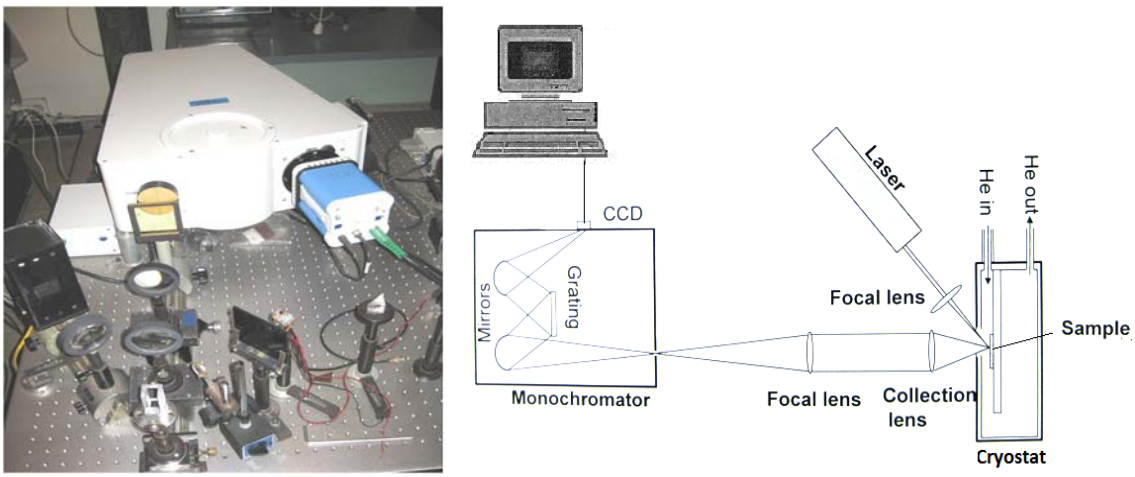

Figure A1.5: *Photo and schematic diagram of a typical PL setup used during this work.*

The light from the excitation source (such as laser or lamp, in the present case 337.1 nm pulsed light of a nitrogen gas laser or 360, 365 nm Xe lamp or 370 nm LED) was focused by a focal lens onto the sample, which is mounted in cryostat, to enhance its excitation density. Consequently, the signal emission was collected and focused onto the entrance slit of a monochromator by a collection and focal lenses. (This can be realized with one or better two lenses). Inside the monochromator, a parabolic mirror is used to reflect the entrance signal to a grating for wavelength separation and another parabolic mirror is utilized to focus the signal onto a detector. As the energetic resolution of the final spectrum is proportional to the

square of the number of slits of the grating, in the present case 600 or 1800 (Jobin-Yvon HRD1 or iHR550), it is important to enlight all the area of the grating. Finally, the PL signals were detected by a thermoelectric cooled Si-CCD camera or photomultiplier tube (PMT).

Measurement of the luminescence quantum yield (QY) [9]

The LQY of the InP/ZnS NCs were determined by comparison to a standard with well-known QY (freshly prepared solution of Rhodamine 6G in ethanol; QY 95%), using the following formula:

$$\Phi_{NC} = \Phi_{Standard} \, (grad_{NC}/grad_{Standard})(n_{NC}^2/n_{Standard}^2)$$

with Φ being the QY, grad the gradient (slope) of the plot of the integrated fluorescence intensity as a function of absorbance and n the refractive index of the solvent (1.375 for n-hexane, 1.36 for ethanol).

Purified NCs samples were put into 1 cm quartz cuvettes and diluted with n-hexane until the absorbance at the first excitonic was below 0.1. The absorbance of the standard was adjusted to be equal to NC dispersion at a certain wavelength (360 nm in our work), which is used to excite the sample

A1.6.3. Photoluminescence excitation spectroscopy

The PLE aims to identify different levels of absorption in the structure, which allows us to determine the mechanisms responsible for the PL emission of the hetero-structure as well as the emission strongly excited at certain photon energies. Indeed, PLE is especially powerful in study the energy transfer process from host crystals to dopant ions.

PLE allows measuring the intensity changes of one chosen emission line as a function of the excitation wavelength. A simplified schema of a PLE system is shown in Figure A1.6. The excitation source is a 500 W high-pressure Xenon lamp. The white light is filtered by using a monochromator to vary the excitation wavelength. The beam from this monochromator is focused the sample, which is placed in a cryostat. The generated photons are collected by using a set of lenses and detected by another monochromator that is fixed wavelength detection. The analysis of the photons is realized by a CCD camera or a PMT.

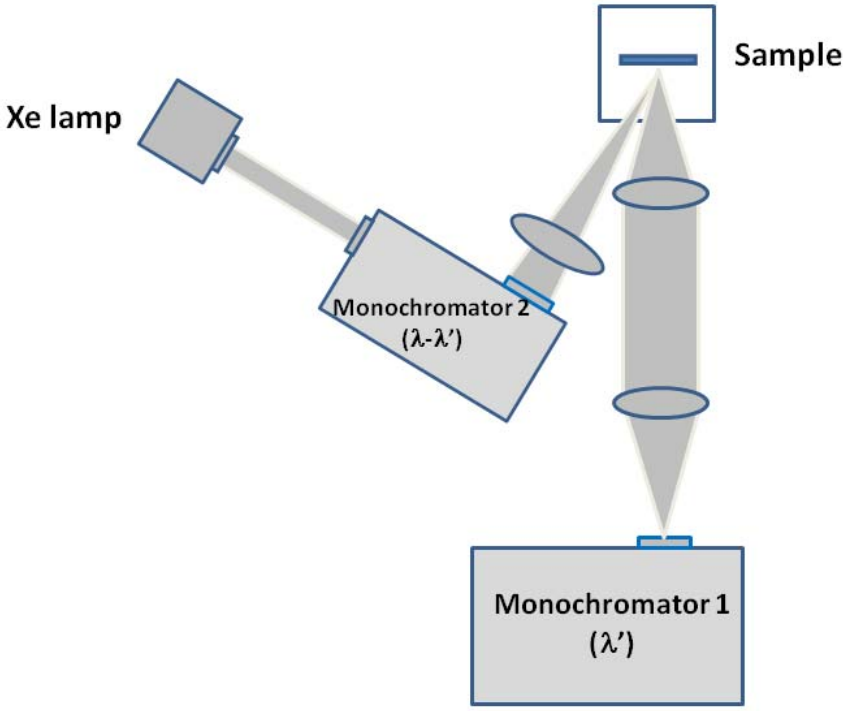

Figure A1.6: *Schematic diagram of a typical PLE system.*

A1.6.4. Time-resolved photoluminescence

In TRPL spectroscopy, the emission spectrum is recorded as a function of delay time after the pulse arrives. TRPL provide direct information about the carrier relaxation and recombination mechanisms and allow to measure the radiative lifetimes.

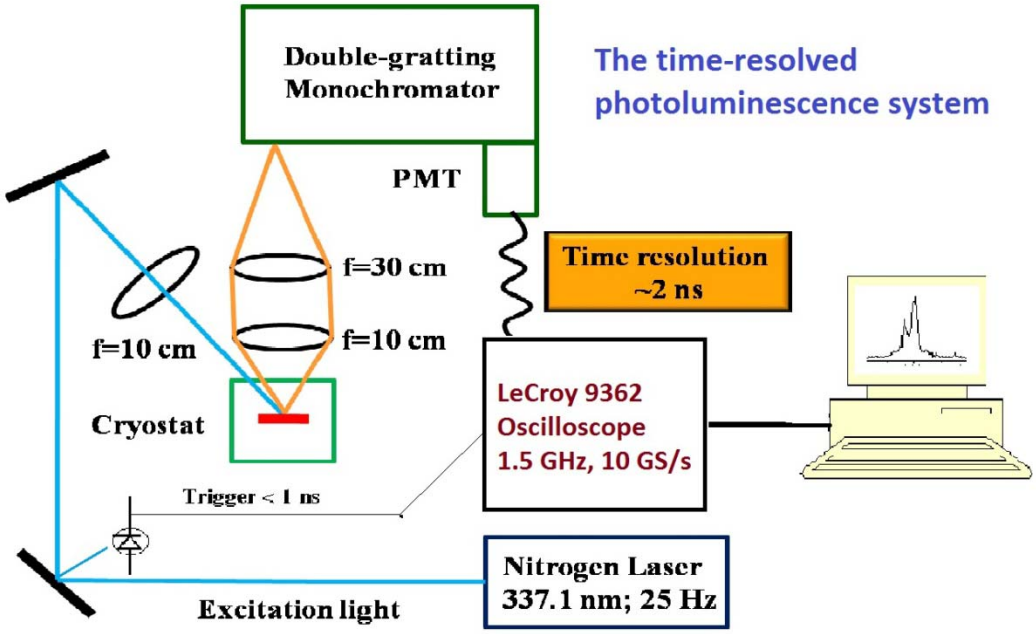

Figure A1.7: *Photo and schematic diagram of a time-resolved photoluminescence system.*

In this work, the TRPL have been setup as shown in Figure A1.7. Typically, the 337.1 nm pulsed light from a nitrogen gas laser was used as the excitation source, whose excitation power density could be varied in the range from 100 W/cm^2 to 100 kW/cm^2, with a pulse duration of 1 ns. A small part of the excitation light is split by a glass or quartz mirror and directed to a fast photodiode to produce

triggering pulses. The PL signals were dispersed by means of a 0.6 m grating monochromator (Jobin-Yvon HRD1) and detected using a fast photomultiplier (Hamamatsu model H733, with a rise time of 700 ps). Averaging the multi-pulses at each spectral point using a 1.5 GHz digital oscilloscope (LeCroy 9362) strongly improved the signal-to-noise ratio.

References

[1] U. T. D. Thuy, T. T. T. Huyen, N. Q. Liem, P. Reiss, *Mater. Chem. Phys*. **112**, 1120 (2008).

[2] L. Li, M. Protière, P. Reiss, *Chem. Mater.* **20**, 2621 (2008).

[3] L. Li, P. Reiss, *J. Am. Chem. Soc.* **130**, 11588 (2008).

[4] U. T. D. Thuy, P. T. Thuy, L. Li, P. Reiss, N. Q. Liem, *Appl. Phys. Lett*. **96**, 073102 (2010).

[5] U. T. D. Thuy, P. Reiss, N. Q. Liem, *Appl. Phys. Lett*. **9**7, 193104 (2010).

[6] S. V. Mahajan, J. H. Dickerson, *Nanotechnology* **18**, 325605 (2007).

[7] R. Xie, U. Kolb, J. Li, T. Basche, A. Mews, *J. Am. Chem. Soc*. **127**, 7482 (2005).

[8] N. V. Tkachenko, *Optical spectroscopy: Methods and Instrumentations*, Elsevier, Amsterdam (2006).

[9] J. N. Demas, G. A. Crosby, *J. Phys. Chem.* **75**, 991-1024 (1971).

[10] P. Reiss, M. Protière, L. Li, *Small* ***5***, 154–168 (2009).

[11] D. Talapin, PhD. Thesis, University of Hamburg, Germany (2002).

Appendix 2

Publications

1. **U. T. D. Thuy**, N. Q. Liem, D. X. Thanh, M. Protière, P. Reiss, *Appl. Phys. Lett.* 91 (2007) 241908. Optical transitions in polarized CdSe, CdSe/ZnSe, and CdSe/CdS/ZnS quantum dots dispersed in various polar solvents. **Selected for**: Virtual Journal of Nanoscale Science and Technology.
2. T. T. K. Chi, **U. T. D. Thuy**, N. Q. Liem, M. H. Nam, D. X. Thanh, *J. Korean Phys. Society* 52 (2008) 510-513. Temperature-dependent photoluminescence and absorption of CdSe quantum dots embbeded in PMMA.
3. N. Q. Liem, L. Q. Phuong, T. T. K. Chi, **U. T. D. Thuy**, D. X. Thanh, *J. Korean Phys. Society* 53 (2008) 1570-1574. Polarization of colloidal CdSe quantum dots.
4. **U. T. D. Thuy**, T. T. T. Huyen, N. Q. Liem, P. Reiss, *Materials Chem. Phys.* 112 (2008) 1120-1123. Low temperature synthesis of InP nanocrystals.
5. **U. T. D. Thuy**, P. T. Thuy, N. Q. Liem, L. Li, P. Reiss, *Appl. Phys. Lett.* **96** (2010) 073102. Comparative photoluminescence study of close-packed and colloidal InP/ZnS quantum dots.
6. **U. T. D. Thuy**, P. Reiss, N. Q. Liem, *Appl. Phys. Lett*. **97** (2010) 193104. Luminescence properties of In(Zn)P alloy core/ZnS shell quantum dots.

Proceedings

1. N. Q. Liem, L. Q. Phuong, T. T. K. Chi, **U. T. D. Thuy**, D. X. Thanh, *the 5th Inter Conf on Advanced Materials and Devices (ICAMD), Jeju Island, Korea*, 12-14 Dec 2007. Polarization of colloidal CdSe quantum dots.
2. P. T. Thuy, **U. T. D. Thuy**, T. T. K. Chi, , L. Q. Phuong, N. Q. Liem, L. Li, P. Reiss, *AMSN08, Nha Trang,* 15-21 Sept 2008, pp. 234. Time-resolved PL measurements of InP/ZnS quantum dots.

3. T. T. K. Chi, L. Q. Phuong, **U. T. D. Thuy**, D. X. Thanh, N. Q. Liem, *Proc. the Fifth National Conference on Solid State Physics, Vung Tau*, 12-14 November, 2008, 654. The passivation of surface CdSe quantum dots by hydrogen.
4. **U. T. D. Thuy**, N. Q. Liem, P. Reiss, *Proc. the Sixth National Conference on Solid State Physics, Da Nang*, 8-11 November, 2009. The influence of zinc on the nucleation and growth of high quality InP/ZnS quantum dots.
5. P. T. Thuy, **U. T. D. Thuy**, N. Q. Liem, *Proc. the Sixth National Conference on Solid State Physics, Da Nang*, 8-11 November, 2009. Optical properties study of InP/ZnS quantum dots.